POLITECNICO
MILANO 1863

SCHOOL OF CIVIL, ENVIRONMENTAL AND LAND MANAGEMENT ENGINEERING
MASTER OF SCIENCE IN ENVIRONMENTAL AND LAND PLANNING ENGINEERING

BALANCING SEDIMENT STARVATION AND HYDROPOWER DEVELOPMENT

THE CASE STUDY OF THE VJOSA RIVER

Master Thesis by:
Tangi Marco
Matr. 837008

Advisor:
Prof. Andrea Castelletti

Co-Advisor:
Dr. Simone Bizzi
Dr. Rafael Schmitt

Academic Year 2017 – 2018

Acknowledgments

A work like this is never a product of a single mind, the result of the work of a single person. I believe this Master thesis to be a testament to the five years I've spent at the Politecnico of Milan, and as such to contain within traces of all the experiences done, all the knowledge acquired and most importantly all the people I've interacted with in this period, both inside and outside the university.

First of all, I would like to thank professor Andrea Castelletti, for giving me the opportunity to work on this thesis.

I also want to express my heartfelt gratitude to Simone Bizzi, for the patience and passion he had in introducing me to this work's topics and the invaluable advices.

Deep thanks to Rafael Schmitt, who helped me to get the hang of his model and supported me many times along the way.

I'm also sincerely grateful to professor Hervé Piegay, for the chance he gave me to work with him in Lyon and the support and help during this period, along with Barbara Belletti and the team at ENS Lyon.

Last, but not least, I would like to thank my family and my friends, for the love, the help and the encouragement during my entire studies. This thesis is yours, too.

Abstract

Fluvial ecosystem are deeply interconnected natural systems and their functioning is controlled by a number of abiotic and biotic factors and their interactions in space and time. Among these factors, sediment transport and connectivity are key elements for the well-being of both the fluvial ecosystems and the population depending on the goods and services river systems provide. Disturbances to these factors, like the construction of dams for hydropower production, are hence bound to cause changes in the river natural equilibrium. These trade-offs should be taken into consideration in multi-objective analysis, in ordert o find alternatives that provide benefits while limiting the alterations to the natural system. Modelling dam impacts on sediment connectivity requires a whole-network perspective, which is challenging to provide with common sediment transport models. CASCADE (CAtchment Sediment Connectivity And DElivery) (Schmitt et al., 2016) is a modelling framework that has been developed to tackle this problem. CASCADE provides disaggregated information about the provenance and destination of sediment derived from a specific source such as to quantitatively describe sediment connectivity in river networks.

In this work, we propose a new version of the CASCADE model, where the sediment supply from each source is described not by a single sediment size, but as a distribution of sediment classes and the calculation of fractional transport rates is based on the empirical Wilcock and Crowe equation. Furthermore, two models were developed inside CASCADE to provide information of the grain size distribution in different branches of the river system.

This new framework is applied to the Vjosa basin, a gravel bed river in south Albania, with long braided sections on the network. The Vjosa is one of the last untouched braided rivers in Europe with a remarkable ecological valuable. In the basin currently, there are plans for hydropower development that pose a serious threat to this valuable ecosystem. We applied CASCADE on the Vjosa to assess the impact on sediment transport due to alternative scenarios of hydropower development. We defined indicators for sediment connectivity al-

terations and hydropower production and adopted them in a multi-objective analysis to find optimal dam siting. Moreover, given the data scarce context, we performed a sensitivity analysis about initial sediment distribution, which is unknown, and evaluated the robustness of the ranking about the planning scenarios in function of this model uncertainty.

The results show that there are alternatives that guarantee around 50% of the maximum possible hydroelectric production without drastically altering the sediment transport or damaging the braided sections of the river. Usually, those portfolios rely on the construction of hydropower dams on the upper part of the river or on the tributaries, that have lower impact on the overall sediment connectivity. The sensitivity analysis shows that, while changes on the initial conditions significantly affect the estimation of sediment fluxes across the basin, the ranking of alternatives dam siting, and the shape and composition of the Pareto front do not change significantly. Planning solutions are robust in terms of uncertainty related to sediment connectivity assessment, caused by the employment of a basin scale model such as CASCADE and the lack of field data.

Riassunto

I sistemi fluviali sono ambienti naturali strettamente interconnessi e governati da numerosi fattori biotici e abiotici che interagiscono e si influenzano reciprocamente nello spazio e nel tempo. Tra questi fattori, il trasporto solido e la connettivitá fluviale dei sedimenti influiscono grandemente sul corretto funzionamento del sistema stesso e conseguentemente sul benessere degli ecosistemi che dal fiume dipendono e sulle popolazioni che beneficiano di servizi e risorse che esso garantisce. Alterazioni a questi fattori, dovute ad esempio alla costruzione di dighe per produzione idroelettrica , sono dunque destinate a introdurre perturbazioni e cambiamenti al naturale funzionamento del sistema fluviale. Questi trade-off andrebbero presi in considerazione all'interno di analisi multi-obiettivi, al fine di identificare alternative che garantiscano benefici limitando al contempo le alterazioni al sistema.

Modellizzare l'impatto delle dighe sulla connettivitá dei sedimenti richede l'adozione di una prospettiva analitica a livello di bacino fluviale, che manca nei tradizionali modelli di trasporto solido. CASCADE (CAtchment Sediment Connectivity And DElivery)(*Schmitt*, 2016) é un modello sviluppato per fare fronte a questo problema, in quanto é in grado di fornire informazioni disaggregate sulla provenienza e la destinazione di sedimenti derivanti da diverse sorgenti al fine di descrivere quantitativamente la connettivitá dei sedimenti nella rete fluviale.

Lo studio illustrato in questa tesi propone una versione rivisitata del modello CASCADE, nella quale il flusso di sedimenti forniti da ogni sorgente viene descritto come composto non da una singola classe di sedimenti, bensí da una distribuzione di differenti classe di sedimenti. Inoltre, il calcolo della capacitá di trasporto solido attribuite ad ogni classe é basato sulle equazioni empiriche di Wilcock e Crowe. Infine, all'interno di CASCADE sono stati sviluppati due differenti modelli che mirano a fornire informazioni sulla frequenza delle classi di sedimenti in differenti aree del sistema fluviale.

Questo nuovo modello é stato appicato al bacino fluviale del Vjosa, un fiume a letto grossolano che scorre nel sud dell'Albania ed é caratterizzato da ampie

porzioni di fiume con una struttura a canali intrecciati. Il Vjosa costituisce uno degli ultimi pristini sistemi fluviali in Europa, e vanta un eccezionale valore ecologico, minacciato, peró, attualmente da vari piani di sviluppo idroelettrico.

Proprio per questo motivo, e cioé per quantificare gli impatti sul trasporto solido di differenti scenari di sviluppo idroelettrico, che CASCADE é stato applicato al bacino fluviale del Vjosa. Nell'ambito di un'analisi multi-obettivi, sono stati, a questo scopo, definiti due indicatori per quantificare la produzione idroelettrica e l'alterazione alla connettivitá dei sedimenti, utili al fine di indentificare combinazioni e posizionamento ottimali di dighe. In aggiunta, data la scarsa disponibilitá di dati sul campo, é stata condotta un'analisi di sensitivitá sulla distribuzione di sedimenti delle sorgenti, sulla quale non sono disponibili dati su campo, per valutare la robustezza delle prestazioni dei vari scenari di pianificazione in funzione di questa incertezza.

I risultati dimostrano la fattiva possibilitá di identificare scenari di sviluppo che possano garantire circa il 50% della massima produzione idroelettrica possibile senza alterare drasticamente il trasporto solido o danneggiare le porzioni di fiume a canali intrecciati. Tipicamente, questi scenari, puntando sulla costruzione di dighe situate nella zona superiore del bacino idrografico o sui tributari del fiume, mostrano un'alterazione ridotta della connettivitá dei sedimenti del sistema. L'analisi di sensitivitá mette in luce come la competitivitá dei vari scenari di sviluppo, valutata tramite gli indicatori, non cambia significativamente introducendo variazioni nei dati in input al modello CASCADE, e di conseguenza non mutano neppure la forma e composizione della frontiera di Pareto nell'analisi multi-obiettivi. Di conseguenza, gli scenari di sviluppo identificati come ottimali si sono dimostrati robusti anche considerando i fattori di incertezza nella misurazione dei flussi di trasporto solido dovuti all'impiego di un modello a scala di bacino come CASCADE e alla mancanza di dati su campo.

Contents

List of Figures

List of Tables

1 Introduction

1.1 General overview

Key connectors in global geo-chemical and hydrological cycles, rivers channel water, sediment and nutrients from the sources to the sea or to continental sinks, redistributing these resources along their path. (*Milliman and Meade*, 1983). Because of this, rivers are ecological hotspots for plant and animal life, both aquatic and terrestrial.

If water is life, rivers are its arteries.

River basins are renowned as the cradles of civilization and cultural heritage. Water courses have been pivotal for the development of settlements and the growth of complex societies. Early human societies rose and flourished around rivers, and many cities that nowadays have developed into major metropolis were founded in proximity of water streams. (*James*, 2015)

Beside the immediate advantage of guaranteeing an easily available fresh water source, rivers provide a number of invaluable services and goods to human settlers. The *Millennium Ecosystem Assessment* (2005) classified these services into four broad domains, as listed in Table 1.1:

River goods are defined as river ecosystem services that are extracted or diverted from the river system to be put ot societal use. (*Brismar*, 2002). They include water extraction for agricultural, domestic and industrial uses, food provision in form of fishes or other species, wood and timber from the floodplains *Horner et al.* (2010) and aggregate sediment for construction *Kondolf* (1994).

Moreover, rivers provide an effective way of transport of goods and people,

Ecosystem Services	Components
Supporting	Nutrient cycling Soil formation Primary production from photosynthesis
Provisioning	Food Fresh water Wood and fiber Sediment for construction
Regulation	Climate regulation Flood regulation Disease regulation Riverbank Stabilization Water purification
Cultural	Aestetic Educational Recreational Spiritual

Table 1.1: *List of the ecosystem services and relative main components as reported from Millennium Ecosystem Assessment (2005)*

and a source of mechanical energy to be exploited for industry, agriculture or electric energy production.

1.1.1 Fluvial Geomorphology

The functioning, conservation and potential degradation of a fluvial ecosystem are controlled by the interactions in space and time of various components. Abiotic factors include geomorphology, climate, hydrology, and sediment transport while biotic factors comprise the impacts of all the communities living in the ecosystem, such as plant, animals and humans.

Fluvial connectivity is fundamental to guarantee the interactions between these component and therefore to provide the ecosystem services necessary for the well-being and health of the river and its inhabitant. *Ward and Stanford* (1995) described connectivity as the exchange pathways of organic and inorganic matter (i.e. water, sediments, nutrients) energy and organisms among the river network and between the river branches and the system with whom they interacts. The latter include floodplains, deltas and aquifers, that in pristine river systems are regularly resupplied with water and nutrients (*James*, 2015).

Sediment connectivity, in particular, plays a fundamental role in the process of fluvial geomorphology, ecosystem integrity, transport of nutrient and pollutant and erosion and the related risks. Processes of entraining, transporting or depositing of sediment shape the river, creating new paths for the water and

dynamic fluvial forms, and are strongly linked to the health of the river ecosystem itself and the availability of ecosystem services for human use.

In free-flowing rivers, sediments are supplied to the river from the river bed material, and from the watershed through either continuous process of weathering on the hillslopes or singular events like landslides. (*Schmitt*, 2016). Lithological, climatic and topological factor, along with the presence of vegetation and anthropic disturbances, like mines and quarries, influence the physical and chemical processes of weathering and delivery of sediment from the landscape to the river. (*Sklar et al.*, 2017).

The transport of sediment within the river is controlled by the amount of energy available for transport in a section of the river and the availability and type of sediment to be entrained and transported. In return, the sediment transport alters the type of grains in the river bed, and potentially the geomorphology of the bed.

1.1.2 Human infrastructures on fluvial systems

Over millenia, the desire to increase the benefit that the fluvial system provides to the settlers has encouraged the development of human infrastructures on the river channel. Diversions and dams were erected as early as the third millennia B.C, with traces of dams made of rock discovered on the Tigris, Euphrates and Nile. (*Jansen*, 2012).

Until the XXI century, dams were primarily used for irrigations and water supply, as well as for flood control and flood protection. With the advent of electricity, dams started to be used for hydropower generation. By 1949, about 5000 large dams had been constructed worldwide [1]. The construction of large infrastructure peaked in 1970s in Europe and North America, with an average annual number of new large dams built of some 160 to 320 per year. (*World Commission on Dams*, 2000).

As per now, around 46% of the world's major river systems have one or more dams on their branches, and this percentage is bound to increase by another 21% if the 3700 dams planned or under construction are completed. In Europe, most of the major river systems present dams or barriers in some extent, with the exception of few areas like the Balkans and Russia. (*Zarfl et al.*, 2015).

[1] The International Commission on Large Dams (ICOLD), defines a large dam as a dam with a height of 15 m or more from the foundation. If dams are between 5-15 m high and have a reservoir volume of more than 3 million m^3, they are also classified as large dams (*World Commission on Dams*, 2000)

Main benefits

The construction of dams provides a means to store and transfer water in time and space, among different users and uses in a controlled way, therefore increasing the utility for human uses. Water can be stored to be distributed for crops or domestic use in time of scarcity or high demand, and to reduce the impact of high flow events downstream the reservoir.

Furthermore, hydroelectric production guarantees a reliable source of electric energy. Nowadays, hydro-power covers 20% of the global energy production. (*Rosenberg et al.*, 1997). In 2013, up to 1.3 billion individuals still lacked access to reliable electric energy. Population growth, change of diet, increase in consumption and climate change threatens to worsen the energy crisis in the future (*International Energy Agency*, 2015).

Hydropower is seen as a valid instrument to face the global energy crisis. It is regarded as a renewable source of energy, that can reduce the emission of greenhouse gases while increasing the energy independence of countries. Moreover, unlike other renewable energy sources like solar of wind power, hydropower is able to provide an energy output flexible enough to cover the base as well as the peak energy demand. This is due to the predictability of the hydrologic cycle as well as the storage capacity of dams, that shield hydroelectric production from short-term fluctuations. (*Schmitt*, 2016).

Impacts and threats

Dams are infrastructure that deeply change the river system in which they are constructed, disrupting its equilibrium and connectivity and threatening the ecosystems and communities depending on it.

Large dams have many mostly negative impact on the river environment, that have often led to the irreversible loss of species population and unique ecosystems. (*World Commission on Dams*, 2000).

The creation of a storage dam and the inundation of the reservoir area effectively destroys any terrestrial or semi-terrestrial habitats in the area, releasing the CO_2 stored in the plant in the process. (*World Commission on Dams* (2000); *Rosenberg et al.* (1997); *Brismar* (2002)).

Local population is also forced to move from soon to be inundated areas; *World Commission on Dams* (2000) estimates the number of people directly displaced by these infrastructure to be at 40-80 million. Areas close to the newly formed dam impoundment are in danger of flooding due to increases in the reservoir water level during periods with high precipitation.

Evaporation and percolation can lead to considerable water loss, especially

in arid or semi-arid regions. (*Sivapragasam et al.*, 2009). The reservoir itself can be the source of geo-physical hazards. *Liu et al.* (2004) .

Moreover, rivers are deeply connected systems, and therefore negative repercussions can extend beyond the vicinity of the infrastructure. Dams disconnect the flux of water, altering the natural distribution and timing of water flow. To guarantee flood protection downstream the dam, the frequency and magnitude of high flow event can experience a reduction. While this may prove initially beneficial to the human communities living downstream, ecosystem such as floodplains, wetlands and deltas can experience loss in fertility, since they rely on flood events to transport nutrient and sediment, and therefore decreases in crop and fishery production.

Furthermore, water temperature and chemistry are also altered as a consequence of water storage and the altered timing of downstream flows. This could damage the river's ability to dilute pollutant and purify water near the reservoir and destroy animal populations sensible to changes in the water conditions (*World Commission on Dams*, 2000).

All these alterations may also lead to the proliferation of non-native, alien species that are more resilient and therefore can grow to occupy the now vacant ecological niches, causing additional pressure to the local fauna and flora (*World Commission on Dams* (2000); *Richter et al.* (2010); *Brismar* (2002)).

Migratory fish species can no longer access part of the river network, removing access to nesting grounds and causing local extinction, with repercussion to the entirety of the food chain (*Richter et al.*, 2010).

The construction of storage dams has major impact on the sediment connectivity, too; both upstream, downstream and within the reservoir. Since water in the inundated area moves at considerably lower velocity in comparison to the river, hydrodynamic energy drops as rivers enter the impoundment, which decreases the sediment transport capacity in the reservoir (*Kondolf*, 1997). As a result, deltas are formed upstream the reservoir, where sediment is deposited. Deltas, in turn, increases the upstream flood risk and backwater effects. Over time, the deposition of sediment on the bottom of the reservoir reduces the impoundment volume, and the ability to store and redistribute water, incrementing the costs of maintenance due to the periodic need of sediment removal and the risk of failures due to the greater static load on the infrastructure.

Water released from the dam possesses the energy to move sediment, but has little or no sediment load. As a consequence, this so-called "hungry water" (*Kondolf*, 1997) erodes the river bed, causing incision and channel degradation, increasing collapse hazard for building and infrastructures situated close to the river. At the river mouth, the lack of sediment delivery can increase coastal

degradation and shrinking of the river delta. Alterations in the magnitude and frequency of high flow events can also induce changes in the sediment size and distribution downstream the dam, damaging fish spawning grounds (*Kondolf*, 1994).

All these combined impacts can have severe consequences on the livelihood of the whole river system. *Richter et al.* (2010) conservatively estimates 472 million people living in 120 rivers in at least 70 countries were forced to emigrate due to negative effect on their livelihood caused by construction of dams, such as inundated areas, reduced food security and loss of ecosystem goods and services.

Small hydropower plants are not free from impact either. These infrastructure are usually design as so-called derivation schemes: A diversion dam is constructed on the river, that instead of creating reservoir diverts water from the river to generate energy. The water flows through the turbines and is then returned to the river.

The dam itself figures as a barrier, disturbing the natural connectivity of sediment, nutrients and organisms. Moreover, small HPPs are often built in cascades in order to maximise energy production. Downstream of the dam, before the diverted water is returned, the river is left with a smaller amount of water (residual flow). Usually, regulations are present to define the minimum value of water flow to be left on the river bed, but this is often not enough. To minimize impacts, the water regime downstream the dam, determined by the dam release, should in fact mimic as much as possible the natural flow variability, with for example a similar frequency of high flow events and seasonal variability. (*Vejnovic*, 2017).

1.2 State of the art

1.2.1 Models of sediment transport and connectivity

Sediment connectivity and delivery has been approached at multiple spatio-temporal scales, from the single grain size to continental scales. (*Walling*, 1983)

The rate and magnitude of the sediment fluxes in the network is controlled by a multitude of parameters, that are often periodic, time and space dependent, dynamic or highly variable.

Sediment entering a river channel is subject to hydro-dynamic forces generated by the water flow. If those forces exceed a certain threshold, the sediment of the channel is mobilized and transported downstream (*Schmitt*, 2016). This threshold varies with the grain size of individual grains, (*Engelund and Hansen*,

1967), the presence of other grain sizes (*Wilcock and Crowe*, 2003) or other channel mophologic parameters.

Hydrological models (e. g. SWAT) can be applied to model transport of suspended sediments, but at large scale the computational time can rise significantly (*Betrie et al.* (2011); *Ranzi et al.* (2012)).

Hydraulic models at network scale(e.g. HEC-Ras , Mike 11) require instead detailed and spatially-distributed input data to characterise the river morphology and long computational times that limits their use to small and well-studied rivers. (*Merritt et al.*, 2003).

Recent studies have adopted a graph theoretic approach to enable the analysis at large scale of environmental connectivity , including the transport of water, nutrient, fishes and sediments along the network.

One of the fist graph theory approach to sediment transport was performed by *Czuba and Foufoula-Georgiou* (2014, 2015); in their work, paths of single sediment flows were simulated for a relatively homogeneous sand-sized river network. However, the framework used did not take into account the transport of multiple grain sizes, and was not able to derive sediment mass balance fro each reach.

To cope with these issues, *Schmitt* (2016) developed CASCADE (CAtchment Sediment Connectivity And DElivery), a spatially distributed modelling framework that combines graph theory with sediment transport modelling.

CASCADE allows to quantify disaggregated information about provenance and destination of single sediment loads, by simulating how an individual transport process proceeds downstream and interact with the river reaches and other sediment loads. [2]

1.2.2 Multi-Objective analysis for dam portfolios selection

Dam impacts on the river environment is often evaluated on a small scale, in the area directly affected by the construction. River network, however, are deeply interconnected systems, and often multiple dams are present or planned in the same network. The cumulative impacts of these dam on the environment cannot be evaluated by performing risk evaluations for the single infrastructures, instead they need to be evaluated at a network scale. Sustainable river basin design therefore requires an assessment framework to support the decision making process. (*Jager et al.*, 2015).

The aim of such a framework is to provide an estimate of the cumulative impacts of a particular dam portfolio on different stakeholder and environmental

[2] For further references and a detailed description of the CASCADE framework, refer to Chapter 2

services and goods. A dam portfolio is a single development alternative, which describes a unique scenario of dams design and siting, and eventual dams removal. The dams portfolios are selected from all the possible combinations of dam siting and design possible in the network. An optimization process can be adopted to analyze the trade-offs between the benefits and impacts of different dam portfolios, in order to find the optimal ones. (*Kuby et al.* (2005); *Wild and Loucks* (2014); *Null et al.* (2014))

Commonly, dam portfolios are evaluated for energy production, flood protection, ecological alteration and water supply for agricultural, domestic or industrial uses. (*Soncini-Sessa et al.* (2007); *Castelletti and Giuliani* (2011); *Giuliani et al.* (2016)). Sediment connectivity, despite its important role in the maintenance and health of fluvial ecosystems, is rarely accounted in these analysis.

The approach to sediment impact assessment usually consists in measurement of sediment trapping and sediment starvations downstream a single reservoir using empirical formulas. Few studies have this far tried to estimate the impact of dam portfolios on the sediment connectivity on a basin scale.

The CASCADE framework can be used in order to evaluate dam impact on sediment transport on the whole river network.[3] (*Schmitt et al.* (2016, 2018)).

However, previous work on CASCADE has not analyzed the structural uncertainty in the simulated sediment transport processes, due to the complexity of the transport process itself and the sensitivity of the model to the input data.

1.3 Purpose of the study

The general objective of the thesis is to build on the previous work of *Schmitt* (2016), by creating a new version of CASCADE to improve the model's description of the sediment transport process in the network. The revised cascade framework describes the sediment from a single sediment source as composed by different grain size classes, each with its own sediment load, instead of using a single grain size, like in previous version of the model. Moreover, more reliable formulas of differential sediment transport are implemented (*Wilcock and Crowe*, 2003) to calculate for each reach the sediment transport capacity of the water flow for each grain size class.

The model is then applied to evaluate the impact of a series of planned dams on the sediment connectivity, in the context of a multi-objective decision making process for the selection of the best portfolio of dams in the case study of the Vjosa river network, in southern Albania. The results of CASCADE and

[3] Refer to Chapter 3 for details on the implementation of CASCADE for multi-objective decision-making

the assessment framework are then tested by performing a sensitivity analysis, both on the reach *grain size distributions* (hereby referred as *reach GSD*) and the robustness of the Pareto-optimal solutions.

The flow chart in figure 1.1 describes the steps taken to evaluate the performances of different dam portfolios and find the Pareto-optimal solutions. As seen in the chart, the main components in which the thesis is structured are:

- input definition;
- operation of network extraction and preprocessing, data preparation and dam implementation;
- CASCADE framework for the evaluation of the sediment fluxes;
- assessment framework for the formulation of the Multi-objective analysis of the dam portfolios.

Chapters 2 and 3 describe the methodology implemented in the thesis for all these compartment. The definition of the necessary inputs, all the operations of network extraction and preprocessing, data preparation and dam implementation are all contained in Chapter 2, together with the description in detail of the CASCADE framework and the changes brought by the new version implemented in this work. Furthermore, the Chapter describes also the the steps necessary to implement CASCADE in Matlab. In the revised CASCADE framework implemented, two different The assessment framework of the multi-objective analysis is described in Chapter 3, with the indicators used to asses the impact on the main stakeholders involved. The structure and methods applied in the sensitivity analysis are also explained.

The detailed description of the Vjosa basin case study and the design and siting of the planned dams are contained in Chapter 4, while Chapter 5 describes what are the input data and the steps necessary to apply CASCADE on the case study, including the network extraction and data preparation for the local digital elevation model and other data for the case study.

Chapters 6 and 7 present the result of the CASCADE simulation and assessment framework. The new CASCADE framework is applied to the Vjosa case study, both with and without dams presence in the network, to assess its performance (Chapter 6). In Chapter 7, we introduce the result of the ranking of the dam portfolios though a Pareto front and the results of the sensitivity analysis, both on the results of the CASCADE model and the ranking of the alternatives. Finally, discussion on the results and hypothesis on future developments are contained in Chapter 8.

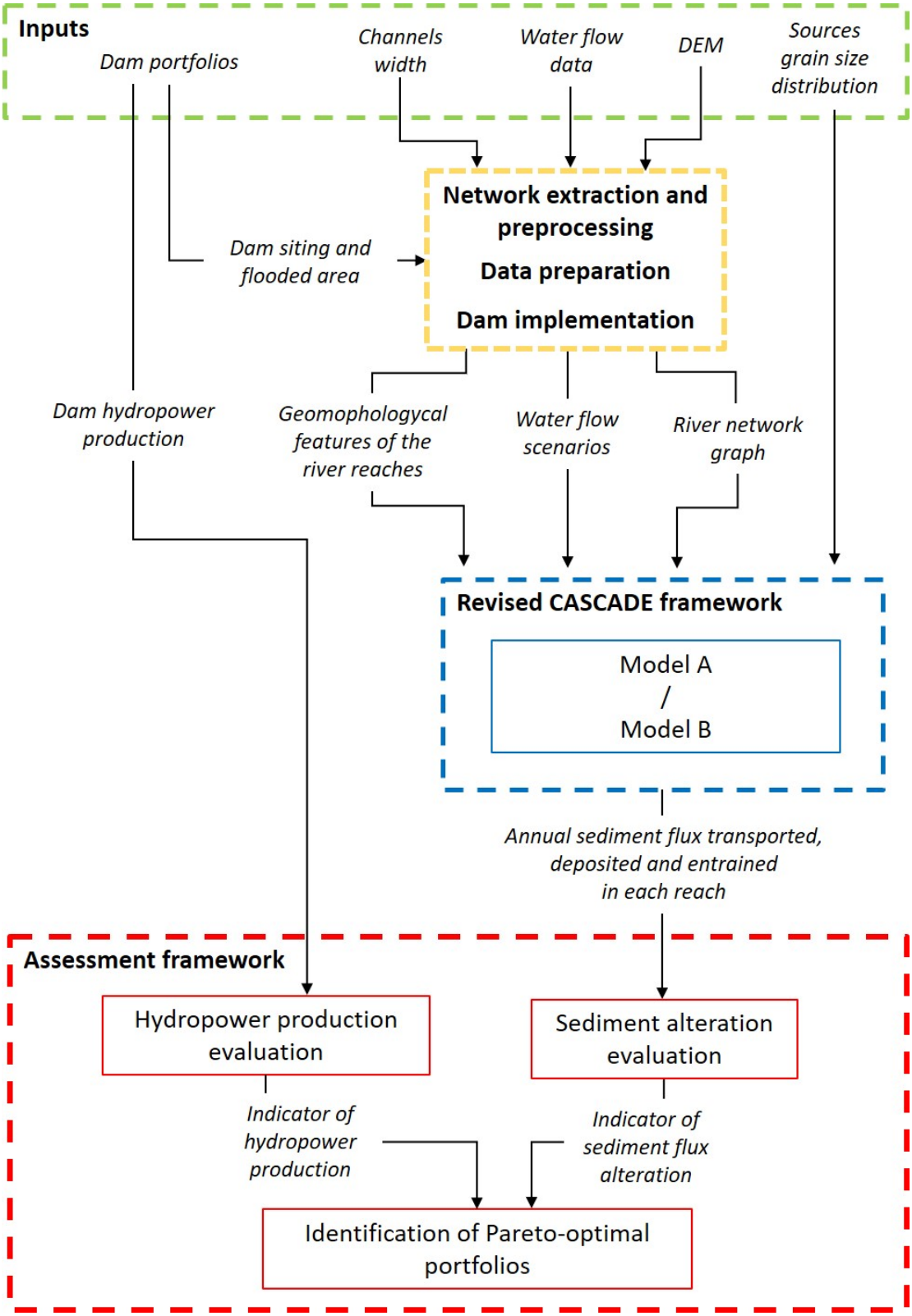

Figure 1.1: *Flow chart describing the methodology adopted in the research to find Pareto-optimal dam portfolios .*

.

2

CASCADE Model

CASCADE (CAtchment Sediment Connectivity And DElivery) is a modelling framework developed by *Schmitt* (2016). It combines graph theory and sediment transport modelling to provide analysis on the sediment connectivity at the river network scale.

In this Chapter, the key concepts and functioning of CASCADE are presented, as well as the practical implementation in MATLAB environment. Furthermore, we introduce two versions of a new CASCADE modelling framework, that aim to increase the level of detail of the model. The MATLAB scripts and functions employed are listed in table A.1 of the appendix.

Over all, this chapter covers the general definition and methodology of the compartments *input data*, *network extraction and preprocessing*, *data preparation*, *dam implementation* and *revised CASCADE framework* in the flow chart in figure 1.1.

2.1 CASCADE original modelling framework

In CASCADE, the sediment delivery is described through the combination of individual transport processes, named "cascades". Each cascade has an unique source in the river network and proceeds downstream. At its source, the cascade is attributed a value of sediment flow and a specific grain size. By proceeding thorough the reaches downstream the source, the cascade can deposit part of its sediment load, until either it depletes completely or it reach the basin outlet. The key concepts of the CASCADE approach are visually described in

Figure 2.1.

The river network of the case study (Figure 2.1 A) must be represented as a direct acyclic graph composed by nodes and edges (Figure 2.1 B). Each edge represents a river stretch, herein named *reach*, while nodes are always located at the confluences and between reaches. To each reach is attributed an unique *reach ID*, that is equal to the *node ID* of its upstream node. The length of each reach is defined by the user, who can choose to use a standard value for all edges or use a different partition to describe changes in geomorphology or fluvial form along the network. The nodes sited at the beginning of each river branches are defined as *source nodes*, and the reaches in the network that has as upstream node a source node as *source reaches*. In the graphical representation, node 1 and 4 and reaches 1 and 4 are respectively, source nodes and source reaches.

Sediment detachment in a reach is represented by a cascade, and each cascade is described by a specific grain size. Each cascade has a single and defined path toward the end node, and multiple cascades can be active in the same reach (Figure 2.1 C and Figure 2.1 D). The quantity of sediment mobilized by each cascade is determined by the reach transport capacity and the eventual presence and magnitude of other cascades in the reach. The *transport capacity* of a reach is defined as the amount of energy available in a reach for the transport of sediment. In CASCADE, the transport capacity is measured using standard sediment transport formulas that requires informations about local geomorphology and hydraulic conditions. The transport capacity vary with the sediment size; under the same local conditions, cascades with finer grain size have higher transport capacity.

If the sediment load exceed the transport capacity, the cascade deposits the exceeding load. If the grain size of a cascade cannot be entrained in a reach, the cascade is interrupted. No new sediment con be added to the load of a cascade, that therefore can only decrease in magnitude going downstream. (Figure 2.1 E) In case there are more cascade passing through a reach, less energy will be available for each cascade. This *competition* causes cascades to deposit more of their sediment load (visualized as reduced line width between Figure 2.1 E and Figure 2.1 F). The informations about sediment deposition and lifting in each reach are stored (Figure 2.1 G), and can be used to provide information about provenance, magnitude and sorting of the sediment in the reach. On a basin scale, these data could help identify dis-connectivity reaches, where most of the sediment is deposited, or area subject to high river bed erosion.

At a reach scale, CASCADE provides information about the magnitude, provenance and type of transported and deposited sediments. At a basin scale,

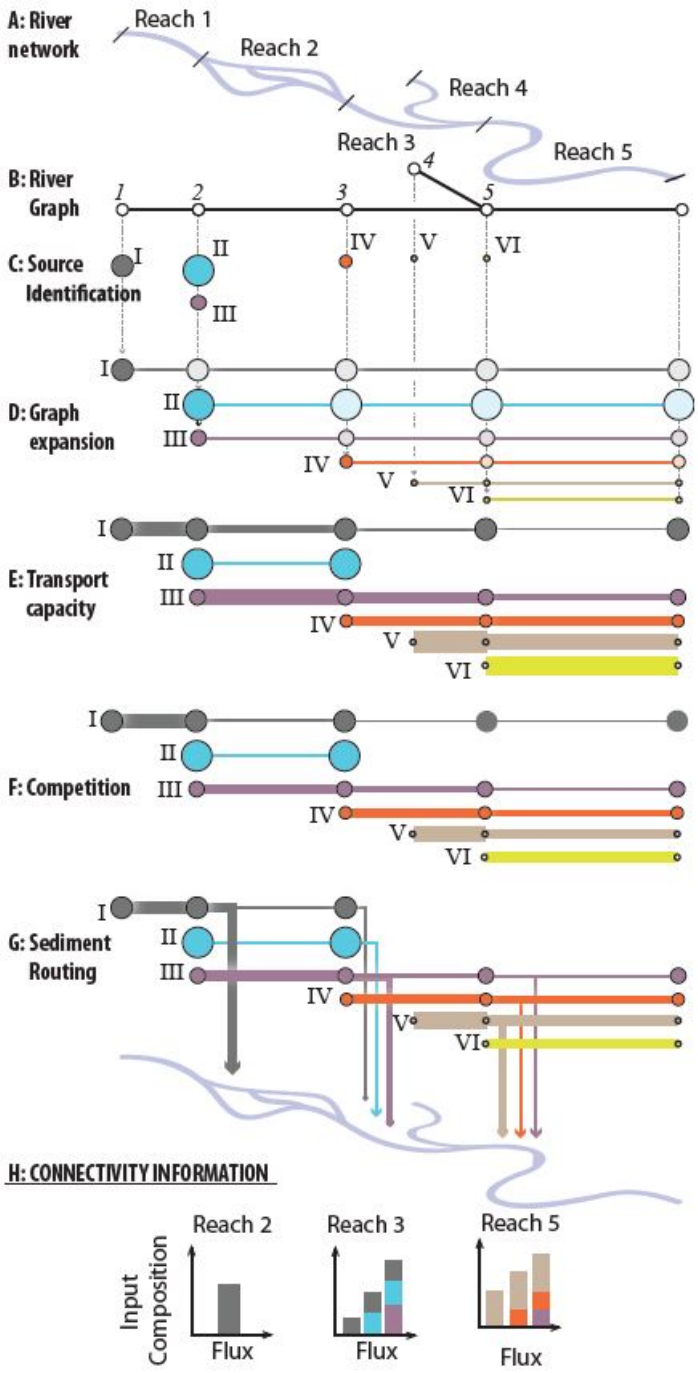

Figure 2.1: *Graphical representation of CASCADE framework. A: river network subdivision in reaches. B: graph representation of the river network by nodes and edges. C: sediment sources identification. D: graph expansion in the possible connected nodes. E: representation of the transport capacity for each grain size and for each reach, indicated by the line width. F: competition corrected transport capacity. G: routing of sediment cascades. H: informations about the sediment flux, provenance, sorting and connectivity are provided to each reach by the multiple cascades crossing it (Figure and caption adapted from Schmitt (2016)).*

the model helps to identify patterns of sediment connectivity in the network and potential bottlenecks where dis-connectivity occurs. Furthermore, CASCADE provides informations on the instantaneous sediment transport and connectivity for a specific water flow regiment, in Kg/s. Each reach is in fact attributed a single water flow value, specific to single scenario.

To gain insight on the yearly sediment transport, CASCADE have to be run multiple time for different water flow scenarios, to simulate both average water flow condition and extreme high flow events. The result are then aggregated considering the yearly frequency of the scenarios, to obtain the sediment transport in Kg/year. (see Section 2.3.5 for further informations)

2.2 Revised CASCADE framework

As seen in Figure 2.1, each reach in the network could potentially act as source for multiple cascades. However, in the previous application of CASCADE, the model associated at each source a single grain size for a unique cascade. The single sediment size associate with the reach was identified with either the use a grain size solver, which would use empirical formulas to estimate the grain size to be attributed to the cascade based on the bankfull hydraulic conditions of the reach; or by resorting to expert opinion and data samples. In this way, however, only a single cascade could be created in each reach , with a single grain size, representing an approximation of the multiple grain sizes of sediment which, in reality, can be supplied at a reach. In response to this problem, a new version of CASCADE was implemented. Each cascade is now described as composed by a number of sub-cascade, each one with its unique sediment size and load. (Figure 2.2)

The number of sediment classes considered is defined a-priori by the user and is the same for all reaches in the network; and each class is defined by an unique grain size. Sub-cascades describe the transport to one of these classes. In each reach, according to the hydraulic conditions and the presence and magnitude of other cascades, a new cascade can be activated. For each cascade, all or just a fraction of the possible sub-cascades can be present. Each sub-cascade proceeds through the river network and interacts only with the sub-cascades of the same size. Proceeding downstream, sub-cascades can lose part of their load or stop altogether. In that case, the cascade they belong will lose one of its sub-cascade. If all the sub-cascades in a cascade disappear, the cascade will stop.

In each reach, *Wilcock and Crowe* (2003) empiric formulas for the calculation of the selective transport capacity of each class were implemented (see Sec-

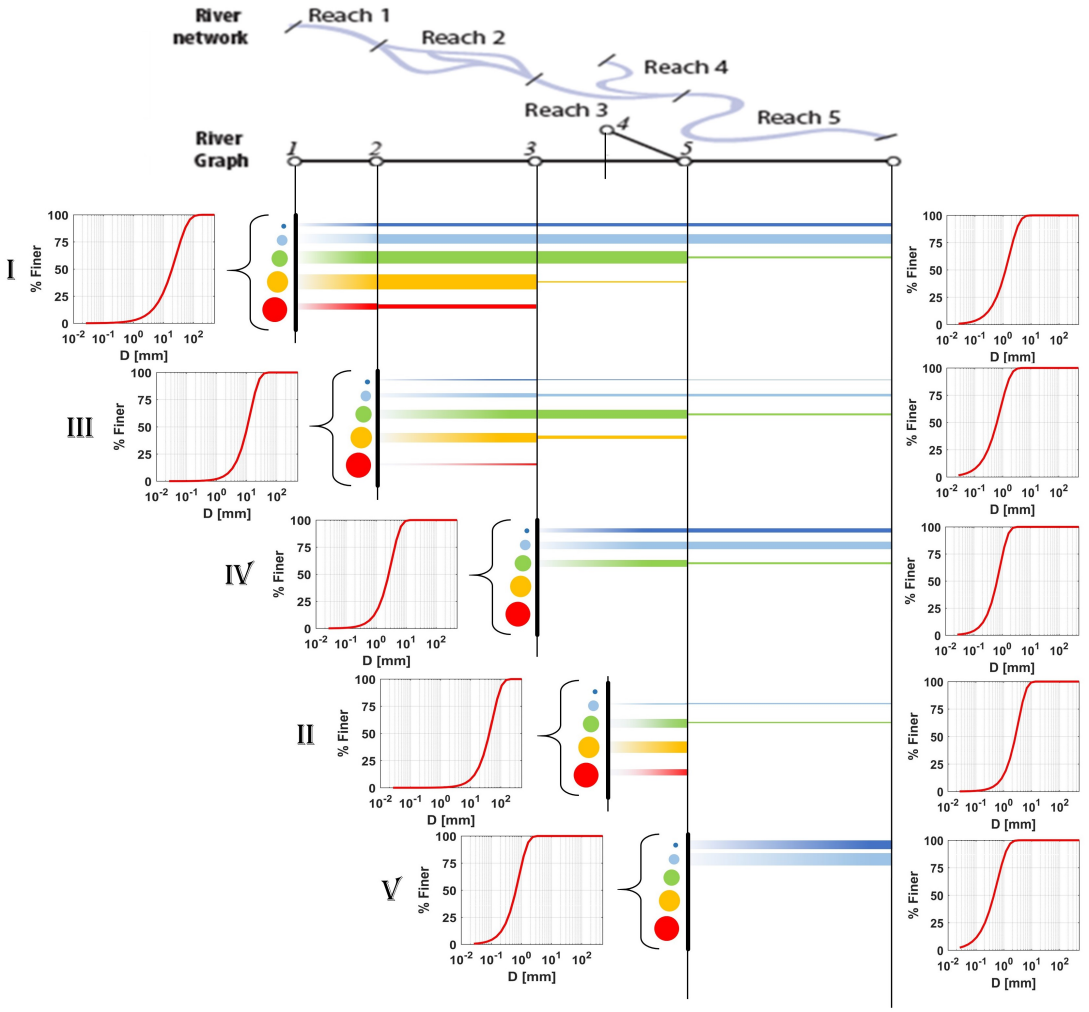

Figure 2.2: *Graphical representation of the new CASCADE framework. The cascades in each reach are now composed by sub-cascades, each with their unique sediment size. The number and grain size of grain classes are determined a priori (5 in this example). For each cascade, all, a fraction or none of the sub-cascades can be activated.*
In each reach, if the reach transport capacity for a specific sediment size exceed the incoming sediment load, no deposition occurs and a new sub-cascade is created. Instead, if the reach transport capacity for a specific sediment size is lower the incoming sediment load, no new sub-cascade is generated and the incoming cascades deposit part of their load.
The sediment distribution of the cascade can change proceeding downstream and usually exhibits a fining process, with deposition of coarse grain classes. The GSD shown on the right refers to the sediment load in its source node, while the one one the left to the load passing through the outlet .

tion 2.2.1). The original CASCADE framework defined for each reach the average D50 of the sediment supply and employed this value to measure the reach transport capacity. However, more sophisticated sediment transport formulas that use the GSDs of the reaches are well known to describe better the selective transport processes for specific grain sizes, since they consider both the characteristic of the single sediment class and its interaction with the other sediment classes on the river bed. These formulas requires as input the reach GSDs and the geomorphological and hydrological features of the reach.

For each grain class, the resulting capacity is subtracted to the sum of the incoming sediment fluxes carried by the sub-cascades. If the flux exceeds the transport capacity, the exceeding sediment load is deposited. Since the sub-cascades have all the same sediment size, the deposition processes cannot distinguish between grains of the same grain size coming from different sub-cascades, therefore the loss of sediment load due to deposition is distributed among the sub-cascades so that each sub-cascade will lose the same percentage of sediment load; thus, sub-cascade transporting higher loads will deposit more (Figure 2.3 (a)). This procedure is further explained through the numerical example in figure 2.4. If the transport capacity for the considered sediment size is more than the incoming flux, the sub-cascades passing through the reach will not suffer losses due to deposition. Moreover, the cascade generated by the reach gains a new sub-cascade, which will have sediment load equal to the remaining transport capacity. (Figure 2.3 (b))

The sediment classes mobilized by the cascade in each reach are therefore not determined a-priori, like in the original model, but during the routing, considering both the geomorphological features of the reach and the incoming sediment fluxes. Moreover, the sediment distribution of each cascade can change moving downstream, due to the selective deposition of some of its sub-cascades. All the reaches are assumed to be *non supply-limited*, meaning that the water flow can entrain a limitless quantity of sediment from the river bed of the reach in order to satisfy the remaining transport capacity, no matter the reach length or GSD. The total sediment flow leaving the reach will thus be equal to the transport capacity of the reach. The competition among cascades present in the previous version of the model, that required the definition of different scenarios to describe how sediments of different size interact with each other, is here replaced by the competitions among sub-cascades for the transport capacity of the grain class.

Modeling sediment transport with sub-cascades allows for the tracking of sediment load of a specific size, and therefore the identification of the river sources that provides the heaviest sediment load to the network of particular

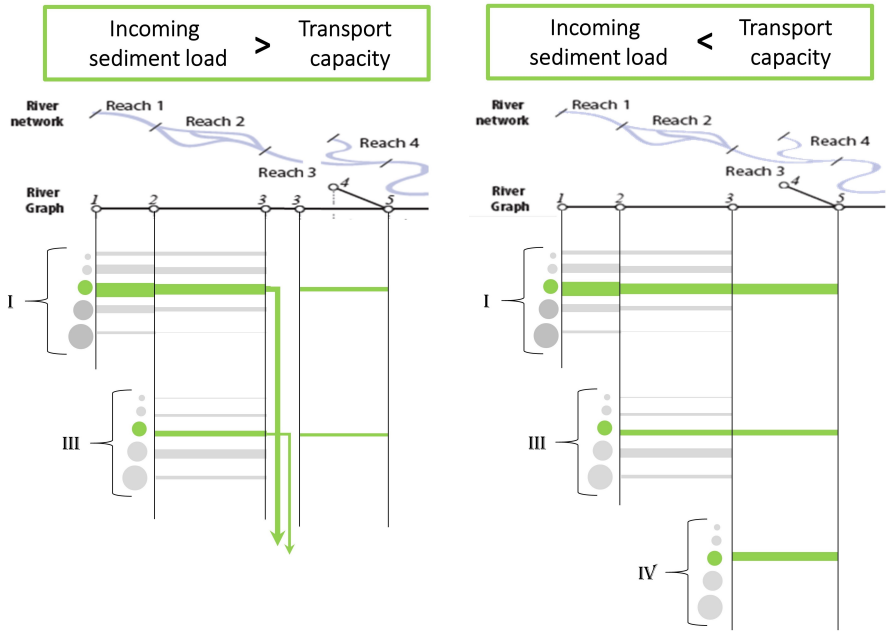

(a) *Graphical representation of the deposition process occurring if the transport capacity is lower that the incoming sediment load*

(b) *Graphical representation of the entraining process occurring if the transport capacity exceed that the incoming sediment load*

Figure 2.3: *Graphical representation of the entraining and deposition processes in the revised CASCADE framework.*

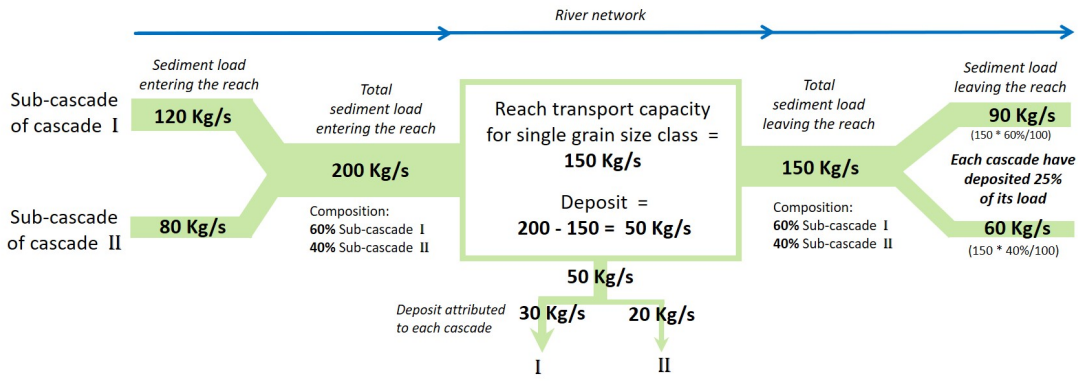

Figure 2.4: *Numerical example describing the methodology used to attribute deposition to sub-cascade transporting the same grain class entering a reach with transport capacity for that grain class lower than the total sediment load entering the reach.*

grain classes.

2.2.1 Transport capacity calculations

The transport capacity for each reach is modelled using the Wilcock and Crowe equations for sand/gravel bed river. Unlike previous mixed-size transport models which use average substrate grains size to derive sediment transport, these formulas make use of the surface grain distribution of the analyzed reach (hereby called *reach GSD*)and are therefore more accurate, since the grain availability for transport depends on the surface sorting, which is typically coarser than the substrate and subject to mechanism of vertical sorting and prior flow transport rate. (*Wilcock and Crowe*, 2003)

The formula incorporates a hiding function, that consider the nonlinear effect of sand content on gravel transport rate. Gravel on sand surfaces will experience increased mobility. On the other hand, the mobility of sand in gravel bed river is in fact dampened by the presence of pockets between the larger grains that shields the sand from the current The hiding function have an equalizing effect on the different sediment transport rates: it reduces the mobility of smaller sediment and increases the mobility of coarser sediment (*Wilcock and Crowe*, 2003). These formulas require as input the reach GSD, that therefore must be defined for each reach.

The sediment flow Q_{bi} for sediment class i, in Kg/s, is calculates as:

$$Q_{bi} = \frac{F_i W_i^* (\tau/\rho)^{1.5}}{(s-1)g} \rho_s W_{ac} \tag{2.1}$$

Where:

- F_i : proportion of size i on the bed surface, from the sediment distribution;
- W_i^* : dimensionless transport rate of size fraction i; (Eq 2.2)
- τ : bed shear stress; (Eq 2.5)
- ρ and ρ_r : respectively, the water and sediment density, set to 1000 kg/m^2 and 2650 kg/m^2;
- s : ratio of sediment to water density. $(s-1)$ is set equal to 1.65;
- g : gravity constant;
- W_{ac} : Active channel width of the reach [m].

The transport rate W_i^* is derived by the equation:

$$W_i^* = 11.2 \left(1 - \frac{0.853}{\phi^{0.5}}\right)^{4.5} \tag{2.2}$$

with $\phi = \tau/\tau_{ri}$, where τ_{ri} is the reference shear stress of size fraction i, calculated as:

$$\tau_{ri} = \tau_{rs50} \left(\frac{D_i}{D_{s50}} \right)^{\gamma} \tag{2.3}$$

D_i and D_{s50} are respectively the sediment size of the size fraction i and the median sediment size of the surface bed distribution. For gravel-bed river with presence of sand such as the case study in analysis, the hiding factor γ is set equal to 0.005.
The shear stress formula for the median grain size τ_{rs50} obtained by *Mueller et al.* (2005):

$$\tau_{rs50} = (0.021 + 2.18S)(1650 * g * D_{s50}) \tag{2.4}$$

where S is the channel slope.
the bed shear stress τ is measured though the equation:

$$\tau = \left(\rho g \left(\frac{nQ}{W_{ac}} \right)^{0.6} S^{0.7} \right) \tag{2.5}$$

With n Manning's coefficient of the reach and Q the water flow related to the specific hydraulic conditions in analysis.

Implementing Wilcock and Crowe equations allows CASCADE to consider how different grain size classes interacts with each other according to their frequency, thanks to the hiding function and the gamma parameter.

2.2.2 Grain size distribution calculations

A critical step in CASCADE consists in finding the appropriate grain size distribution to be attributed for each source. This parameter depends on the type of sediment present in the river bed and banks. Ideally, local measurement of sediment size should be performed in each reach. When this is not possible, other methods must be applied in the model to provide this information.

In this study, we implement two different methods to provide these data and we applied them both to the case study, comparing the their performances and limits.

Both method requires as input data the reach GSD of the *source reaches*. These data will greatly impact the calculations of the GSDs of all the other reaches, and therefore the model results. Moreover, the sediment load transported calculated with the transport capacity formulas defines also the sediment contribution for the hillslopes of the drainage area of the source reaches. For all these

reason, we have included a sensitivity analysis on the model results robustness with changes in the source reaches GSDs in this work.

If field data of bed surface GSD are available, they can be used to validate the model results and therefore to choose which of the two modeling approaches is more effective.

Model A : GSDs from incoming cascades

The first model, hereby called *Model A*, uses the informations carried by the cascades passing through the reach to derive the GSDs. The sediment distribution is derived by calculating, for each sediment class, the total load carried by the relative sub-cascades and then dividing it for the total sediment load arriving in the reach.

$$F_i = \frac{\sum_{n_i=1}^{N_i} Q_{bi}^{(n_i)}}{\sum_{i=1}^{I} \sum_{n_i=1}^{N_i} Q_{bi}^{(n_i)}} \tag{2.6}$$

Where:

- N_i : total number of sub-cascades entering the reach for sediment class i;
- I : total number of sediment classes;
- $Q_{bi}^{(n_i)}$: sediment load carried by the sub-cascade n_i with sediment size belonging to class i.

This model, therefore, assumes that the informations carried by the incoming cascades can give insight on the GSD of the analyzed reach, presuming a continuity regarding the type of grain size present in the bed of the river.

Employing *Model A* in river networks with sediment bottleneck or areas with sudden discontinuity in the GSD and other geomorphic features is likely to give poor results. The presence of sections in the network where huge deposition of sediment occurs causes the GSDs of the reach downstream to be calculated using only the sub-cascades that are able to pass the bottleneck, that are likely to be characterized by fine sediment only. While this is a reasonable results, it also causes the GSDs of all the new cascades created after the bottleneck to have sediment distribution with fine sediment only. This *bottleneck effect* is especially troubling in case of reservoirs and barriers along the river, that act like element of dis-connectivity of the sediment transport in the network.

Model B : GSDs from transport capacity

Model B employ the hypothesis used by *Ferguson et al.* (2015) for the implementation of a sediment transport model on the Fraser river system, a cobble-gravel bed river in British Columbia. Assuming the river to be in an equilibrium state, the bed load transport capacity at each reach is hypothesized equal to the total sediment supply of the incoming cascades. Based on this assumption, the reach GSDs are found using a reach-by-reach optimization of a probability distribution function with adjustable parameters. The optimization process explores possible combinations of the parameters of the reach GSD function to find the one that guarantees that the transport capacity, calculated using the reach GSD and the formulas in chapter 2.2.1, matches the incoming sediment flow transported by the cascades.

The function used is the Rosin distribution, that fits river bed and bed load GSDs. (*Shih and Komar*, 1990).

$$F(\leq D) = 1 - \exp[-(D/k)^s] \tag{2.7}$$

The Rosin distribution is a 2-parameters cumulative distribution function, where k is the mode of the GSD and s is an inverse measure of spread. In each reach, both k and s are optimized to find the best fitting GSD.

Since all the reaches are non supply limited, the total sediment supply entering and leaving the reach will remain the same. The hypothesis, necessary for equilibrium, that in each reach the transport capacity for individual grain size class is equal to the incoming sediment load does not correspond necessarily to sediment immobility. In fact, single grain classes can be deposited or entrained, since the transport capacity can change. Overall, the deposition of some grain classes is always completely compensated by the entraining of others, and therefore the total sediment flow remains constant.

In Model B, the confluences are the only location in the network where the sediment transport can increase. The initial transport capacity, that will remain constant until the first confluence, is calculated using the sediment distribution of the *source reaches* and the formulas in Section 2.2.1. No other types of sediment contributions are considered. Thus, obtaining a good estimate of the sediment distribution of the source reaches is even more pivotal, since these data influence the transport capacity of the whole branch of the river network.

While model A reports for each reach a single value of GSD, given by the incoming sediment load, model B has two: the reach GSDs, obtained by calibration and referring to the sediment distribution in the river bed of the reach, and the cascade GSDs, that is the frequency of each grain class in the sediment

load mobilized and transported through the reach by the cascades.

2.3 MATLAB implementation

The two version of the new CASCADE framework described in section 2.2 are implemented in MATLAB environment. The following section describes the input data required (section 2.3.1), the preprocessing (section 2.3.2) and the actual implementation of the two models. Section 2.4 describes the steps to take to implement reservoirs in CASCADE.

Both version were applied in the case study described in chapter 4, the Vjosa basin in south Albania. The implementation of dams in the model described in section 2.4 was used in the case study to provide a framework on which to establish the effect of the construction of hydropower stations with reservoir on the sediment connectivity of the basin and set up indicators for a multi objective analysis, as described in chapter 3.

Sections 2.3.1, 2.3.2 and 2.3.3 refer to the CASCADE routing for a single water flow regiment; the sediment fluxes are represented in Kg/s. Section 2.3.5 describes the steps necessary to obtain values of annual sediment flow in Kg/year.

The functions and script employed are listed in Table A.1 of the appendix.

2.3.1 Input data

Both Model A and Model B requires the same basic input data. The main input are the bed sediment distribution for the source reaches and the graph representation of the river network, containing the morphological and hydrological features each reach. For convention, we assume N to be the number of reaches in the network and K the number of sediment classes considered.

River network

The model CASCADE represent the sediment transport in a river network represented as an direct acyclic graph composed by nodes and reaches (Figure 2.1 B). The graph is implemented in MATLAB through the matrix *Aggdata*, which is a $Nx16$, in which every row refers to a reach in the graph, while each column represents a field containing a different information about the network.

These fields are listed in the table below.

1. Reach identification code;
2. Identification code of the upstream node ("*From Node*"), equal to the reach ID;

3. Identification code of the downstream node. ("*To Node*");
4. Mean slope of the channel [m/m];
5. Active channel width of the reach [m];
6. Water flow of the reach for the chosen water flow scenario [m^3/s];
7. Manning's n of the reach;
8. Reach length [Km];
9. East coordinate of upstream node [m];
10. East coordinate of downstream node [m];
11. North coordinate of upstream node [m];
12. North coordinate of downstream node [m];
13. Average water flow [m^3/s], needed for the implementation of reservoirs in the basin;
14. Upstream node elevation [m];
15. Downstream node elevation [m];
16. Drainage area [Km^2].

The method of extraction of the Matrix *AggData* for the case study of the Vjosa river system is described in section 5.2.

Source reaches GSDs

The input data for the source node are the vector *psi* and the matrix *Fi_Sn*.

Vector *psi* of length K contains all the average values of sediment size in the Krumbein (ϕ) scale for each sediment class, and therefore describing the number and amplitude of the sediment classes implemented in CASCADE. The Krumbein (ϕ) scale is a logarithmic scale for listing grain sizes computed by the equation:

$$\phi = -\log_2 D/D_0 \tag{2.8}$$

where D is the diameter of the sediment [mm] and D_0 is a reference diameter, equal to 1 mm (*Krumbein and Aberdeen*, 1937).

Matrix *Fi_Sn* contains the frequency in the river bed of the sediment classes described in *psi*, for each source node. The first column in *Fi_Sn* reports the reach ID or the sources as reported in *AggData*, the other K columns list the frequency for each class. The frequency will be used in the Wilcock and Crowe equations to derive the transport capacity of the source reaches, that in turn will influence the GSDs calculations for all the downstream reaches

2.3.2 Preprocessing

This section contains all the operation of preprocessing that are required before running the CASCADE main function in MATLAB environment. All the operations described are contained in the main script `CASCADE_script`.

Graph Preprocessing

The section `graph preprocessing` in the main script `CASCADE_script` contains the operation of graph preprocessing. The network's informations contained in matrix *AggData* are processed in order to derive topological informations, stored in the struct *Network*, with the following fields:

1. matrices *downstream path* and *distance*, containing, for each reach, the IDs of the stretches composing the path downstream to the outlet node and the distance between the reach itself and each stretch;
2. matrices *upstream path* and *distance*, containing, for each reach, the IDs of the stretches composing the path upstream to the farthest source node and the distance between the reach itself and the each stretch;
3. matrix *II*, which contains, in each cell (*i,j*), the topological distance proceeding downstream from reach *i* to reach *j*, or *NaN* if it do not exists;
4. vector *NH*, which contains the node hierarchy, which lists the river reaches by the number of upstream nodes up to the farthest source.

Slope correction

The extraction of the river network is usually conducted employing a *Digital Elevation Model* (DEM) of the case study area, which could be subject to errors in the measurement of the elevation or could be affected by poor ground and elevation resolution. The resulting river network could therefore show errors in the values of elevation of the nodes, with repercussion on the measurement of the channel slope, especially for short reaches, where the elevation of the *From Node* and *To Node* is similar due to their proximity. To correct these potential errors and avoid erroneous calculation of the transport capacity, the function `slope_smoothing` was developed.

This function smooths the slope of a reach by performing a weighted average between the original channel slope and the slope or the neighboring reaches. The weight of the original slope increases according the reach length. For reaches longer than 10 Km, the weight is equal to 1 and the slope remains unaffected In case the reach is situated before a confluence or it is a source, only the reach directly upstream or downstream is used.

2.3.3 CASCADE routing

The computation of the sediment routing and the sediment transport and deposition of each sub-cascade are performed by the functions `CASCADE_model_A` and `CASCADE_model_B`. The differences in the two functions are limited to the method of measurement of the reach GSD, while inputs, outputs and routing process remain the same.

The functions process the network reach-by-reach, according to their hierarchy; source reaches are processed first, while the outlet reach is the last. In this way, the model assures that all the precesses in the upstream reaches have been measured before processing a reach. (that is why, in the CASCADE representation in Figure 2.2, the cascade form reach 4 is the second to be calculated (and is therefore identified with **II**).

If the node is a source node, the model calculates the transport capacity of the reach for each sediment class using the formulas in Section 2.2.1 and the input data in matrices *AggData* and *Fi _Sn*. A new cascade is activated, with sub-cascades with sediment fluxes equal to the transport capacity of each class.

If not, the model receives the informations on the incoming cascades and proceeds to use one of the two models to obtain the GSD of the reach. The transport capacity is then calculated; for each sediment class, depending on whether the sediment supply from the sub-cascades exceeds or not than the available energy, the cascades deposit part of their load according to their magnitude or a new sub-cascade is created in the reach.

In model A, in the rare case that no incoming cascades are present, the GSD is derived proceeding upstream until the first available cascades in the closest reach possible is found.

In model B, a genetic algorithm is used to perform an optimization on the parameters k and s of the GSD, to find the sediment distribution function that most closely matches the incoming total sediment load. The model also contains an error correction tool: if the difference between the transport capacity fro the optimized GSD and the incoming total sediment load is more than 0.01, it guarantees that erroneous values of transport capacity are not propagated downstream. K ranges from the 10th to the 90th percentiles of the size of the sediment classes, while s ranges between 0.8 and 1.5 [1].

[1] *Shih and Komar* (1990) found that best fit values of s for the bed surface, subsurface, and high-flow bed load for grave-bed rivers were in this range.

2.3.4 Model outputs

Most of the outputs of the functions `CASCADE_model` are the same, Model B however returns additional outputs describing the performance and results of the optimization process .

F_i^R is a NxK matrix (where N is the number of reaches and K the number of sediment classes) in which every row, that corresponds to a reach, contains the sediment distribution obtained by the GSD calculus.

$Q_{bi}^{(tr)}$ and $Q_{bi}^{(dep)}$ are 3-dimensional matrices $NxNxK$ which contain informations about respectively the sediment load and the amount of sediment deposited of the sub-cascade passing thought each reach.

The rows are referred to cascade sources, while the columns are reaches crossed by cascades. A generic vector with S-elements a_{ij} located in the i^{th} row and j^{th} column of the matrices contains the sediment load that the s sub-cascades originated by the reach with ID equal to i carry while crossing the reach with ID j, or the sediment deposited by the sub-cascades in said reach.

$Q_B^{(tr)}$ and $Q_B^{(dep)}$ are NxN matrices that are structured like $Q_{bi}^{(tr)}$ and $Q_{bi}^{(dep)}$, with the difference that each element a_{ij} in the matrices contains the total sediment transported and deposited in the j^{th} reach by the cascade originated in reach i, data obtained by simply aggregating the sediment load and deposition of the sub-cascades composing it.

In all the matrices described above, the elements in the i^{th} row refers to the cascade originated from reach i. In the same way, elements in column j^{th} refers to the cascades and sub-cascades crossing reach j.

If a reach j is not topologically connected to a cascade source i, the element a_{ij} is set to NaN.

The initial sediment load of the cascade i in its source, stored in the diagonal of matrix $Q_B^{(tr)}$, provide informations on the instantaneous sediment load lifted from each reach, and therefore on the erosion of the river bed in the reach.

Lastly, Model B supply also the $Nx2$ matrix par, which contains the parameters k and s of the Rosin sediment distribution obtained by the optimization for each reach.

2.3.5 Annual sediment transport calculation

As previously mentioned, CASCADE simulates instantaneous sediment flow on a single water flow scenario. In order to gain insight on the annual sediment transport regime, and therefore the actual load of sediment lifted and deposited in each reach, CASCADE needs to be run multiple times with different water

flow values, describing all the possible hydrological scenarios.

Therefore, the model requires informations about the daily water discharge in each reach, in order to derive the hydrograph of the river stretch.

To compress hydrological informations and save computational time, only a limited number of scenarios are used. Each hydrograph is dissected into p discharge classes, with a different annual frequency $n_e(p)$, indicating the number of day per year in which the water flow falls in the class. The mean values of classes and the relative frequency can thus provide a good representations of the whole hydrograph of the reach, provided that the classes are in sufficient numbers and covers also rare but high-magnitude events.

Once CASCADE has been run for each mean value of the discharge classes, the data on instantaneous sediment flow are converted in annual sediment flow for the discharge class using the annual frequency of the class, and then added together to obtain the total annual sediment flow.

For example, the information stored in matrix $Q_B^{(tr)}$ and $Q_{bi}^{(tr)}$ are joined by the formula:

$$Q_B^{(tr,ann)} = \sum_{p=1}^{P} Q_B^{(tr)}(p) * n_e(p) \tag{2.9}$$

and

$$Q_{bi}^{(tr,ann)} = \sum_{p=1}^{P} Q_{bi}^{(tr)}(p) * n_e(p) \tag{2.10}$$

The annual sediment eroded in each reach is indicated by the initial sediment flow of the cascade generated in each reach, stored in the diagonal of matrix $Q_B^{(tr,ann)}$:

$$Q_B^{(erod,ann)} = diag(Q_B^{(tr,ann)}). \tag{2.11}$$

The annual sediment deposited in each reach, instead, is obtained by aggregating the information on the sediment deposit stored in matrix $Q_B^{(dep)}$ and then summing up column-wise, to add together the sediment loads deposited by all the cascades passing through each reach:

$$Q_B^{(dep,ann)} = \sum_{j=1}^{N} \left(\sum_{p=1}^{P} Q_B^{(dep)}(p) * n_e(p) \right) \tag{2.12}$$

where N is the number of reaches in the network and j is ID of the source node of the cascade.

Both $Q_B^{(dep,ann)}$ and $Q_B^{(dep,ann)}$ are $Nx1$ vectors, containing the annual sediment load deposited and eroded for each reach.

Since in both Model A and B the cascade GSDs of the reaches will be different for each CASCADE run, the annual average frequency for each class $F_i^{R(year)}$, corresponding to the cumulate grain size distribution of the sediment load carried by the cascades thought a reach, is obtained by dividing the annual sediment flow carried by all the sub-cascades passing through the reach by the total annual sediment load carried by the cascades along all the spectrum of sediment classes considered.

For model B, the reach GSD is obtained by performing an average of the F_i^R for each percentile, weighted by the fraction of the total annual sediment load that is transported in the water flow scenario. The results are stored in matrix $F_i^{R,year}$.

In this way, the final values of reach GSDs will be more influenced by simulations in water flow regiment that contribute more to the annual sediment transport process.

The operations to obtain the annual sediment transport and the relative GSDs for both Model A and B are contained in the sections `Annual cascade routing - Model A` and `Annual cascade routing - Model B` in the main script `CASCADE_script`.

2.4 Implementations of reservoirs in CASCADE

A stated in Section 1.2.2, the common approach to impact assessment of the construction of a barrier or a reservoir on the sediment routing consists in measurement of sediment trapping and sediment starvation downstream the reservoir using empirical formulas. CASCADE, instead, can be programmed to consider the effect of the presence of a reservoir on the cascades routing and to measure the transport capacity in different compartment of the reservoir.

In the model framework, the compartments are identified as the reaches submerged by the reservoir impoundment. (see Figure 2.5)

For each compartment, the flow depth and width are needed. Both variables can be provided by using the Digital Elevation Model (DEM) of the case study area and the Fully Supply Level (FSL) of the dam, that is the elevation of the water table at the dam when the reservoir is at full capacity. (Figure 2.5 A).

The model introduces simplification in the shape of the component to ease the calculations (Figure 2.5 B), as reported in Section 2.4.1.

CASCADE recalculates the channel slope of the inundated reach, and sub-

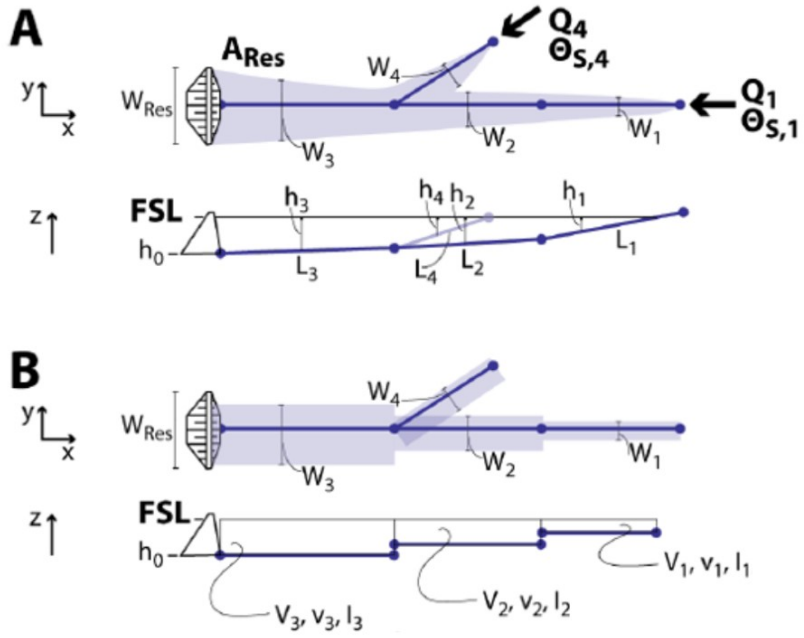

Figure 2.5: *Reservoir routing in CASCADE. A: example of a plan-view and cross-sectional parameters of the inundated reaches by a dam construction. B: subdivision of the reservoir in compartments, as operated by CASCADE, and the relative variables. (Figure and caption adapted from Schmitt (2016))*

.

stitute it with the active water slope of the reservoir's component, typically smaller. The slope is then used to calculate the new value of transport capacity, using the Wilcock-Crowe equations reported in Section 2.2.1. (*Wilcock and Crowe*, 2003).

In case Model B is used, the sediment distribution is not recalibrated, but is kept equal to the value obtained in the optimization for the undisturbed state, contained in matrix $F_i^{R,year}$. This is due tot he fact that we are evaluating the alteration that the implementation af a dam portfolios will have on the features of the pristine river. If a calibration was to be performed on the inundated reaches, the new value of slope would be often too low to allow the optimization tool to find suitable parameters of the GSD that fit the upcoming sediment supply.

In CASCADE, all dams are supposed to have a bottom outlet, therefore every sub-cascade that manage to reach the dam without being deposited in the impoundment can be routed downstream. Otherwise, the dam will stop all sediment to be transported downstream.

Typically, the flooded area of the dams is divided in *compartment*, along the direction of the river, and to each compartment is attributed a simple geometrical shape to aid the calculations. The energy slope of the compartment k is

calculated as:

$$I_k = \frac{v_k^2}{2g} \tag{2.13}$$

Where:

- L_k : inundated length of the reach, equal to the reach length if the stretch is fully submerged;
- v_k : average flow velocity in the compartment:

$$v_k = L_k \frac{V_k^2}{Q_k} \tag{2.14}$$

- V_k : compartment volume [m^2];
- Q_k : average water inflow [m^3/s];
- $\frac{V_k^2}{Q_k}$: residence time in the compartment [s];

2.4.1 Reservoir routing in MATLAB

The following section reports the steps taken to integrate in MATLAB a component for recalculating the slope in the inundated reaches.

The implementation of the sediment routing in MATLAB is conducted by the function `dam_slope_correction`, called in the section `dam_correction` of the main script.

In case Model B is used, a new CASCADE function is implemented, named `CASCADE_model_B_optimized`, lacking the optimization tool and with the additional input of the matrix $F_i^{R(year)}$ containing the calibrated GSDs for the reaches, obtained from a previous run of `CASCADE_model_B` without reservoirs.

The input of the function `dam_slope_correction` are:

- *AggData* : matrix describing the river network, described in section 2.3.1
- *Network* : struct containing topological informations of the network, obtained in section 2.3.2
- *DamDatabase*: struct reporting informations on the position and the size of the dams and the reservoirs in the river network

DamDatabase contains the following fields:

- *id_FN* : ID of the node in the river network closest to the dam location;
- height : height of the water surface at with reservoir at full supply, from the base of the dam [m];

- Name : cell array reporting the name of the dams;
- portfolio : vector containing '1' if the dam is present, '0' if absent;
- calcResArea : vector reporting the superficial area of the reservoir [m^2].

As highlighted by the list above, in order to represent in a meaningful way the reservoir in the network, a node must be located as near as possible to the dam location. To do so, the river network can be partitioned using the dam locations as breaking points, as in the case of the Vjosa river case study (see section 5.2.1).

Moreover, the height is kept constant, meaning that the reservoirs are assumed always at maximum capacity. This hypothesis is reasonable for reservoirs build for hydropower production, like the one in the Vjosa case study.

The FSL (Full Supply Level) is obtained by summing the elevation of the node where the dam is sited with the dam height.

The function finds for each dam the IDs and inundated length of the reaches in the reservoir impoundment, using the elevation of the nodes reported in *AggData* and the FSL.

It calculates then the maximum width of the reservoir (considered to be near the dam), assuming an impoundment of triangular shape, employing the data on the impoundment area stored in *calcResArea* and the total inundated length.

The mean width of the components is derived by performing a regression with the maximum width calculated above and the average distance of the component to the dam. The surface area of each edge is calculated considering each component to have a rectangular surface.

The mean water level at FSL in each inundated reach is obtained performing an average between the water levels of the nodes delimiting the component, acquired by performing a difference between the FSL and the node elevation.

The water volume is calculated assuming the component to be shaped as a parallelepiped with constant depth, equal to the mean water level.

Finally, the active slope in each inundated reach is measured using the Equation 2.13 and Equation 2.14 and substituted to the reach channel slope in *AggData*.

The function returns a new matrix *AggData*, with the corrected slopes for the dams reported as present by the vector *DamDatabase.portfolio*.

To obtain the annual sediment fluxes with reservoirs, the methodology described in Section 2.3.5 is implemented, with CASCADE runs for each water flow scenario with slope corrected to account for the dam implementation. For Model B, the optimized model `CASCADE_model_B_optimized` is used.

2.5 Sensitivity analysis on reaches GSDs

Both Model A and B procedure to identify the bed GSDs of the reaches, described in Section 2.2.2, is extremely dependent to the GSDs of the source nodes, that provide both an estimate of the sediment supply from the different river branches and the sediment supply form the hillslopes. Thus, in this work, a sensitivity analysis is performed to evaluate the range of uncertainty of the resulting reach GSDs, obtained from CASCADE simulations with the methodology described in Section 2.3.5, with variation of source reach GSDs.

A single simulation for the sensitivity analysis requires as input a data sample containing the GSDs of the source nodes, to be stored in the input matrix *Fi_Sn*.

These data samples must be derived form a *sn*-dimensional space containing all the possible combination of source D50 given by the D50 range, where *sn* is the number of source nodes in the network. In order to generate random, low-discrepancy data samples that allows to effectively describe the sample space, the MOEA framework was used to perform a Sobol sampling of the sample space (*Hadka*, 2015).

The sample size needed for performing a reliable Sobol sensitivity analysis depends on two main factors, such as the complexity of the model and the number of parameters evaluated. While no general consensus has been achieved on the optimal number of generated sets, the general rule of thumb is that the larger numbers of model parameters, the higher the number of parameter sets to be used. However, it should be noted though that increasing the number of evaluations comes with an increases also in the computational cost. The appropriateness of the number of evaluations selected can be tested using the bootstrap confidence intervals. Generally speaking, the most sensitive parameters should have narrow confidence intervals, which are less than 10% of the sensitivity indices.

The operations to conduct the sensitivity analysis of the GSD in MATLAB are contained in the script `Script_sensitivity_GSD`.

3

Assessment framework

As introduced in Section 1.2.2, multi-objective assessment frameworks are developed on river systems to evaluate the impacts of the implementation of different *alternatives* on a number of stakeholders or environmental goods or services at a basin scale, and provide the decision makers with tools to quantify the trade-offs between the considered objectives, and to select the alternative that they deem preferable.

In this Chapter, we explore the definitions of the assessment framework we used for the multi-objective analysis on the dams portfolios on the case study. In the case in analysis, an alternatives is defined as a single dams portfolio. As reported in the flow chart in figure 1.1, the main objective of the framework is to identify the optimal (*non-dominated*) dam portfolios, defined as the portfolios for which there are no other alternatives that performs better for all the analyzed objectives. These portfolios compose the Pareto front of the multi-objective analysis, and are thus hereby referred also as *Pareto-optimal* portfolios.

Two indicators were defined to evaluate the performance of the portfolios in two different objectives, the hydropower production and the alteration in the sediment transport processes. The latter is measured using the outputs of the annual CASCADE simulation. Each portfolio option correspond to a decision variable vector $[\mathbf{u}]$, composed by boolean decision variables: each decision variable, therefore, assumes value 1 if the dam is selected in the portfolio, and 0 otherwise. The assessment framework aims to identify the portfolios that minimize the indicators:

$$\min_{u}(L^{hpp}, L^{sed}) \tag{3.1}$$

where L^{hpp} is the hydropower production indicator, and L^{sed} is the sediment alteration indicator.

3.1 Indicators

Given the high degree of uncertainty surrounding the case study, we choose to limit the number of indicators and to consider two objective in clear competition. The two objective analyzed, as mentioned before, are the hydropower production and the sediment alteration, the latter evaluated using the CASCADE model.

3.1.1 Hydropower indicator

As stated in Section 1.1.2, dam construction and management can provide a number of benefits to the stakeholders involved in the construction and the people living in the affected area, among which flood control, water for agriculture and hydropower production. The purpose of the dams planned on the Vjosa case study, however, is mainly the hydropower production.

The annual hydropower production for each dam, expressed in GWh/year, is provided by *Sogreah Consultant* (2009). Since the definition of the indicator requires a single value for each dam portfolio, the annual hydropower productions of the dams selected in the portfolio is added together:

$$L^{hpp} = -\sum_{d=1}^{D} G_d * u_d \tag{3.2}$$

Where:

- d : ID of the dam in the portfolio, from 1 to D;
- D : number of planned dams;
- u_d : boolean reporting 1 if dam n is selected, 0 otherwise;
- G_d : annual hydropower generation of dam n [GWh/year].

The negative value of the indicator is necessary since, as seen in equation 3.1, the identification of the non-dominated solutions is performed by minimizing both indicators.

3.1.2 Sediment connectivity

The alteration of sediment connectivity in the network determined by the dams can be observed in the CASCADE framework with both deposition of sediments in the reach upstream the reservoir and erosion in the reach downstream. The indicator for this alteration must therefore take into account both phenomenons to provide a good estimate on how the dams in the portfolio alters the connectivity.

The indicator L^{sed} is derived with the following formula, from the data of annual sediment transport, depositions and erosion obtained from CASCADE, as described in Section 2.3.5.

$$L^{sed} = \sum_{i=1}^{I} |Q_{B,i}^{(dep,ann)} - Q_{B,i}^{(erod,ann)}| \tag{3.3}$$

Where:

- $Q_{B,i}^{(dep,ann)}$ is the annual deposited sediment load in reach i [Kg/year], stored in row i of vector $Q_B^{(dep,ann)}$, obtained by equation 2.12.
- $Q_{B,i}^{(erod,ann)}$ is the annual sediment load lifted in reach i [Kg/year], stored in row i of vector $Q_B^{(erod,ann)}$, obtained by equation 2.11.

The indicator adds together, for all the reaches, the absolute value of the difference between deposited and eroded sediment load, i.e. each reach sediment budget.

3.2 Matlab implementation

The implementation of the assessment framework in Matlab is performed by the script `Script_Assessment_framework` that contains the operations to obtain the Pareto front. The Pareto front is derived by an exhaustive method: all the possible combinations of dam portfolios are tested and the indicators for each portfolio are derived. This requires to run a simulation on annual sediment transport with CASCADE for each portfolio. The number of possible dams portfolios, given the 14 dams described by *Sogreah Consultant* (2009), is 16,384.

The optimal portfolios solutions are derived with the function `getNonDominated`.

3.3 Sensitivity analysis on Pareto-optimal portfolios

The identification and ranking of non-dominated portfolios in the two-objective assessment framework depend on the performance each individual dam portfolios has for the two identified indicators.

In particular, the sediment alteration indicator depends on the results of the CASCADE simulation of the sediment transport in the network with the selected portfolio. As described in Section 2.2, the revised CASCADE framework requires as input the sources reach GSDs, in order to derive the GSDs for all the reaches in the network, that in turn will influence the transport capacity of the reach and ultimately the processes of sediment transport, deposition and entraining. Changes in these input data could therefore alter the score of a dam portfolio in the sediment alteration indicator, and consequently make the alternative more or less competitive in compare to the others.

Because of this, in this work we have carried a sensitivity analysis on the robustness of the Pareto-optimal solution to changes in the input source reach GSDs. If the shape and composition of the Pareto front remains similar for CASCADE simulation run with different values of source reach GSDs, it indicates that the Pareto-optimal dam portfolios are robust and therefore uncertainties in the CASCADE framework do not influence the ranking of the alternatives for the sediment alteration indicator.

Thus, the Pareto-optimal solutions were identified for different scenarios of source reach GSDs. To perform a single iteration of this sensitivity analysis, we need to measure the value of each of the possible dam portfolios for the two indicators. To evaluate the performance for the sediment alteration indicator, the annual simulation of sediment flow without dams must first be performed with as input a single set of values of sources D50, in order to find the reach GSDs for all reaches, with the methodology explained in Section 2.3.5. Then, for each dam portfolio, Model B optimized framework is used, with the reach GSDs found as input[1] and the value of the indicator is evaluated. Finally, the values of the two indicators for each portfolios are used to identify the Pareto-optimal solutions for the analyzed scenario.

[1] As described in Section 2.4.1.

4

Case Study

4.1 Geographical Setting

The Vjosa river is situated in the southern part of Albany, in the mountain range of the Balkans. It originates from the Pindus mountains in Epirus, in the northwest of Greece, and flows into the Adriatic Sea. Throughout its 272 km of length, the river passes through a variety of different landscapes, receives water from several tributaries, and exhibits a variety of fluvial forms. While in Greece, the river, locally named Aaos, flows thought the Vikos-Aaos National park, where it forms impressive canyons. The river then meets its first important tributary, the Voidomatis, which, before joining the Vjosa, passes through the Vikos Gorge, one of the world deepest canyon. (Figure 4.3 (a)) The Vjosa enters in Albania near Perat, where it is joined by the Sarantaporos river. Proceeding downstream, the river flows in a narrow valley, maintaining a relatively small width except for small areas, where if briefly widens with low terraces on both side of the river. After the Dragot gorge, the river meets one of its two main tributaries, the Drinos. After that, the valley widens considerably, the slope reduces and the river meanders, forming impressive braided sections where the riverbed expand up to two kilometers in width (Figure 4.3 (b)) The river is joined by the second large tributary, the Shushica, near its mouth and enter the sea north of the Narta lagoon, within the boundary of the Vjosa-Narta Protected Landscape (Figure 4.1)

The Vjosa is draining a total area of 6700 Km^2, while the Drinos river and the Shushica river have a catchment of respectively 1 302 Km^2 and 715 Km^2.

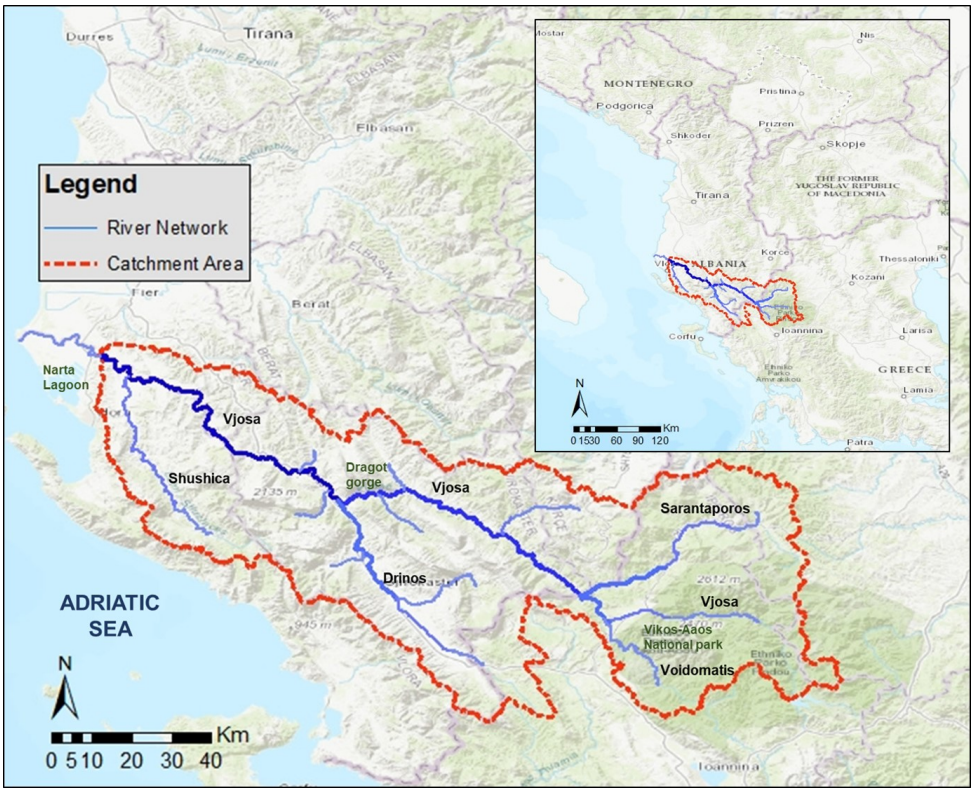

Figure 4.1: *Geographic localization of the Vjosa and its main tributaries and catchment area*

Along its course, the river passes through different climatic region. The coastal lowland has a typical Mediterranean climate, with mild winters and summer with high temperature and humidity. The inland is dominated by a Mediterranean continental climate; the temperatures is affected by the changes in elevation, but winters are usually cold due to continental air masses stationary over the Balkans and constant winds, while summer temperature can be higher than the lowland.

Regarding the precipitation, the Vjosa river basin has the highest average total annual rainfall in Albany, up to 2500 mm on some upper part of the basin. The average annual rainfall is around 1500 mm, of which approximately 70 % is concentrated in the cold period of the year. Rainfall is typically higher in the mountainous area. Due to the Mediterranean climate, there can be whole months without rainfall during any period of the year.

The Vjosa river system is considered one of the last wild river system in Europe outside Russia. The different territories and river formations along the path of the river and its tributaries host a variety of often unscathed and pristine fluvial ecosystem. Figure 4.2 shows the most significant river forms found in the basin. Braided sections are situated in the lower part of the Vjosa and on the Voidomatis, while in the middle Vjosa the river flows though *U* shaped

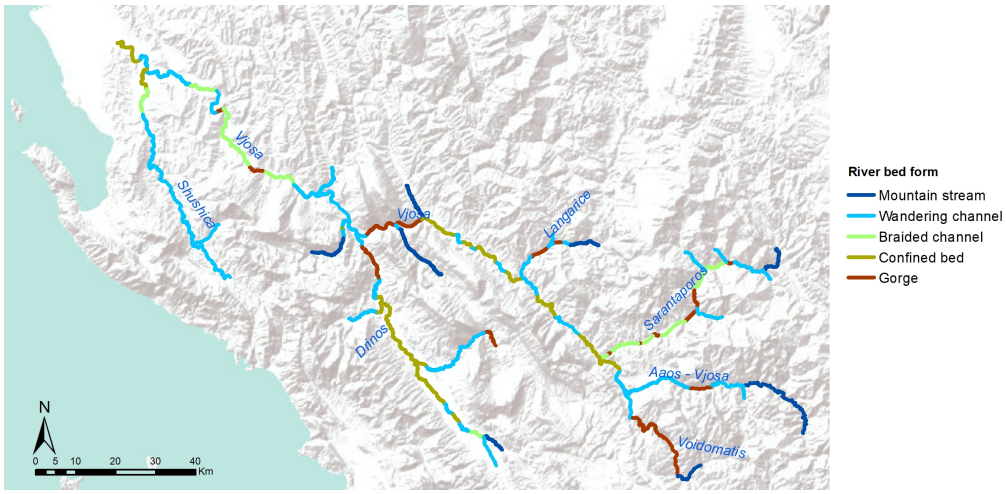

Figure 4.2: *Most significant fluvial forms found in the Vjosa river network*

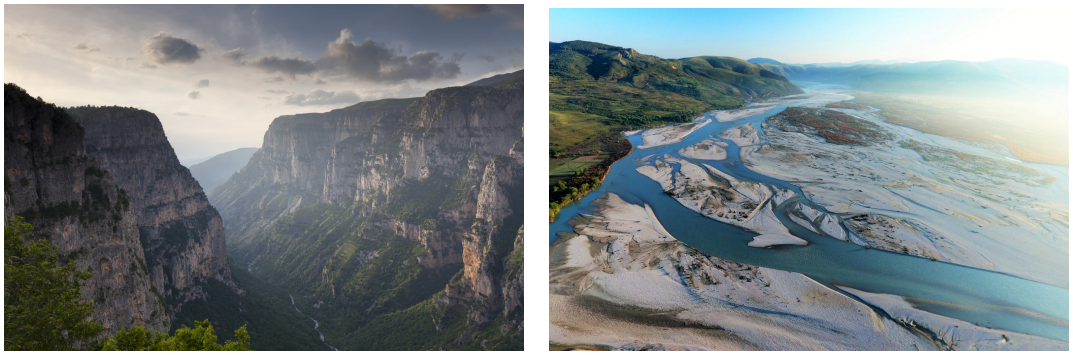

(a) *The Vikos Gorge, in the Upper Vjosa basin*

(b) *Braided channel in the lower Vjosa*

Figure 4.3: *The Vjosa river network cross wildly different areas*

beds, confined by almost vertical, rocky hillslopes.

The Vjosa river network is characterized by a sediment bed distribution mostly composed by gravel and cobbles, with presence of boulders in the canyons areas in the upper basin. The scientific knowledge on the Vjosa river system is still very limited, with few studies at hand so far and scarce field data available about the sediment transport and the sediment contribution, and limited comprehension of the river's biotic and abiotic components.

However, the researches conducted so far highlight how this river system is of great ecologic and natural value, and could be one of the last large pan-European ecological hotspot. The fauna and flora that populate these ecosystems are typical of unimpaired, highly dynamic rivers, with viable animal communities of land and fish fauna due to the high connectivity between the river and the surrounding (semi)-terrestric habitats. It harbours species that have disappeared from other European rivers due to river fragmentation, and that

are considered critically endangered. (*Graf et al.*, 2017)

Evaluations on the extend of the human impact on the river and the water quality indicates that the for most of its course, the river present a pristine or predominantly unmodified ecosystem. The overall physiochemical character of the Vjosa is mainly governed by natural processes. The unregulated state of the Aoos-Vjose River allows the free development of geomorphologic features (such as riffles, pools, extensive braided channels, lateral connectivity) which enhance self-purification and retention processes. (*Chatzinikolaou et al.*, 2008).

4.2 Hydropower development plan in the area

The Balkan region is recognized as a global biodiversity spot, but during the last 15 years major pressures have arisen concerning the development of hydropower plants in this previously untouched area. Thousand of hydropower plants have been planned in the area, and many of them are supported by European public money, with investment coming from the European Bank of Reconstruction and Development and the European Investment Bank (*Vejnovic*, 2017). In Albania alone, 313 hydropower plants are currently planned, and 24 are under construction. (*Schwarz and Vienna*, 2017).

While the Vjosa catchment crosses many protected areas, the river as a whole do not have a special protection status, making it a viable candidate for the development of hydropower stations.

Figure 4.4: *The planned construction site of the Kalivaç dam. The infrastructure is predicted to greatly damage the braided sections downstream and upstream the reservoir*

Right now, 38 HHPs are planned on the catchment, 6 of which in Greece and the other in Albany. Most of the projects consist in small diversion hydropower plants on the tributaries, with limited capacity (usually below 10 MW), that do not require the construction of a dam, but divert the water from the river, channel it thought a pipe towards the plant and then return it to the main stream. (*Schwarz and Vienna*, 2017).

On the Vjosa and its two main tributaries, the Drinos and the Shushica, 14 large HHPs are planned to be build in the near future. (*Sogreah Consultant*, 2009). (Figure 4.5). These project features storage dams built directly on the river and reservoirs, flooding the area upstream the barrier. (Table 4.1)

Figure 4.5: *HPPs planned siting and power production, data from Sogreah Consultant (2009)*

The planned dams will have a major impact on the river. Apart for the immediate effect of ecosystem destruction due to flooding, there are bound to be lasting effect on areas not directly occupied by the future reservoir. The rupture of river connectivity will damage the ichthyic species, while the regulation of the river flow will cause the wetlands to recede or disappear completely. In particular, the barriers situated downstream the braided section of the river are bound to deeply damage these ecological hotspots. Figure 4.4

Regarding the sediment connectivity, the creation of reservoirs will deeply impact the sediment transportation, causing alteration on the transport of nutrient and the natural morphological processes of the highly dynamic Vjosa river system. Phenomenons of bed erosion will probably occur downstream the dams, while we expect sediment deposition in the impoundment and upstream the reservoir, where the energy available for sediment transport drops.

4.3 Fieldwork results

The 21-23 of February, 2018, five researcher from University of Trento and Politecnico of Milano, including Simone Bizzi and myself, have conducted a field analysis on the Vjosa, with the support of collegues for the University of Tirana.

The targets of the fieldwork were:

- Conduct a geological survey of the Vjosa basin, with support of geologists from the university of Tirana and lithological and geological maps of the area. The analysis focus on the geological features of the river hill-slopes and the sediment on the river bars;

River	Name	Power Production	Height	Reservoir Area
Vjosa	Karbonari	240 GWh/year	7 m	5.4 Km^2
	Pocem	204 GWh/year	33 m	22 Km^2
	Kalivaç	308 GWh/year	30 m	12 Km^2
	Memeliaj	39 GWh/year	5 m	1 Km^2
	Dragot	332 GWh/year	45 m	3.2 Km^2
	Grabova	88 GWh/year	20 m	1.1 Km^2
	Kosina	84 GWh/year	20 m	1.7 Km^2
	Permeti	83 GWh/year	20 m	0.48 Km^2
	Badelonja	104 GWh/year	25 m	2.5 Km^2
	Kaludh	224 GWh/year	49 m	7.3 Km^2
Drinos	Ura Subashit	104 GWh/year	40 m	7.2 Km^2
Shushica	Brataj	104 GWh/year	55 m	6.5 Km^2
	Ura e Gjormit	12 GWh/year	20 m	15 Km^2
	Kota	8.1 GWh/year	1.1 m	0.58 Km^2

Table 4.1: *List of planned dams along the Vjosa and its tributaries (Sogreah Consultant, 2009)*

- collect data on the grain size distribution of the river bed on different sites on the Vjosa and its tributaries, and information about the river section geometry;
- survey the sites of the planned dams;
- propose project and ideas on future collaboration with the University of Tirana on the Vjosa river system.

The survey of the river bars highlighted a strong presence of coarse sediments, in the cobble-pebble grain class, with presence of sand deposits ranging from 5% to 20% of the total GSDs.

The geological survey on the river bars highlighted the strong presence of carbonatic sediment, with lower percentage of flints and magmatic and metamorphic rocks. Lithological maps of the area identify the origin of the latter from surfacing magmatic rock formations situated mainly on the Sarantaposos basin. The field data collected confirm this hypothesis, since the river bear on the Sarantaporos present a larger fraction of cobbles from magmatic rocks.

The GSDs data were collected with Wolman sampling method on four sites on the Vjosa and the tributaries Sarantaporos and Drinos, at the confluences (*Wolman*, 1954).

In two sample points, *1_Vjosa_Drinos* and *3_Sarantaporos*, two sampling areas were identified, one closer to the water flow and one on the riverbank. In this work, the sample most representative of the reach GSDs has been identified as the one closer to the water flow, since the bars are more likely to be affected by the water flow in lower water flow scenarios. The results for each

sampling site are shown in figure 4.6. The results seems to highlight a sensible sediment size fining proceeding downstream. The river bars are however always composed mostly by cobbles and pebbles. The data from the Drinos shows that the river bed of the tributary is characterized by a finer sediment distribution than the Vjosa, both downstream and upstream the confluence. This is reasonable, since in gravelly-alluvional systems such as the Vjosa, it has been extensively reported that, at basin scale, the grain size is characterized by downstream fining (*Hoey and Bluck* (1999); *Rice* (1999)). Usually the grain size decreases with the distance downstream following an exponential law. (*Moussavi-Harami et al.*, 2004). However, the fining process is often undermined in where considerable sediment supply from tributaries and lateral sediment sources occurs. (*Rice*, 1999). The two processes that have been considered to explain this phenomenon are the abrasion of the grains proceeding downstream and the selective deposition of larger grain sizes due to different transport capacity of the current. It is widely agreed that downstream fining depends on some combination of the two processes. (*Gomez et al.* (2001); *Moussavi-Harami et al.* (2004)).

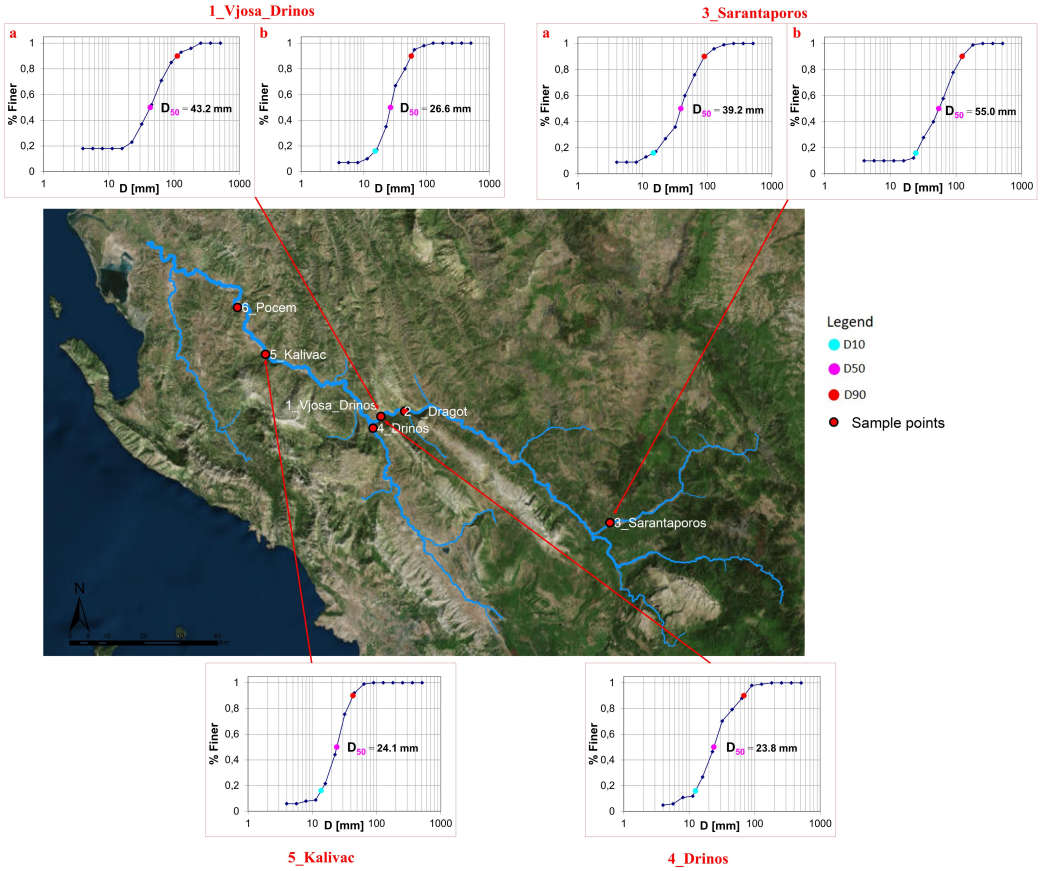

Figure 4.6: *Grain size distribution from Wolman sampling for the 6 sampling areas on the Vjosa*

5

CASCADE Implementation

In this Chapter, we describe the steps taken to implement CASCADE in the Vjosa basin case study. As seen in Chapter 2 , the model demands the matrix *Fi_Sn*, which contains the sediment distribution for the source nodes. Moreover, the model requires the definition of the river network by mean of the matrix *AggData*.

Since no field data are available for the Vjosa river network about the reach GSDs, we had to resort to data relative to other braided river network where field data are available. *Piegay et al.* (2009); *Liébault* (2003) report informations on the geomorphology of braided rivers in the south-east part of France, including sampling of D50 for different river bed morphotypes. *Piegay et al.* (2009) also describe the relationship between the maximum channel width and catchment size of braided sections in the rivers in south-est France, Italian rivers in Piedmont and the Tagliamento river in Friuli-Venezia Giulia. The braided sections are classified by their absolute normalized width $W*$ parameter, measures as:

$$W^* = W^{(bed)} / Ad^{0.44} \tag{5.1}$$

Where Ad is the drainage area of the reach in the *ToNode* and $W^{(bed)}$ is the bed channel width. The bed channel width is identified as the section of the river bed with little or no vegetation present, as permanent plant life denotes that the area is not subject to frequent flooding events and sediment mobilization.

By selecting the braided and meandering sections in the Vjosa river and confronting the W^* with the W^* from the other case studies, we can observe that

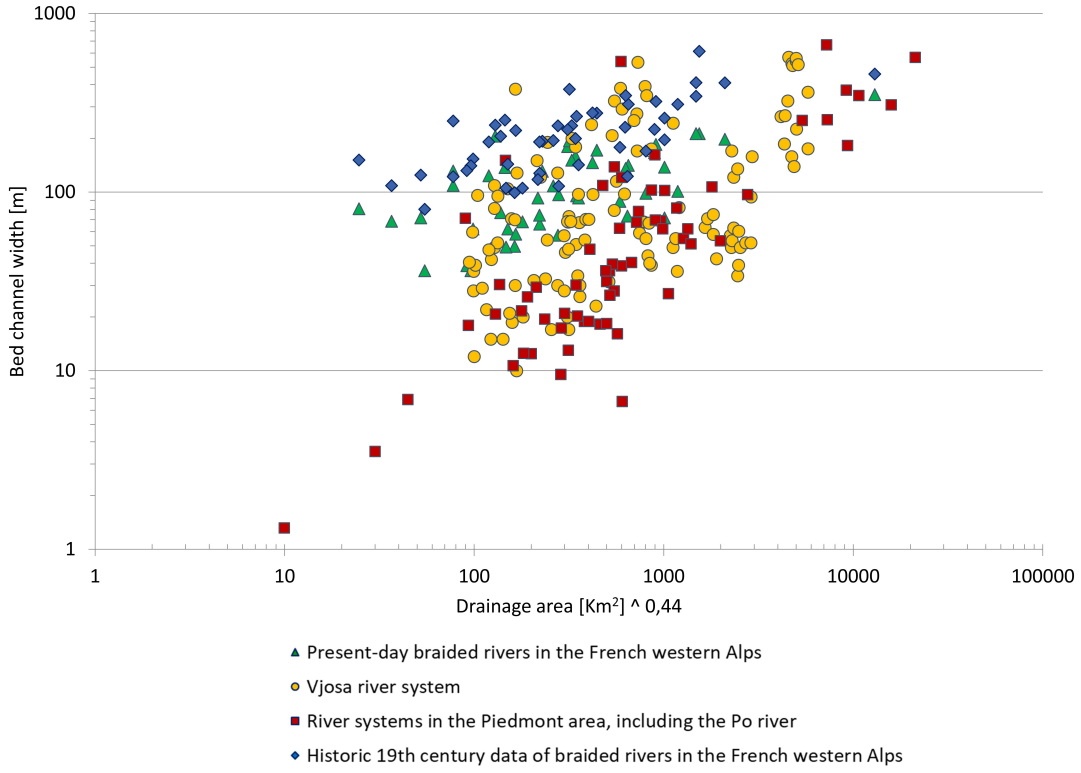

Figure 5.1: *Comparison between the W* of the braided and meandering reaches of the Vjosa river system and other European river systems.*

all the $W*$ values are in the same range (Figure 5.1). Therefore , we can suppose that the the Vjosa basin present similar geomorphological features of these other rivers flowing into the Mediterranean.

The data and the hypothesis used in this section were analyzed with the help of professor Hervé Piegay, during a 8 weeks period spent in the University of Lyon, France. In particular, we looked at the issues of determining the source reach GSD and how the active channel width of the reaches changes with the water flow.

5.1 Model initialization: defining initial condition

In this section, we explore how the initial conditions stored in the matrix *Fi_Sn* have been defined. *Fi_Sn* contains, for each source node, the frequency of sediment for each class, described by the function.

Given the similarity between the Vjosa and the braided rivers in the southeast of France, we can use data collected for these river to provide an estimate of the reach GSDs of the sources. *Liébault* (2003) classify mountains stream in the

(a) *Morphotype D source reach on the Voidomatis.*

(b) *Morphotype C source reach on a tributary of the Drinos.*

(c) *Morphotype B source reach, on the Vjosa-Aaos, near the river spring.*

(d) *Morphotype A source reach, on a tributary of the Shushica.*

Figure 5.2: *Example of morphotype on the rivwer network source reaches.*

south-east part of France according to the characteristics of their beds into four morphotypes, and provide informations on the D50, D90 and D10, and their relative range of uncertainty, for each of them In order to use these data on the Vjosa, each reach defined as source in the model is classified into one of the four morphotypes described by *Liébault* (2003), by observing satellite images of the area and expert base analysis.

These typologies, ordered from finer GSD to coarse, are:

- A - beds with gravel river bars;
- B - beds with gravel flat bottoms;
- C - beds with coarse flat bottoms;
- D - block beds or rocky bottoms.

Figures 5.2 show satellite images of source reaches of the network that be-

long to each one of the morphotypes. Morphotype D is characterized by a high density of boulders in the bottom of the bed (particles whose diameter is greater than 256 mm) a bottom marked by a strong topographic irregularity, which implies a high hydraulic roughness, and an almost total absence of gravelly or stony sedimentary deposits. These morphotype is common for streams flowing through gorges, and often offers scarce supply of sediment to the network.

Morphotype C is similar to block beds rivers, but it shows a smoother alluvial bed, with less boulders emerging from the stream and an overall reduced roughness. Alluvial bars on the sides of the main channel are almost non existent, and the bed width is often lower than 20 m.

The absence of coarse elements emerging from the bottom of the bed and the presence of stony lateral accumulations distinguish morphotype B to the previous one. The bed appears flat and covered by an homogeneous stony filling. The low-water channel still occupies a significant part of the active band, but this time, the presence of alluvial surfaces become more important.

Finally, morphotype A differs from the others by the presence of large alluvional bars that follow one another continuously over a wide linear range. The low-flow channel becomes a minor element of the river bed, which is occupied mainly by large gravelly and stony river bars that occupy most of the bed width. Reaches of this morphotype can present main channels with high sinuosity or can behave like braided section, with multiple active channels in the same sections. The particle size distribution of the bottom of the bed is rather homogeneous. River belonging to this morphotype are often regarded as prime supplier of sediment to the network.

Figure 5.3 shows the morphotype class to which each source reach of the network belongs. Tributaries that have source reaches of morphotype A or B carry more sediment load and contribute more to the overall sediment transport in the network.

Liébault (2003) lists, for each morphotype, the average D50, D90 and D10 of the reach GSD, and the interquartile interval, that can be considered a valuable range of uncertainties for the sensitivity analysis described in Chapter 3. (Tables 5.1, 5.2, 5.3).

The values of K for each morphotype are identified by inverting equation 2.7 using the relative average D50 value.

The most appropriate value of s for each morphotype was found by performing an optimization to find the Rosin distribution that best fit the average D10 and D90 reported in tables 5.3 and 5.2, given the value of K obtained from the average D50 in table 5.1. The values ranges from 1.2 form morphotype D to

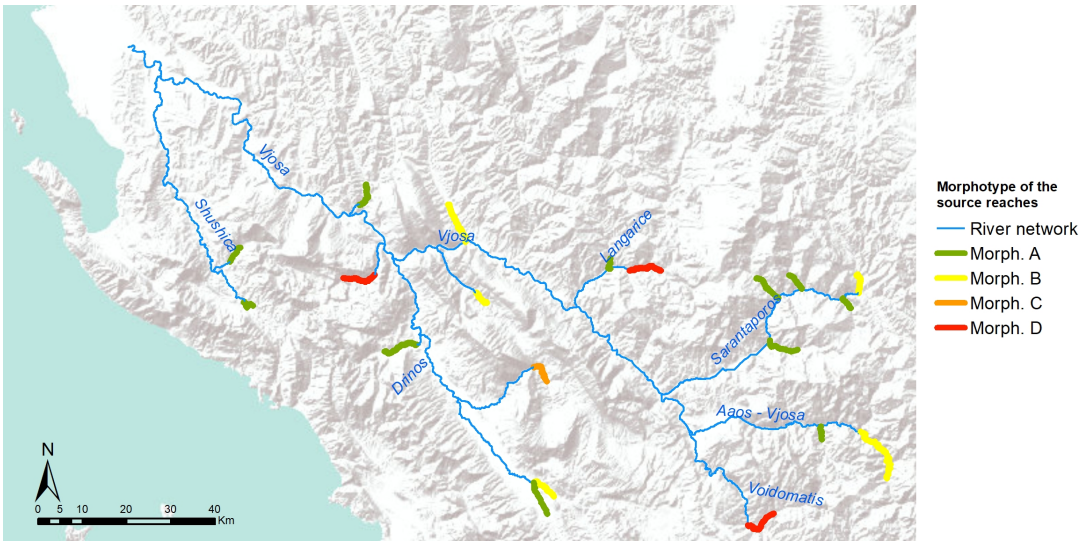

Figure 5.3: *Morphotypes to which each source belong in the network. This graph can give insight on the overall contribution of sediment of a river branch to the network. Branches with sources belonging to morphotypes A or B usually transport higher sediment load.*

D50		
Morphotype	Average	Interquartile interval
A	36.68	[27.80 - 40.87]
B	43.76	[33.06 - 52.17]
C	66.37	[44.57 - 79.43]
D	84.35	[63.29 - 100.99]

Table 5.1: *Estimated D50 for the different morphotypes and their associated range of uncertainty.*

D90		
Morphotype	Average	Interquartile interval
A	94.83	[63.12 - 117.05]
B	125.5	[103.16 - 146.49]
C	206.65	[135.15 - 256.00]
D	264.37	[187.67 - 298.68]

Table 5.2: *Estimated D90 for the different morphotypes and their associated range of uncertainty.*

D10		
Morphotype	Average	Interquartile interval
A	14.83	[11.96 - 17.00]
B	15.2	[11.74 - 18.21]
C	24.08	[14.69 - 32.11]
D	25.41	[18.22 - 33.71]

Table 5.3: *Estimated D10 for the different morphotypes and their associated range of uncertainty.*

1,5 for morphotype C and 1.6 form morphotypes A and B.

Then, the rows of matrix *Fi_Sn* are filled with the frequency value of the Rosin distribution linked with the morphotype of the stream associated to the source.

5.2 Data Preparation

The operations described in this section aim to define the *AggData* matrix and to populate the matrix with the data listed in Section 2.3.1.

5.2.1 River Network Extraction

In order for Cascade to work, the river network needs to be modeled as a series of nodes and reaches. This was conducted by means of MATLAB coding and the use of GIS software, both requiring a Digital Elevation Model (DEM) of the case study area.

The extraction of the river network from the DEM was carried out by a set of functions for topographic analysis contained in *Topotoolbox*,a MATLAB tooolbox developed by *Schwanghart and Kuhn* (2010) .

Function `Extract_River_Network` and script `Script_River_Network_Vjosa` were developed to provide a framework where to use the *Topotoolbox* functions and obtain the *AggData* matrix.

User-defined parameters need to be specified within the script, such as the standard length of a reach and the minimum drainage area for a cell to be considered as part of the network. High values of the latter lead to a river network that contains only the main tributaries, while lower values guarantee that shorter water streams will be present in the network too.

While it might seems favorable to choose low value of minimum drainage area, it must be noted that this could cause the appearance in the river network of non-existing tributaries, especially in plain areas where the changes in altitude are minimal and sink areas can be present in the DEM, which the algorithms in *Topotoolbox* are not entirely capable of correcting. In this case study, the drainage area was set to 100 Km^2.

The tools in *Topotoolbox* process the DEM given as input, fill the sink areas and calculate the flow directions and the flow accumulation, which contains for each the number of upslope cells, and hence the drainage area. From that, the cell with drainage area higher than the defined threshold are used to derive the stream networks in the basin, and select the largest connected component, that is the main river network in the area defined by the DEM. Once the river

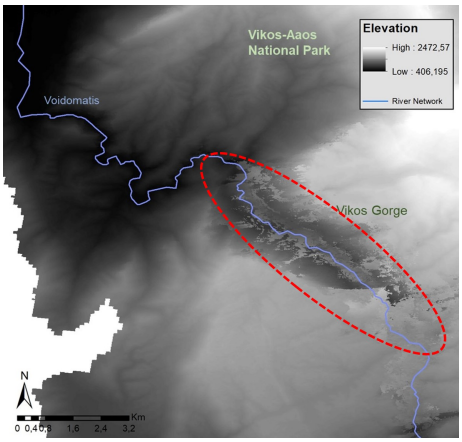

Figure 5.4: *Example of errors in the DEM in the area of the Vikos-Aaos National Park, around the Vikos Gorge (red circled area)*

network is identified, the *AggData* matrix is composed with the data reported in Section 2.3.1. Each reach and node is given an ID, the DEM is used to derive the channel slope and the drainage area of each node is measure from the flow accumulation.

Digital Elevation Model

The Digital Elevation Model used is the novel TanDEM-X DEM. This DEM is the product of a four year campaign, from December 2010 to January 2015, of bistatic X-band interferometric SAR acquisitions and covers the entirety of Earth landmasses. The independent Pixel Spacing of the DEM is 0.4 arcsec equator, equal to a ground accuracy of ~10.9 m at the case study longitude. The absolute vertical accuracy is inferior to 10 m. (*Wessel et al.*, 2016)

While having a high ground resolution, this DEM suffers from localized errors, that appear as area where the elevation contains abrupt changes, pixel with no data and clear discontinuity from the surroundings. These errors are especially present in mountainous and shaded areas, like the canyons or gorges common in the upstream part of the river system. (Figure 5.4) Because of this, the river network is extracted solely using this DEM do not consider whole tributaries and present errors in the channel slope or in the section shape.

To correct these errors, another DEM was used, obtained by the European Union's Earth Observation Programme, Copernicus (*European Environment Agency*, 2017). This European Digital Elevation Model, is a contiguous dataset subdivided into tiles 100 km x 100 km. Each tile is 4000x4000 pixels wide with ground resolution of 25 m and vertical resolution of +/- 7 meters. The version used by this work is EU-DEM v1.1. The European DEM is used to

derive the tributaries that the other DEM could not identify and connect them to the main river network, as well as checking the effective accuracy of parameters such as slope and drainage area for different reaches in *AggData*.

The extraction of the river network present difficulties in the area of the Vjosa river mouth, due to the presence of a cultivated flat area near the Narta lagoon which causes errors in the calculation of the flow direction. The basin outlet node was therefore positioned 16 km upstream the mouth.

Reach partitioning

In order to increase the accuracy of the model and the depiction of the changes in sediment transport, the river network was not partitioned using a standard length, which would have created reaches with all the same length. Instead, the river network was divided in sections manually, in order to create reaches with homogeneous geomorphological properties within and discontinuity with the neighboring reaches.

Given the high variability of fluvial forms in the basin, this partitioning method allow us to reduce the variance of the parameters to be attributed at each reach, while allowing the results of the model to be contextualized in the environment in which the reach is located.

The parameter mainly used to conduct this partitioning was the bed width of the reaches (see Section 5.2.2), while satellite images of the study area were also used to find discontinuities in the geomorphology of the area. A vector of "breaking points", which contains the coordinates of the point of separation between two reaches, was inserted in the script and used to obtain the final river network.

The input value of standard length of the reaches, necessary to run the functions in *Topotoolbox*, was set to a really high value to guarantee no further partitioning was allowed in the river network. Moreover, in order to partition the network at the location of the dams reported in Table 4.1, the coordinates of the dams in the river network were added in the vector of breaking points. Some river tributaries with lower drainage area than the threshold of 100 Km^2 were manually inserted in the network, if they appeared on satellite images as sources of sediment to the network. This is the case for streams passing thought gullies or badland, that typically convey sediment from the landscape to the river.

The resulting river network consist in 139 reaches and 20 source nodes, with length ranging from half a kilometer to 15 Km, with an average of 4.35 Km. Such differences in length is due to high variability of fluvial forms in the

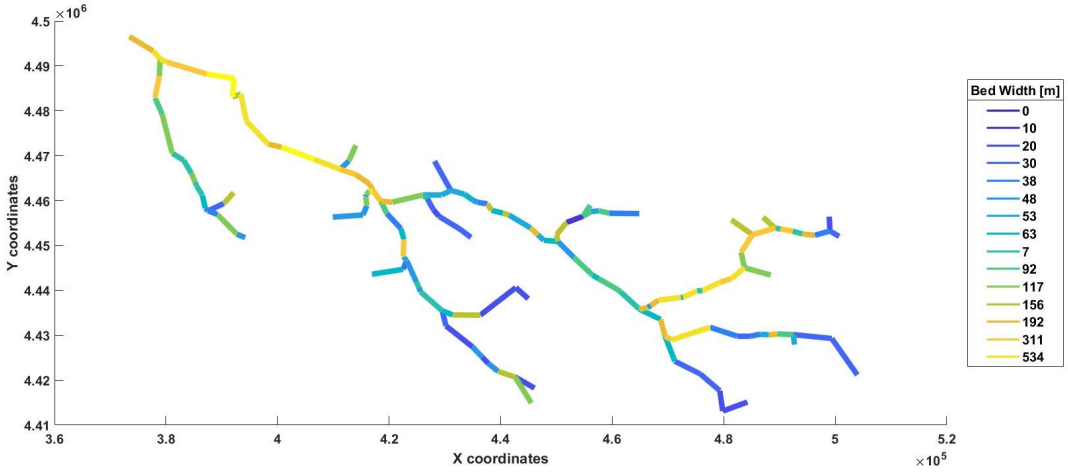

Figure 5.5: *Representation of the Vjosa river network in Matlab environment and the bed channel width of the reaches.*

river basin, where areas where the river rapidly alternates between gorges and braided sections are present alongside long, confined river stretch with no sensible change in geomorphology. Figure 5.5 shows the final partitioning of the network as it is represented in MATLAB environment, as well as the bed channel width of the reaches.

5.2.2 Active Channel Width

As stated in Chapter 2, in order for CASCADE to work, to each reach it must be attributed a value of active channel width.

Primary informations about the bed width can be found using satellite images. The bed width is identified as the section of the river bed with little or no vegetation present, as permanent plant life denotes that the area is not subject to frequent flooding events and sediment mobilization.

Around 400 sections were identified in the river basin using Google Earth Imagery, and the observation were used to identify the breaking point for the reach partitions, as described in Section 5.2.1. In order to reduce the errors in the measurement for long reaches, more section were taken and the bed width was identified as the average value.

The patterns and changes in bed width in the basin, as seen in figure 5.5, denotes how, as stated in Section 4.1, the Vjosa river network is highly dynamic, with interchanging fluvial forms and different type of river environments.

However, employing the bed width in CASCADE would not be realistic, since even for high flow events only a limited portion of the river bed section is flooded and displays sediment mobilizations on the river bed. The param-

eter that therefore should be employed is the active channel width, defined as the channel width perpendicular to the main flow, over which measurable bed material motion occurs during a water flow with given return period. (*Ashmore et al.*, 2011). Even so, measuring the bed material motion has often proven difficult, especially in case studies like the Vjosa, with few data available.

The active channel width seldomly corresponds to the bed channel width, since bedload transport processes in gravel-bed rivers are limited to threads of transport that are much narrower than the river bed itself, even during high flow events. (*Ferguson* (2003); *Ashmore et al.* (2011)).

The similarities between the Vjosa and other Mediterranean rivers, described at the beginning of the chapter and used already in Section 5.1 to derive the reach GSDs of the source reaches, can be used to provide insight into the relationship between the water flow and the active channel with in braided basin with similar characteristics.

First of all, it is necessary to classify the reaches based on the shape of the river bed. According to their shape, in fact, the active channel width will change differently with the water flow. The absolute normalized width W^*, calculated using equation 5.1, can be used to classify the river reaches according to their bed width compared to their drained area.

Using W^* instead of $W^{(bed)}$ to classify the reaches provide better results, since it removes the effect of the drainage area, and therefore the position of the reach in the network. For example, $W^{(bed)}$ will be higher in confined sections near the mouth of the river than is confined sections close to the source, since the latter drains a smaller area and therefore is subject to lower water flow conditions. W^*, on the other hand, will report similar results for both reaches, since it rescale the bed width according to the drainage area, and therefore allows us to classify them according to the shape of their bed. High values of W^* are characteristic of the wide river channels, like braided sections, while low values of W^* are associated with river sections that have unusual narrow bed width compared to area drained, such as confined reaches or gorges. (Figure 5.6). W^* give us also informations on the sediment supply that the reaches provide to the network.

To provide informations about changes in active channel width, a simple power law function was implemented to describe how this parameter changes with the water flow. (Equation 5.2).

$$W_i^{(ac)} = aQ_i^b \tag{5.2}$$

where Q_i is the water flow relative to scenario i $[m^3/s]$ and W_{ac} is the active

Figure 5.6: *Representation of the Vjosa river network and the W^* of the reaches defined as* $W^* = W^{(bed)} / Ad^{0.44}$

channel width [m].

Parameter a is specific to the geomorphology of the area, while b is linked to the characteristic of the river bed section, and in particular the magnitude of changes in the active channel width with changes in water flow. Confined river beds have typically low values of b, around 0.4, while we expect higher values for braided areas, close to 1.

In this case study, parameter a can be assumed constant for the entire river basin. To obtain this we analyze river sections with low W^*, that typically present no gravel bars and U shaped beds. In these reaches the active channel width does not change significantly with the water flow, and is equal to the bed width. Therefore, the active channel width of the reach depends only on its drainage area and the geomorphological features of the area, described by parameter a.

The reaches with $W^* < 2$ were then selected, and a fit power law function was determined, with the same structure as equation 5.2, where $W^{(bed)} = W^{(ac)}$. The function was derived for water flow with 1.5 return period. (Figure 5.7).

The parameter b is instead specific for each reach. To derive this parameter, we assumed an direct correlation between the W^* and the b parameter. *Piegay et al.* (2009) found a relationship between W^* and the supply of sediment of the reach. Sediment-rich reaches with high W^* , like morphotype A and B sources, have typically flat beds with large river bars, where the active channel width varies significantly with the water flow and therefore high b values. On the other hand, reaches that provide less sediment load have usually confined-U-

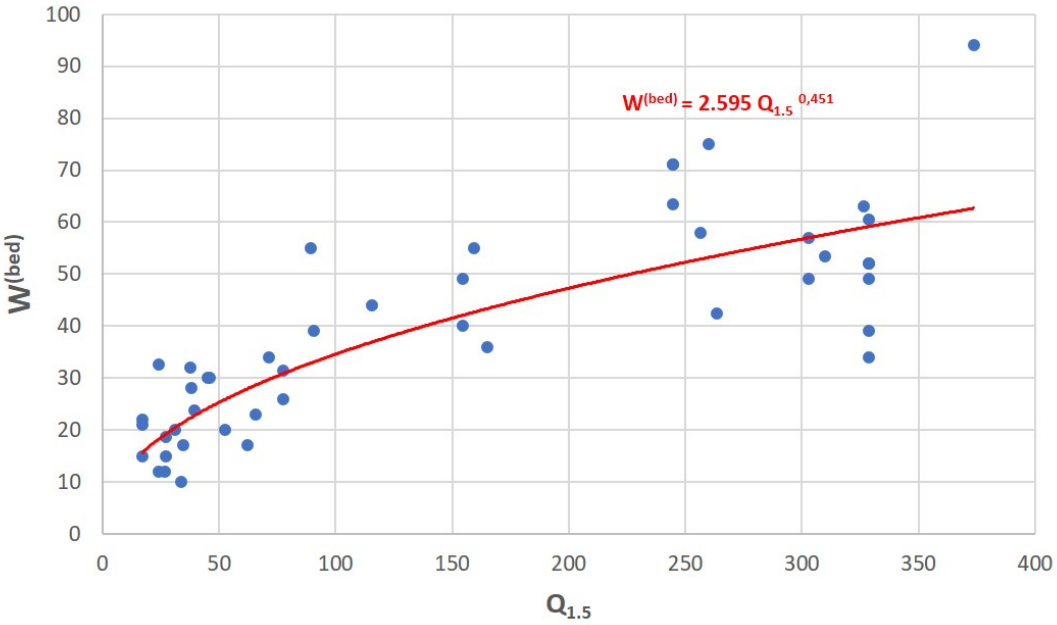

Figure 5.7: *Fit function for reaches with $W^* < 2$.*

shaped beds, where the width does not change significantly with the water flow and therefore b is low.

The b parameter will therefore vary between 0.45, the minimum value found for confined reaches, and 1, attributed to braided sections of the river, proportionally to the W^* of the reach itself:

$$b_i = \frac{(W_i^* - min(W^*)}{max(W^*) - min(W^*)} 0.55 + 0.45 \tag{5.3}$$

where b_i and W_i^* are respectively the b and W^* for reach i, 0.55 is the range of b values and 0.45 is the minimum b value. Thus, braided section will have a b value closer to 1, and will experience a more pronounced active channel width widening with increasing water flow regime.

Having obtained both the parameter a and b for all the reaches, the active channel width can be derived for each water flow conditions. Figure 5.8 shows the power function for different reaches in the river network. As we can observe, gorges and confined section have the lowest b values, while braided reaches have the highest, especially if sited in the upper part of the river, since their W^* is higher due to the lower drainage area.

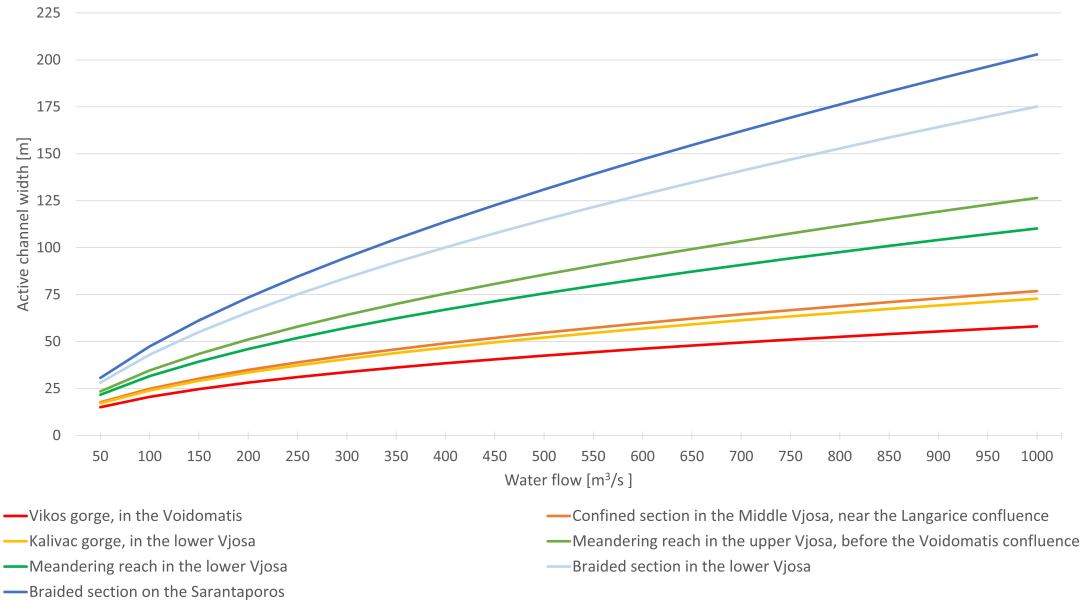

Figure 5.8: *Examples of power laws functions linking active channel width with water flow, for selected reaches in the network with different fluvial forms.*

5.2.3 Hydrology

To calculate the transport capacity for each reach, as stated in chapter 2, hydrological informations are needed. In particular, the model needs locally spaced hydrographs, that will be divided into discharge classes. The average values of each class will be used to perform the separate runs of the model, in order to have a representation of the sediment transport and connectivity in the basin under different flow conditions.

To acquire the hydrographs, we require data series of water flow for each reach. Since no data is available for gauging stations on the river, we resorted to hydrodynamic models to acquire the information needed. In detail, we employed LISFLOOD, a two-dimensional hydrological rainfall-runoff model, capable of simulating hydrological processes in a catchment and provide daily information of water discharge in a 5 km x 5 km window for the period from 1990 to 2014 (*De Roo et al.*, 2003).

The spatially-distributed data acquired from LISFLOOD were then attributed to the reaches that fall inside the tile. Errors that ensued from the low ground resolution of the hydrological model, such as faulty attribution of discharge data series at confluences, where the smaller tributaries would fall inside the tile containing the data for the mail channels, were corrected with the use of GIS software.

The hydrographs derived by the data series have to be divided into dis-

charge classes, as stated in Section 2.3.5. Eight classes have been thus identified by using nine percentiles values, spaced of one standard deviation paces from -4σ to +4σ in a normal standard distribution. The probability values associated to the percentiles are 0.1%, 2.3%, 15.9%, 50%, 84.1%, 97.7% and 99.9%.

The σ-intervals used allow to consider the effect of normal flow conditions as well as infrequent high magnitude flow event. For each discharge class, the average value of water flow was calculated, as well as the average number of days per year where the water flow falls into the class.

5.3 Dam implementation

The implementation of the dams listed in Table 4.1 in CASCADE is performed through the matrix *DamDatabase*, with the techniques described in Section2.4.

Figure 5.9 (a) reports the reaches in the network that the function `dam_slope_correction` report as flooded.

Sogreah Consultant (2009) presents for each dam a cartographic representation of the predicted flooded area, that was used to verify if the flooded reaches reported by the function `dam_slope_correction` actually correspond to the planned reservoir impoundment (Figure 5.9 (b) and figure 5.9 (c)).

Due to the simplification introduced in the function described by Section 2.4.1, these results may diverge. The dam height is therefore corrected, if needed, to obtain a flooded area as similar as possible to the one recounted by *Sogreah Consultant* (2009).

5.4 Implementation of the sensitivity analysis on reaches GSDs

As stated in Section 2.2.2, both Model A and B requires as input data the GSDs of the source reaches to provide the GSDs of all the other reaches in the network, and therefore the associated transport capacity.

The sensitivity analysis, described in Section 2.5, is thus performed on the resulting reach GSDs from CASCADE, obtained with the methodology described in Section 2.3.5, to evaluate their range of uncertainty with variation of source reach GSDs.

In the Vjosa case study, 20 source nodes were identified, each of one belonging to a Morphoype for which is reported the range of uncertainty of the D50 (the interquartile interval of the morphotype associated with the reach , reported in table 5.1).

In Section 2.5, however, we stated that the sensitivity analysis requires the

(a) *Planned dams siting and flooded reaches*

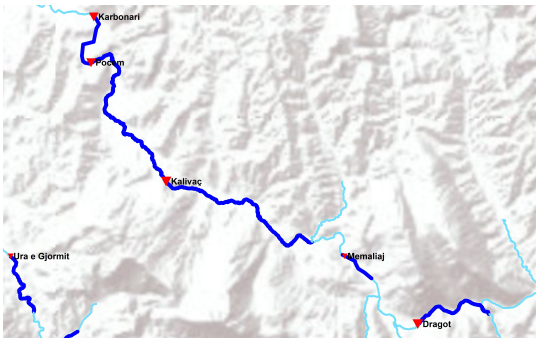

(b) *Planned inundated reaches in the lower Vjosa, obtained by the function* `dam_slope_correction`

(c) *Planned impoundments in the lower Vjosa (from Sogreah Consultant (2009))*

Figure 5.9: *Annual sediment fluxes from CASCADE simulation with Model A, in bankfull conditions*

GSD of the sources, not only the D50. However, by keeping the s parameter in the Rosin distribution equal to the fixed value specific for each morphotype found in Section 5.1, the D50 of the sources can be used to derive the K parameter, and therefore the sediment distribution of the reaches.

For a single simulation for the sensitivity analysis, the data sample containing the D50 of the source nodes is first used to derive the sources GSDs, to be stored in matrix *Fi_Sn*, that in turn are given as input to the CASCADE framework.

These data samples must be derived from a 20-dimensional space containing all the possible combination of source D50 given by the D50 range. In order to generate these data, a Sobol sampling of the sample space (*Hadka*, 2015). In total, 2100 data samples were created for the sensitivity analysis, a number that balance computational time and extensive sampling of the search space.

To the script `Script_sensitivity_GSD` is thus given as input a 2100x20 matrix containing for in the rows the D50 values of source GSDs for each sample point and returns, for all the CASCADE runs with the different Sobol samples, the matrix $F_i^{R,year}$ and the vectors with the values of D50, D90 and D10 for all the reaches.

6

CASCADE model simulations

In the following chapter, we implement the new versions of CASCADE on the case study.

The annual sediment transport process is simulated using the methodology and the water flow percentiles described in Section 2.3.5 and Section 5.2.3 to obtain the annual sediment load and the average reach GSDs for each reach. The input source GSDs is derived from the average D50 of the morphotypes described in Section 5.1.

The results of Model A and B are then confronted and validated using the data from the fieldwork described in Section 4.3. Model B seems to perform better and therefore the dams effect on the sediment connectivity is evaluated using this model. The cumulative impact of all the future planned dams is determined by performing a simulation with all the reservoir present on the network at the same time.

For the simulations, 30 sediment classes have been selected with constant range equal to 0.5ϕ and average size ranging from 5.25 ϕ to -9,25 ϕ, corresponding to the range 0.026 mm - 608 mm, from coarse sand to boulders.

In the results of CASCADE for the Vjosa, we expect to see a fining process in the reach GSDs for both Model A and B. As stated in Section 4.3, downstream fining is often attributed to the combination of processes of selective grain transport and abrasion. Since the latter is not considered in the model the fining is solely due to preferential transportation of fine grain classes.

6.1 Model A simulations

Figure 6.1 reports the annual instantaneous sediment load transported each reach. The simulation does not account for dams in the system.

The sediment flux increases moving downstream in the tributaries and the upper part of the Vjosa, as reported by figure 6.1 (a). On the middle and lower part of the main river, the sediment load remains more or less constant, slightly increasing moving downstream. In reaches passing through gorges and confined areas, the sediment transport increases, due to the increasing transport capacity, in turn connected to the higher slope and narrower active width.

The annual sediment load delivered to the outlet node is reported to be around 5 million tons of sediment each year. These informations are obtained by aggregating the fluxes of all the cascades leaving the reach, therefore by performing a sum of each column on the matrix $Q_B^{(tr)}$.

The Sarantaporos is, among the main tributaries, the one which contributes the most to the sediment supply, followed by the Voidomatis. The latter is passing for most of its course through gorges, where typically the river bed is composed by rocks and boulders. This phenomenon is not unique to the Voidomatis. In the river network, the various fluvial forms that the river channels take deeply influences the sediment connectivity and transport. [1] Moreover, the GSD tend to be slightly coarser in gorge areas, due to the higher transport capacity of the current, that in turn is able to lift bigger sediments.

Figure 6.1 reports the annual sediment load transported, eroded and deposited in each reach, obtained as described in Section 2.3.5. The data reported in the figures present trends similar to the one previously described for the instantaneous fluxes.

The average D50 is derived from the annual average GSDs of the reaches (see Section 2.3.5). The average D50 of the sediment loads passing through each reach is understandably lower than the D50 in bankfull conditions, since the average water flow in the reaches is lower, and therefore less energy is available for lifting coarser sediments. (Figure 6.1) The D50 varies form 117 mm to 9 mm, in the pebble-cobble size range, in compliance with the range of sediment size observed in the river beds in the basin. The figure highlights a clear fining process on the river system, as expected for a gravel bed river system such as the Vjosa (*Moussavi-Harami et al.* (2004); *Rice* (1999); *Gomez et al.* (2001)). The grain size decisively decreases on the tributaries, while on the main channel the magnitude of the fining is more contained, but nevertheless present.

[1] See figure 4.2 for a representation of the main fluvial forms which characterize the reaches of the river.

(a) *Total annual sediment load transported thought each reach.*

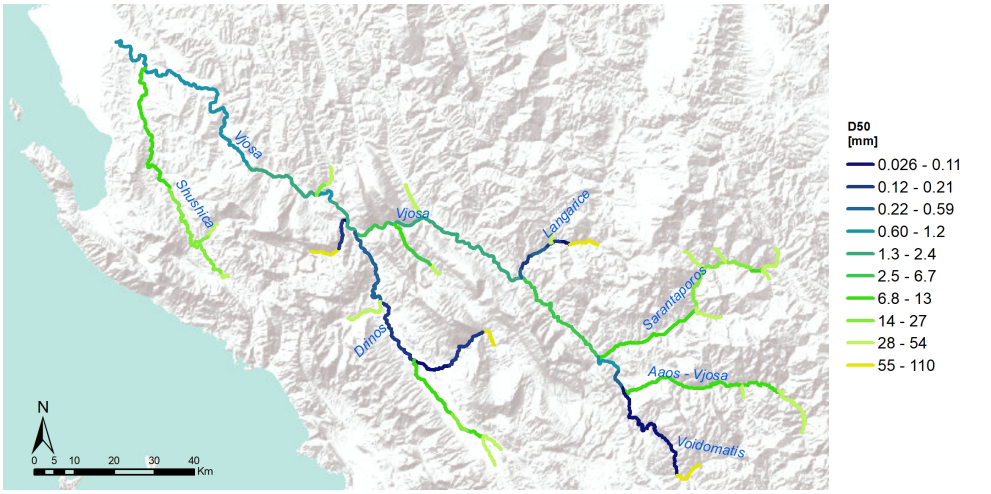

(b) *D50 of the cumulate annual sediment fluxes passing thought each reach, from CASCADE simulation with Model A.*

Figure 6.1: *Annual sediment fluxes and bed D50 from CASCADE simulation with Model A.*

Since CASCADE cannot account for sediment abrasion in the transport process, the grain size fining is only due to the selective and preferential transport of finer grain size due to the higher transport capacity of the current for finer sediment classes. The fining trend, however, reverses near the confluences, where the tributaries often supply the main channel with cascades with coarser sediment loads. Prime examples of this phenomenon are the confluences on the Drinos and the Vjosa-Drinos junction.

On the Voidomatis and other minor tributaries, the simulated D50 falls in to the lowest grain classes. This is due to the *bottleneck effect* of Model A, described in Section 2.2.2. For low and average water flow scenarios, the only sediment classes lifted at the sources are the extremely fine one, and the sediment load is very low, since the source is characterized by a bed with rocky bottom, with minimal presence of fine sediment.

Model A derives the reach GSD and thus the transport capacity by the distribution of the incoming cascades. Therefore, in the reach directly downstream, the derived distribution will present exclusively fine grain classes, and so will the cascade eventually created. In this case, however, since the frequency for the fine grain classes will be high, the sediment load lifted will be large. The new cascade will continue affecting the downstream reaches GSDs, thus propagating the error.

While, in these simulation, the errors induced by this effect influence only a limited portion of the network, it could be especially troubling when dams are included. Reservoirs are in fact prime example of bottleneck areas, where only the fine sediment loads can reach the dam and leave the impoundment, while all the other sub-cascades are deposited.

6.2 Model B simulations

The measurement of the annual sediment transport for model B is performed by running the model and calibrating the reaches reach GSDs for all the selected water flow scenarios. The fluxes and reach GSDs are then aggregated as described in Section 2.3.5. The annual sediment load delivered to the outlet node is reported to be around 1 million tons of sediment each year.

The GSDs calculation in Model B is based on the hypothesis that the transport capacity of the network ought to remain constant thorough the river, increasing only at the confluences, where the river is supplied with new sediment. Thus, the total sediment load deposited and eroded in each reach is always equal, and the sediment transport increases only at junctions. (Figure 6.2 (a)).

(a) *Total annnual sediment load transported thought each reach.*

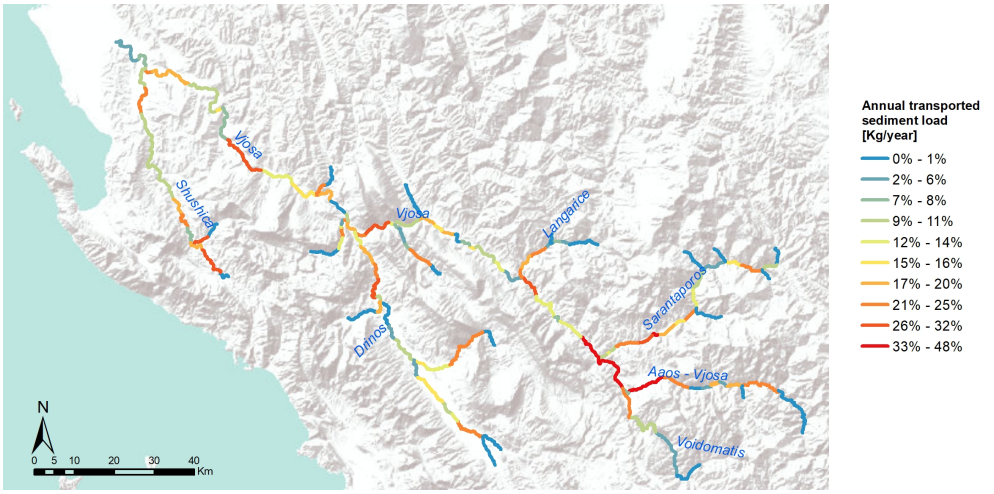

(b) *Fraction of sediment passing through the reach closing section composed by local erosion in the reach.*

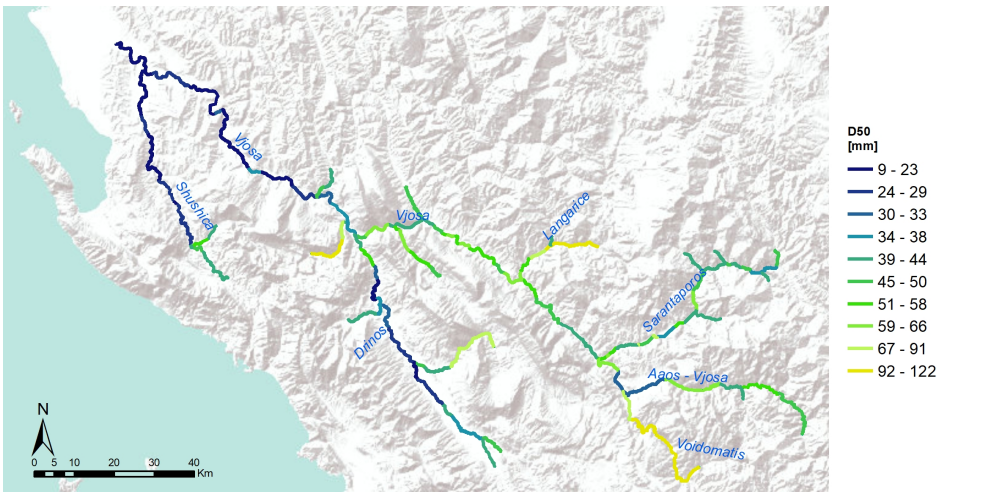

(c) *D50 of the calibrated GSD for each reach.*

Figure 6.2: *Annual sediment fluxes and respective D50 from CASCADE simulation with Model B.*

Processes of erosion and deposition for single grain classes can still occur, however they are at equilibrium, with the same amount of sediment load deposited and eroded, to maintain the transport capacity constant. The magnitude of the erosion and deposition in a reach depends on how marked the differences in the geomorphological features, and therefore the GSD, of the neighboring reaches are. For example, the steep fining in the reach GSD passing from a gorge to a wide braided area causes the deposition of coarse sediment classes and lifting of fine grains.

A way of detecting those discontinuities is to measure how much of the total sediment load leaving each reach is transported by the cascade generated in the reach itself. This indicator is higher when the river present geomorphological discontinuities, such when the river transition from one fluvial form to another. (Figure 6.2 (b)).

In model B, as stated in section 2.2.2, the reach GSDs the cascade GSDs are different. The figures and graphs hereby reported always refers to the reach GSDs. These two values tend to diverge considerably in reaches with rocky bottoms, where the reach GSDs is very coarse (with D50 falling into the boulder grain class), while the cascade GSD is much finer, since the water current can only lift the finer sediment classes. If the reach source node has a coarse reach GSD and therefore the cascade originated transport a low sediment load, all the reaches downstream until the first confluence will be attributed low transport capacities. The behavior of the model on the Voidomatis is a prime example of this phenomenon.

The reach GSD obtained from the calibration process tends to be coarser in reaches with high slope, low channel width or in general in reaches with high energy availability. Figure 6.2 (c). In this way, the exceeding energy is employed to lift coarser sediment, that requires more energy compared to the fine grains to lift the same weight, and the total load transported thought the reach stays the same, as the model requires.

If the calibrated reach GSD of the reach differs from the frequency of the sediment classes in the incoming cascades (which depend on the reach GSD of the reach upstream), we will observe the deposition of sediment classes less common in the reach and the lifting of grain sizes with higher frequency. The more pronounced the difference between the reach GSDs, the higher the deposition and erosion. The reach GSDs calibrated appears to fall inside the pebble-cobble size range, like Model A, but the D50 values reported are usually higher.

Figure 6.3: *Reach D50 from CASCADE simulation with Model A, in bankfull conditions. The network contains all the planned dams.*

6.3 Model discussion and confrontation

Model A reports the total annual sediment load to be one order of magnitude higher than Model B. Since the reach GSDs are on average finer for Model A, we can expect the magnitude of transport and erosion to be higher due to the lower energy requirement for transport of the finer grain classes. Both Models presents deficiencies when simulating the changes in sediment transport due to discontinuity in the geomorphological features of the reaches.

The hypothesis that the reach GSDs can be described using the cascade GSDs of the cumulate incoming sediment loads works well for river networks with small basins or that show constant or slowly changing geomorphological features or similar fluvial forms, however here it causes the already described *bottleneck effect* in areas with marked differences is slope or channel width.

As stated before, this effect is especially troubling when reservoirs are introduced in the network. The method of identification of the reaches GSDs in Model A can in fact lead to errors in the simulation when the cascades proceeding downstream pass through a reservoir, that allows only sub-cascades carrying fine sediment size to pass.

Figure 6.3 reports the changes in D50 in the network for a simulation in bankfull conditions with dams. The *bottleneck effect* is clearly evident, the D50 drops down to the lowest sediment class as soon as the routing process arrives at the series of dams on the middle Vjosa.

Model B seems to be more reliable to study river network with frequent discontinuities in fluvial forms. The model strong hypothesis of sediment equilibrium forces reaches with high different morphology to have the same transport

capacity and to transport the same amount of sediment, allowing the model to modify the reach GSDs to better describe the geomorphological features of the various river sections. However, this also causes unusual behaviors in gorges and confined reaches, where the need to maintain the same total sediment load while having available more energy forces the model to attribute a coarse GSD, with low frequency of fine sediment classes, and therefore low transport capacity. Thus, we observe a deposition of fine grains, which is most unusual in reaches with high energy availability.

6.3.1 GSDs validation

A validation of the results of the model can be performed using the data collected during the fieldwork, described in figure 4.6 in Section 4.3.

The GSD obtained from the models can be compared to the data collected on the field. Table 6.1 compares the values of D50, D10 and D90 found in the field with the one reported by the annual simulations of model A and B.

As we can see, Model B gives results of reach GSDa that are considerably closer to the observed data. Model A tends to report a finer GSDs than the one found on the river bars, most likely because the hypothesis at the base of this model works poorly in river basin with rapidly interchanging fluvial forms, that can induce the already described *bottleneck effect*.

Model B instead seems to report data on the D50 remarkably close to the one found in the field. Only on the Drinos the model reports a coarser grain size. Nevertheless, as previously stated, the model is sensible to the GSD of the source nodes, and as reported in tables 5.1, 5.2, 5.3 the D50 attributed to the various morphotypes presents a quite broad range of uncertainty. Therefore, the error in the calibration of the GSDs on the Drinos could be caused by input GSD of the source nodes of the Drinos and its tributaries coarser than reality, or inaccuracies in the estimation of geomorphological features of the river reaches, such as the slope or the active channel width.

Over all, Model B seems more suited to describe the sediment transport processes in the Vjosa case study and the effects of the construction of dams on the sediment connectivity. That said, Model B measurement of reach GSDs seems to be more realistic for non-confined reaches. In fact, in reaches situated in gorges, where visual surveys reported the river beds to be composed by large boulders or bedrock, the model predict a GSDs coarser than the surrounding non-confined reaches, but still much finer than the actual GSDs. Model A is definitely not suited for the task of evaluation the alterations caused by the dam implementation. However, for river in pristine conditions, it can provides

Sample site		Field data	Model A	Model B
1_Vjosa_Drinos_a	D10	Sand	0.03	11.09
	D50	43.21	2.93	46.22
	D90	112.40	38.81	119.16
3_Sarantaporos_a	D10	24.61	0.39	12.93
	D50	55.00	8.56	52.59
	D90	124.36	43.11	133.42
4_Drinos	D10	12.46	0.01	9.68
	D50	23.80	0.55	38.36
	D90	68.36	41.74	95.95
5_Kalivaç	D10	13.75	0.03	4.61
	D50	24.15	1.10	19.75
	D90	43.27	32.17	52.94

Table 6.1: *Comparison between the D10, D50 and D90 obtained from the field data and from the simulations of annual sediment transport of Model A and B*

results that decently represent natural processes of sediment transport, since they do not diverge greatly from the field values.

Therefore, Model B was employed for the study on the dam effect, the sensitivity analysis of the D50 and the assessment framework and sensitivity analysis of the Pareto front.

6.4 Annual sediment transport analysis

As stated in Section2.3.5, instantaneous sediment flows obtained from CASCADE simulations performed with various water flow regimes are aggregated to obtain the annual sediment transport. These results, however, also provide insight on which discharge scenario contribute the most to the sediment transport for each reach in the network. This depends on the average number of days per year when the scenario realizes and the instantaneous sediment fluxes mobilized.

This analysis was performed on the results of Model B and highlights that on reaches on the main river branches the classes defined by the quantiles [84.1-97.7] and [97.7-99.9] contribute respectively 43% and 48% each to the annual load transported, while occurring respectively 50 and 8 days per year, the last class [99.9 - 100] contribute to another 7% while occurring 0.3 days a year. On the small tributaries with coarse reach GSDs, like the Voidomatis, the class [99.9 - 100] can contribute up to 30 %, while the contribution of class [97.7-99.9] rise to 70 %. This is due to the fact that for river bed composed by cobbles and boulders, only rare events with high discharge can mobilize a significant amount of

sediment, while in normal conditions no processes of sediment transport occur. Over all, around 98% of the annual sediment transport take place on average during the 58 day with higher water flow conditions.

6.5 Dam Effect

As described in Section 2.4), the model takes into account the presence of storage dams on the network by changing the channel slope of the inundated reaches with the much lower energy slope of the water current in the impoundment.

The energy available for transporting sediment in the reaches drops considerably, and most of the sub-cascades with coarse grains size approaching the reach deposits all of their load. Downstream the reservoir, on the other hand, we observe high level of erosion, due to the release of "hungry water" form the reservoir, which has regained its transport capacity, but is deprived of sediments.

For the evaluation of the sediment transport with dams on the network, Model B is used without performing a calibration of the GSDs, instead using the one obtained in the undisturbed state, for the reason, explained in Section 2.4, that we are evaluating the alteration caused by reservoirs implementation on the river in pristine conditions, that still retains its geomorphological features, including the reach GSDs.

The results shows that the presence of reservoirs alters the magnitude of the total sediment load transported only inside the inundated reaches, where the grain transport becomes minimal or stops altogether (Figure 6.4 (a)). In the other reaches, the sediment transport is equal to the undisturbed state, since both the GSDs and the geomorphological features remains the same. However, the provenance of the cascade supplying sediment to the considered reach can change, since reservoirs effectively stops the sediment connectivity between the reaches upstream and downstream the impoundment.

Sediment erosion increases in respect to the undisturbed state in the reaches directly downstream the reservoir. The releases of hungry water, deprived of sediment load, causes the transport capacity to be satisfied mostly, of at all, with sediment eroded from the reach itself. Sediment depositions is mostly concentrated in the fist inundated reach of the reservoir. (Figure 6.4 (b)).

On the Vjosa, several dams are located directly upstream the impoundment of another reservoir, like the *Karbonari*, *Pocem* and *Kalivaç*. In this case, the model do not report erosion downstream the impoundment.

(a) *Total annual sediment load transported thought each reach, with dam.*

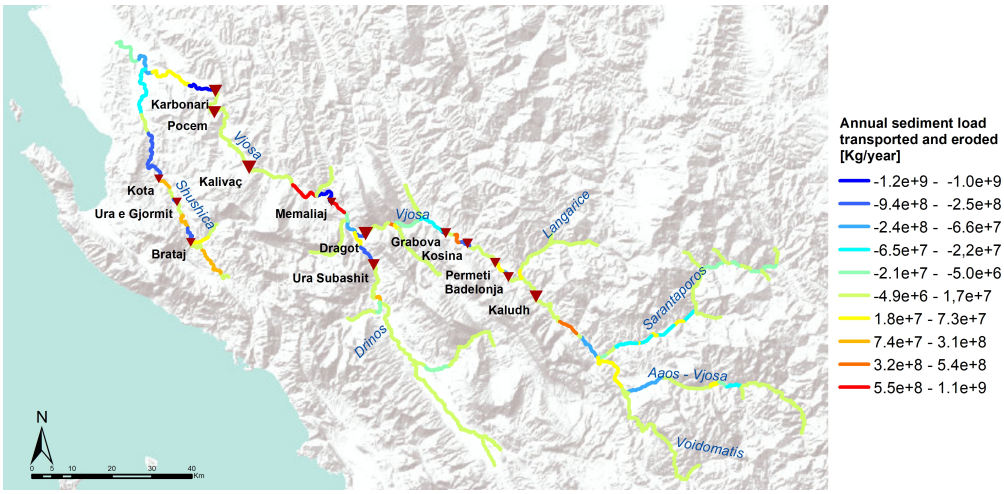

(b) *Total annual sediment load deposited (positive) or eroded (negative) in each reach,with dams.*

Figure 6.4: *Annual sediment fluxes from CASCADE simulation with Model B. The network contains all the planned dams.*

6.6 Results of the sensitivity analysis on reaches GSDs

The sensitivity analysis was performed with the methodology described in Section 5.4 on 2100 source D50 samples generated with Sobol sampling. Since, as stated in Section 6.3, Model B performs better for our se study, we employed it for the GSDs calculation in the sensitivity analysis. For each Sobol sample, the reach GSDs of all reaches is measured with the methodology described in Section 2.3.5. From the GSDs, the range of possible values of D50 obtained from the model simulations is found for each reach.

The results are shown with the box-whisker plots for the sections on the Vjosa and the main tributaries (Figure 6.6), for selected reaches in the network (Figure 6.5).

The sensitivity analysis shows that the calibration processes of the reach GSD in Model B were successful for each of the Sobol sample, and the range of values of bed D50 all the reaches in the network remains contained and does not present outliers or values that deviate excessively for the values for the average D50 scenario. The first element that the plots highlight is that, as seen also in the GSDs calculations in the Figure 6.2 (b), reaches in confined bed of passing through gorges reports a coarser D50. Moreover, the results of the sensitivity analysis show that the range of possible D50 values increases in confined reaches, while it is the most contained in braided sections. This is possibly due to the fact that the sediment classes were identified using the logarithmic Krumbein (ϕ) scale, and therefore, the range in mm of the coarser grain size classes is higher than the finer classes. Therefore, reaches with finer GSDs reports a lower range of D50 values in mm.

Over all, we do not observe a broadening of the range of values of the reach GSDs moving away from the sources. Moreover, the range of possible values is similar to the range of the D50 morphotypes that most influence the sediment transport. This is most evident in rivers with uniform geomorphological features, like the Voidomatis, that flows through gorges for most of its course, and the Shushica, that presents mostly meandering river brances. In fact, the Voidomatis has source reaches belonging to the coarser morphotype (D), that has the larges uncertainty D50 range[2] and thus its reaches presents a broader range of D50 (Figure 6.6 (e)). On the other hand, the Shushica river has sources that belong to morphotypes A and B, with D50 values with tighter uncertainty range, and therefore its D50 range is more contained (Figure 6.6 (c)).

The green bars in the plot represent the D50 value found on the field for the reaches for which the data were collected. Except for the Drinos data, the field

[2] See table 5.1 for the morphotype range

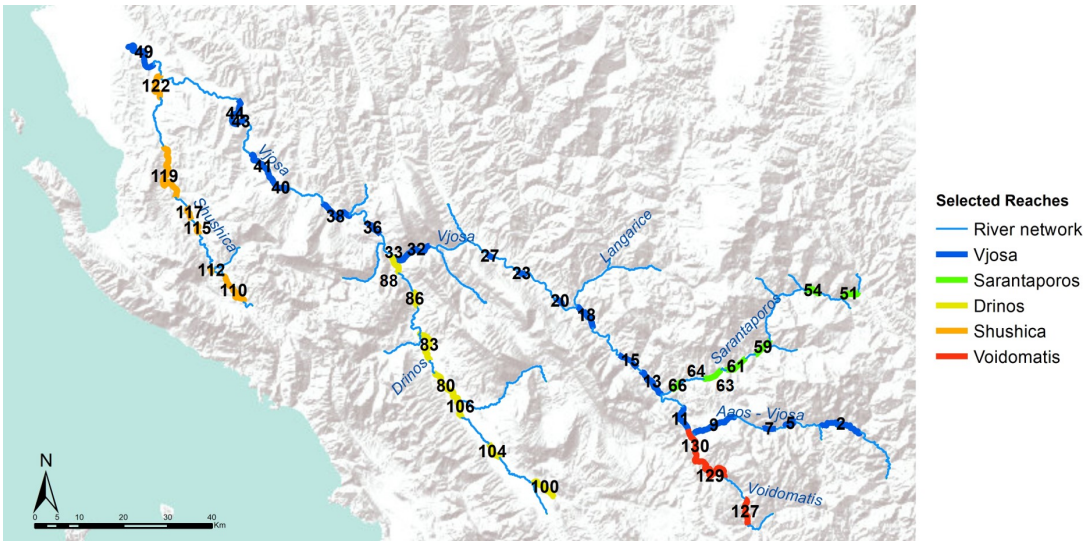

Figure 6.5: *Position in the network of the selected reaches for the sensitivity of the bed D50 and their relative ID. The reaches were selected to provide a good variety of fluvial forms and to accurately depict the changes in morphology of the river branch proceeding downstream.*

data fall within the possible range of D50 values predicted by the model. The field data on the Drinos, however, is not far from the range of possible D50 value for the reach.

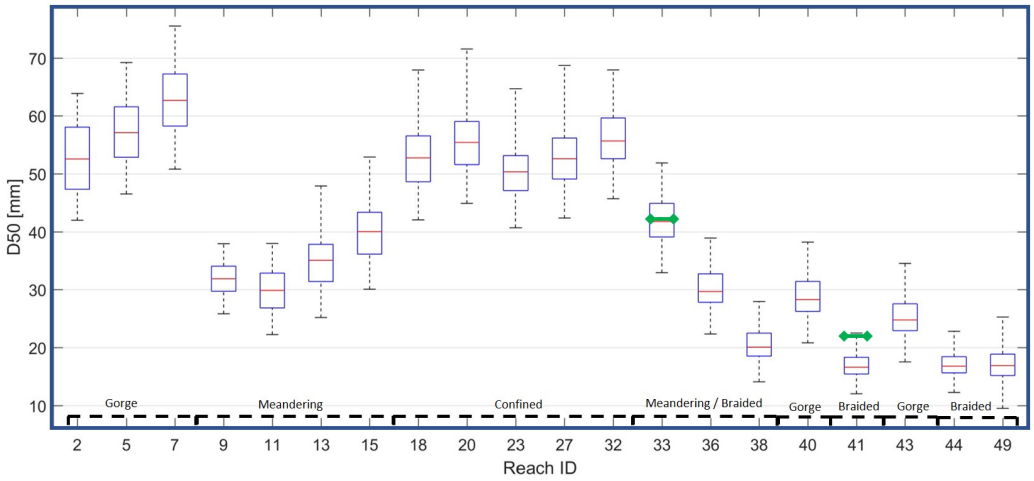

(a) *Vjosa river*

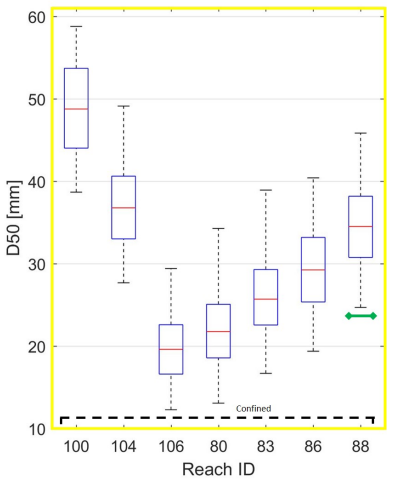

(b) *Drinos river*

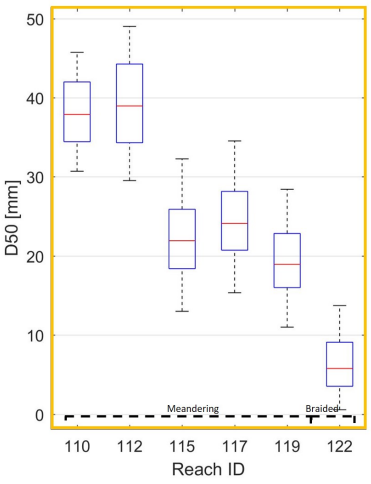

(c) *Shushica River*

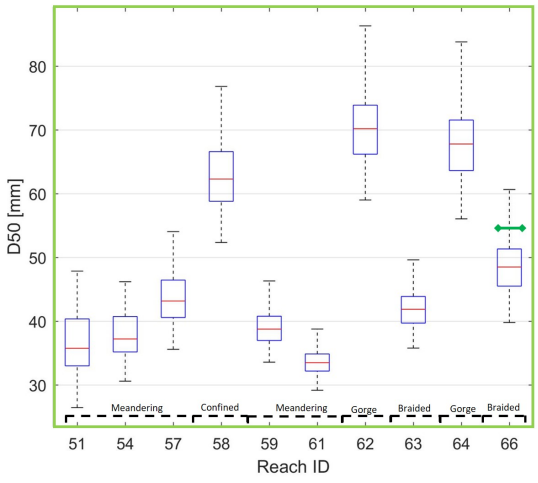

(d) *Sarantaporos river*

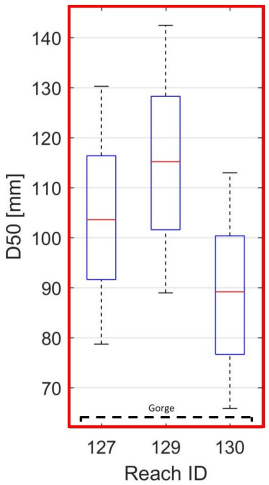

(e) *Voidomatis river*

Figure 6.6: *Box-whisker plots of selected reaches in the river network, shown in Figure 6.5. In the plots are reported the typology of river channel of the reaches. The bed D50 from field data (see Section 4.3) are shown as the green line on the respective reaches.*

7

Assessment framework results

In the following chapter, we show and comment the results of the assessment framework found with the methodology described in Chapter 3.

The ID of the dams ranges from 1 to 14 and correspond to the position of the decision variable in the vector. It is attributed proceeding upstream on the Vjosa main channel, and then considering the Dams on the Shuschica and Drinos. For example, the following decision variables vector:

u = [0 1 1 0 1 0 1 0 0 1 0 0 1 1]

correspond to the dam portfolio shown in figure 7.1.

The integration of a dam and the relative impoundment on the river system is implemented in CASCADE as described in Section 2.4.

Regarding the indicator of sediment alteration, we expect that, for reaches unaffected by the dams implementation, the difference between the two sediment flows to have values orders of magnitude lower than the reaches affected by the dams and the relative reservoirs, since we hypothesize that the pristine river is at equilibrium and sediment alteration occur only when dams are implemented. If the reservoir impoundment is composed by more than one reach, the only reach that will report sensible sediment alteration will be the first upstream, where deposition occurs. In all the other inundated reaches few sediments are deposited, since the upcoming sediment load was mainly deposited upstream, in the first inundated reach, and no sediment entraining can occur, due to the low transport capacity.

Figure 7.1: *Example of dam portfolio.*

7.1 Non-dominated solutions and Pareto front

This section contains the results of the evaluation of the Pareto front for sediment alteration indicators measured with CASCADE simulations of annual sediment transport with dams performed with Model B. The source GSDs is derived from the average D50 of the morphotype the sources belong to.

Figure 7.2 shows the performances of all the 16384 dam portfolios for the two indicators defined in Section 3.1, and highlight the Pareto front composed by the non-dominated solutions. On the x and y axis is reported the value of the hydropower indicator, and sediment alteration indicator, respectively.

The Utopia point, defined as the point which coordinates are the best possible results for both indicators, is situated at the intersection of the axis. The x coordinate of this point is the value of the hydropower indicator with the portfolio with all dams implemented, while the y coordinate is the sediment alteration reported when no dams are positioned in the network.

In total, 34 Pareto-optimal dams portfolios are identified. Among the non-dominated alternatives are included the two portfolios, with no dams or all dams implemented in the network, that perform the best for respectively the sediment alteration indicator and the power produced indicator.

From the figure, we can notice that there are portfolios that performs worst regarding the sediment alteration indicator compared to the portfolio with all dams (the red dot with the highest sediment alteration among the non-dominated portfolios). That is due to the effect of series of dams placed in rapid succession. If a dam is situated directly upstream the impoundment of another reservoir, the model will not report erosion nor deposition in the downstream reach, since the dam will discharge water deprived of sediment directly

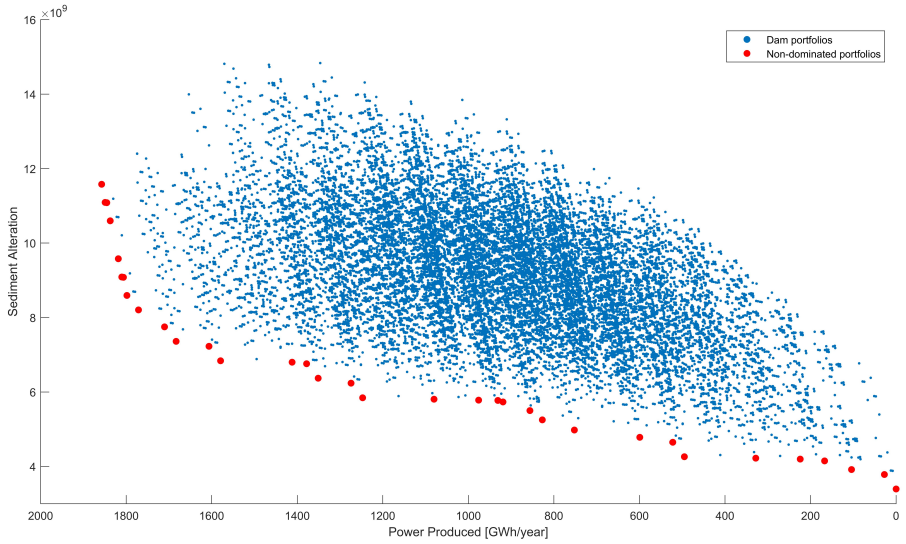

Figure 7.2: *Performance of all the possible dam portfolios for the two indicators defined and Pareto front.*

in the reservoir downstream, where the transport capacity of the current is low and no sediment will therefore be entrained.

This effect have a great influence in the selection of the non-dominated solutions, since it favors portfolios with tightly packed dams series, that acts like a single, large reservoir. Example of this are the series Karbonari - Pocem - Kalivaç in the upper Vjosa, the Kosina - Permeti in the middle Vjosa and the Kota - Ura e Gjormit in the Shushica [1].

Moreover, the size and inundated area of a dam have a limited effect on the alteration indicator, since, as explained in Section3.1.2, all but the first inundated reach reports alteration due to the abundance of sediment deposited that influence the indicator. Large dams benefits from this fact, since their alteration of the sediment fluxes is comparable to the one of small dams, while their hydropower production is higher.

Figure 7.3 reports the frequency with which a dam is included in a non-dominated portfolio.

The dams with higher frequency are Badelonja (79%) and Kaludh (74 % , followed by Permeti and Kosina (both 71%), all sited in the middle Vjosa. These dams have a good hydropower production, and they are sited before the confluence with the Drinos, that provides a huge sediment load to the network. Therefore, the sediment deposition, and erosion, consequently, caused by their construction is lower than the dams after the confluence.

The Karbonari, Pocem and Kalivaç dams possess a high frequency too (all

[1] See Figure 5.9

Figure 7.3: *Spatial distribution of the dams in the Vjosa basin. Each dam is colored according to the probability to be selected in a non-dominated portfolio of the Pareto front*

three 67%) . While their alteration on the sediment transport processes is the highest due to their positions, after the confluence with the Drinos, their power productions are among the highest. Moreover, they greatly benefit from the fact that they are positioned one after the other, and therefore the model considers them as an unique reservoir, as described before. This is proven by the fact that they all present the same frequency and appear always together in the Pareto-optimal portfolios.

The Dragot and Ura Subashit dams appears with lower frequency (47% and 50%). While they both present a high energy output and are sited before the Drinos confluence, meaning the alterations of sediment flow should be less, they are less attractive than the series of dams on the lower Vjosa, since the latter appers as one single reservoir for the calculation of the benefit from the effect described before.

The dams on the Shushica are the least attractive, since they produce a small energy output while altering the sediment transport of this tributary.

Analyzing the dam distribution of the 43 optimal portfolios, it si possible to identify spatial patterns in the non-dominated portfolios. Therefore, we divided the Pareto-optimal solutions into three groups (Figure 7.4):

- Set A : portfolios with low hydropower production, with dams mainly in the middle Vjosa;
- Set B : portfolios with medium hydropower production, with dams mainly in the upper and middle Vjosa;
- Set C : portfolios with high hydropower production, with most of the dams

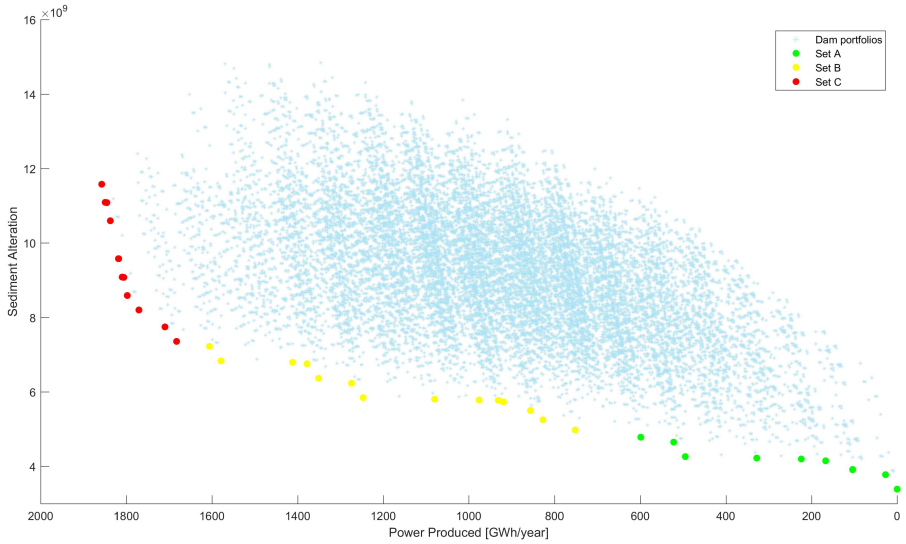

Figure 7.4: *Spatial subdivision of the non-dominated portfolios into three sets, with similar dam siting.*

selected;

Set A portfolios present different combinations of dams from in the middle Vjosa and from the tributaries. The latter are the Ura Subashit dam on the Drinos and the Brataj on the Shushica, that present the largest energy output among the HPP on the tributaries (Figure 7.5 (a)). These portfolios guarantee a production of maximum 930 GWh/year, equal to 50 % of the maximum possible production in the basin. On the other hand, the sediment alteration reach at worst only 28% of the maximum sediment alteration, reported by the indicator for the alternative with all dams implemented.

Non-dominated portfolios of Set B, instead, rely heavily on the series of three dams in the lower Vjosa. In this case the hydropower production ranges between 40% and 86% of the maximum possible production, while the sediment alterations indicator ranges between 20% and 47%. (Figure 7.5 (b)) The close siting of the sequence of three dams on the Vjosa, that acts like a single reservoir, and their large energy output guarantee a contained sediment alteration and with a high hydropower production. However, the sediment alteration indicator does not take into account the ecological damage of flooding the braided section in the lower Vjosa.

The point of maximum curvature of the Pareto front, i.e. the point where the slope of the front steepen abruptly, can be identified between Set B and C. To the left of the point of maximum curvature, small increases in the hydropower production corresponds to high increases in the sediment alterations. Because of this, while the energy output of the portfolios of Set C varies only between

(a) *Frequency of dams in non-dominated portfolios from set A.*

(b) *Frequency of dams in non-dominated portfolios from set B.*

(c) *Frequency of dams in non-dominated portfolios from set C.*

Figure 7.5: *Representation the dam frequency in each of the three sets of the Pareto-optimal solutions.*

86% and 100% of the maximum power production, the sediment alteration increases from 48% to 100%.

7.2 Results of the sensitivity analysis on Pareto-optimal solutions

A sensitivity analysis was performed to quantify the robustness of the Pareto-optimal solutions found in the previous section for average values of reach GSDs in the source nodes, as described in Section 3.3

Since the Pareto front is identified by performing a time-expensive exhaustive procedure of indicators evaluation on all the possible dam portfolios, it is not possible to perform a sensitivity analysis using as source reach GSDs input the 2100 Sobol samples described in Section 2.5 and used in Section 6.6.

Instead, we performed the sensitivity analysis with different extreme scenarios of source GSDs, derived from the limit values of the interquartile range of the morphotype GSDs. The sediment supply from the various river branches is directly linked with the GSDs of their sources, since as described in Section2.2, for Model B the transported sediment load is constant along the branches and increases only at confluences, and depends to the source GSDs.

The scenario used are:

1. Average scenario , used in Section 7.1;
2. all source nodes D50 set to the coarser value possible for the morphotype;
3. all source nodes D50 set to the finer value possible for the morphotype;
4. all source nodes D50 on the Drinos, Shushica and Langarice set to the finer value possible for the morphotype, all the others set to the coarser value;
5. all source nodes D50 on the Drinos, Shushica and Langarice set to the coarser value possible for the morphotype, all the others set to the finer value;
6. all source nodes D50 on the Shushica set to the coarser value possible for the morphotype, all the others set to the finer value;
7. all source nodes D50 on the Shushica set to the finer value possible for the morphotype, all the others set to the coarser value;
8. all source nodes D50 on the Drinos set to the coarser value possible for the morphotype, all the others set to the finer value;
9. all source nodes D50 on the Drinos set to the finer value possible for the morphotype, all the others set to the coarser value.

In addition to scenario 2 and 3, where all the source GSDs were set to their coarse and fine extreme values, the other scenario aims to analyze how the Pareto-optimal solutions change if just the contribution of sediment from the three largest tributaries of the middle and lower Vjosa is higher or lower than the average scenario.

Table 7.1 shows the frequency each dam appears in the Pareto-optimal solution for each scenario.

While there is quite some variability in the frequency of the dams in the non-dominated solutions, the trends observed in the average scenario persist also on the others, such as the importance of the three dams on the lower Vjosa and the Badelonja and Kaludh in the middle Vjosa, and the low frequency of the Brataj and Ura e Gjormit dams on the Shushica. In fact, table 7.2 report a low value of standard deviation for these three series of dams. The frequency of the three dams on the lower Vjosa is the higher in scenario 3 and 5, where the sediment load coming from the middle Vjosa is the highest.

This is due to the fact that, if the sediment load coming from the Drinos is low, the sediment load transported through the lower Vjosa does not increases significantly compared to the load transported in the middle Vjosa. Due to this fact, in this scenarios the sediment alteration index for dams from the middle and lower Vjosa becomes similar and therefore the dams on the lower Vjosa becomes more competitive due to their higher power production.

On the other hand, the dams whose frequency change the most are the dams on the tributaries and the low-production dams in the middle Vjosa (Dragot, grabova, Kosina, Permeti). The frequency of dams on tributaries in non-dominated solutions increases or decreases if the tributary transport respectively less or more sediment load, since the sediment alteration is higher if the river transports higher sediment load.

On the other hand, the frequency of the low-production dams on the Vjosa is extremely sensible to the sediment contribution of the Vjosa and the tributaries. In fact, their frequency is the highest in scenario 7 and 9, where the sediment contribution from the middle Vjosa is the lowest. In this case, their low sediment alteration make them more preferable to the dams in the lower Vjosa and Drinos (scenario 9) or on the Shushica (scenario 7), due to the high sediment load coming from these tributaries.

To verify the robustness of the Pareto-optimal portfolios in the average scenario, we also checked the position of these portfolios in the graph with the performance of all the possible dam portfolios for all the other scenarios (Figure 7.6). From the results, we can observe that the Pareto-optimal solution for the average scenario perform generally well also for in the other scenarios. In

River	Name	Frequency for each scenario								
		1	2	3	4	5	6	7	8	9
Lower Vjosa	Karbonari	68%	73%	79%	68%	78%	74%	72%	75%	59%
	Pocem	68%	73%	79%	68%	78%	74%	72%	75%	59%
	Kalivaç	68%	73%	79%	68%	78%	74%	72%	75%	59%
	Memeliaj	12%	15%	12%	14%	8%	6%	27%	11%	12%
Middle Vjosa	Dragot	47%	54%	48%	68%	38%	35%	50%	44%	71%
	Grabova	26%	34%	27%	50%	20%	13%	33%	25%	66%
	Kosina	71%	80%	67%	68%	53%	48%	78%	61%	94%
	Permeti	71%	80%	67%	68%	53%	48%	78%	61%	94%
	Badelonja	74%	73%	70%	82%	67%	64%	67%	72%	91%
	Kaludh	79%	73%	76%	96%	67%	67%	67%	78%	90%
Drinos	Ura Subashit	50%	54%	52%	36%	67%	44%	56%	67%	28%
Shushica	Brataj	12%	15%	15%	14%	24%	35%	11%	16%	25%
	Ura e Gjormit	12%	15%	15%	14%	24%	35%	11%	13%	25%
	Kota	41%	50%	48%	32%	63%	74%	22%	41%	66%

Table 7.1: *Frequency of each dam in the Pareto-optimal solution for each scenario*
scenarios :

1. *Average scenario;*
2. *all source nodes D50 set to the coarser value possible for the morphotype;*
3. *all source nodes D50 set to the finer value possible for the morphotype;*
4. *all source nodes D50 on the Drinos, Shushica and Langarice set to the finer value possible, all the other to the coarser;*
5. *all source nodes D50 on the Drinos, Shushica and Langarice set to the coarser value possible, all the others to the finer;*
6. *all source nodes D50 on the Shushica set to the coarser value possible, all the others to the finer;*
7. *all source nodes D50 on the Shushica set to the finer value possible, all the others to the coarser;*
8. *all source nodes D50 on the Drinos set to the coarser value possible, all the others to the finer;*
9. *all source nodes D50 on the Drinos set to the finer value possible, all the others to the coarser.*

River	Name	Min	Max	St. Dev.
Lower Vjosa	Karbonari	59%	79%	6.0
	Pocem	59%	79%	6.0
	Kalivaç	59%	79%	6.0
	Memeliaj	6%	28%	6.2
Middle Vjosa	Dragot	35%	72%	12.9
	Grabova	14%	66%	15.9
	Kosina	48%	94%	14.0
	Permeti	48%	94%	14.0
	Badelonja	64%	91%	10.5
	Kaludh	67%	96%	10.6
Drinos	Ura Subashit	28%	67%	13.0
Shushica	Brataj	11%	35%	7.8
	Ura e Gjormit	11%	35%	7.9
	Kota	22%	74%	16.7

Table 7.2: *Statistics for the frequency of each dam in the Pareto-optimal solution for each scenario.*

particular, the two Pareto fronts overlap almost entirely when the sediment supply from the tributaries is low due to their coarse source GSDs (scenarios 5, 6 and 8 in figure 7.6, and when the reach GSDs is proportionally coarser or finer in all the river (scenarios 2 and 3 in figure 7.6).

On the contrary, the two Pareto fronts diverge the most for some portfolios in scenarios where the source GSDs from one or all of the main tributaries is finer and the source GSDs on the Vjosa is coarser (scenarios 4, 7 and 9 in figure 7.6). In these scenarios, the contribution of the tributaries to the total transported sediment load on the river is relatively higher compared their contribution on the average scenario, and therefore building dams on these rivers becomes less recommended. The Pareto-optimal portfolios on the average scenario that contains those dams, therefore, appears further away from the Pareto front in these scenarios.

Overall, however, all the Pareto-optimal solutions for the average scenario seems to be positioned close or on the Pareto front in all the other analyzed scenarios, and no portfolios seems to performs remarkably worst in those scenarios. Therefore, we can assert that the Pareto-optimal solutions found for the scenario with average source GSDs are robust for the assessment framework set up in this work.

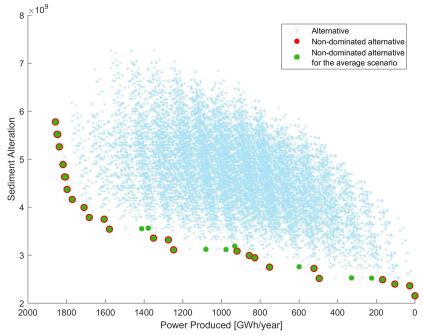

Scenario 2

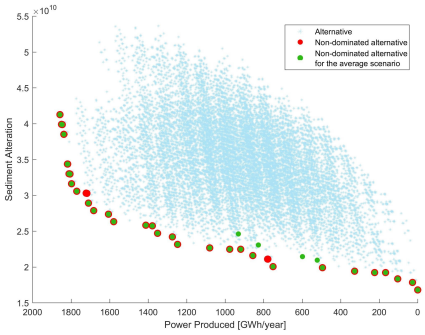

Scenario 3

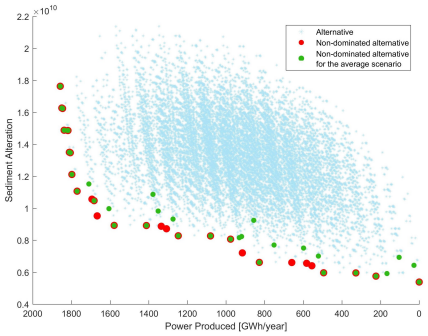

Scenario 4

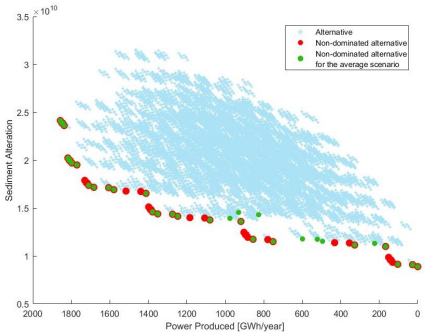

Scenario 5

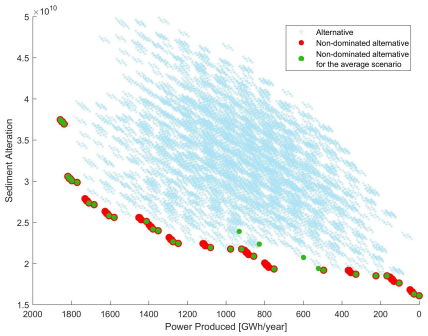

Scenario 6

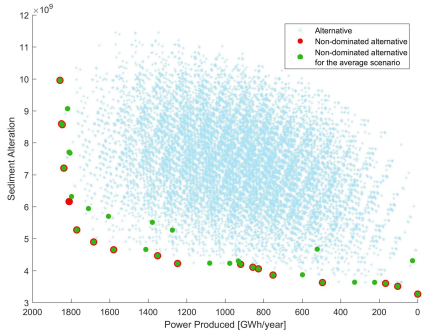

Scenario 7

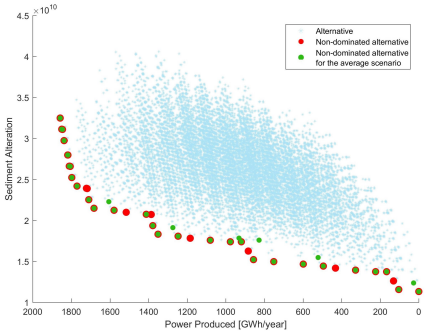

Scenario 8

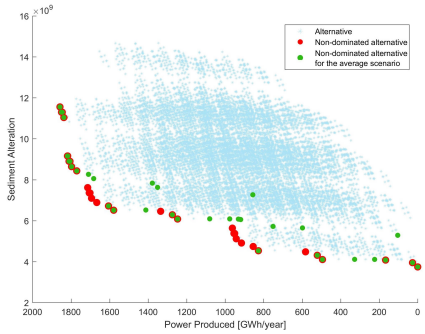

Scenario 9

Figure 7.6: *Results of re-simulating performance of portfolios that are optimal for the average scenario for different alternative scenarios (green) with portfolios that are optimal for each scenario (in red).*

8

Discussion and Conclusion

Main findings

CASCADE's ability to evaluate and quantify the sediment fluxes at a basin scale opens a broad range of uses for impact evaluation is multi-objective analysis framework. *Schmitt et al.* (2018) used CASCADE to evaluate the sediment alteration that would be caused by a series of planned dams in the Mekong river, and identify Pareto-optimal solutions that minimize the trade-off between hydropower production and sediment connectivity.

The revised CASCADE framework introduces widely used and robust formulas of selective sediment transport, by implementing Wilcock and Crowe equations of transport capacity (*Wilcock and Crowe*, 2003) and defining cascades not with a single grain size, but by subdividing them into multiple subcascades with different grain size. In this work, the revised CASCADE model is employed to evaluate the sediment connectivity on the Vjosa river network case study, in southern Albania, one of the last wild river system in Europe, and to evaluate the alteration due to the planned construction of a series of large storage dams on the river and the main tributaries.

The calculation of the GSDs of all the reaches in the network, necessary to measure the transport capacity, has been conducted by developing two different methodology, named Model A and B. Model A derives the bed surface GSDs (named in this work reach GSD), by the sediment distributions of the incoming sediment load, and the results on the case study compared to the field data shows that this model behaves poorly when used in riven networks com-

posed by reaches with rapidly interchanging fluvial forms and geomorphological features, and especially if reservoirs are implemented in the network. Model B, instead, implements the hypothesis of sediment equilibrium introduced by *Ferguson et al.* (2015) for gravel-bed rivers. For each river reach, an optimization is performed to find the bed GSD that correspond to a transport capacity equal to the total incoming sediment supply. Both models requires as input the bed GSDs of the source reaches.

Due to the lack of field data on the Vjosa case study, we have extracted the river network and derived geomorphological informations such as the slope from the European TanDEM-X DEM, with ground accuracy of 11 m (*Wessel et al.*, 2016). Another DEM, the Copernicus EU-DEM (ground resolution 25 m), was employed to correct errors in the network extraction and validate channel slope for the reaches (*European Environment Agency*, 2017).

Other input data, such as the reach GSDs of the source reaches, were obtained by comparing the analyzed case study to well documented braided rivers in south-eastern France and using data employed in these case study. Moreover, for each reach, a power function was derived to model the changes of active channel width with water flow regime. Both these data were obtained with the consult of river geomorphology expert prof. Hervé Piegay.

A fieldwork was conducted on the Vjosa,the 21-23 of February, 2018 and GSDs measures were collected using the Wolman sampling method (*Wolman*, 1954) in 5 different locations in the network (Figure 4.6). The data collected on the field highlighted a fining process of the reach GSDs proceeding downstream, as often reported for gravel-bed rivers (*Hoey and Bluck* (1999); *Rice* (1999)). According to the validation with the field data, Model B allows for a realistic estimation of the reach GSDs on a basin scale in non-confined areas. The results of D50 from the model run with average values of source GSDs and the field data are very similar (Table 6.1). However, Model B presents limitations in predicting the actual sediment routing in gorges and confined areas, and the GSDs in river sections with bedrock.

Annual simulations of sediment transport showed that, on average, 98% of the annual sediment transport in a reach take place during the 58 days with higher flow, and 48% during the 8 days with higher water flow in the year (Section 6.4)

The sensitivity analysis on the reaches D50 (used as proxy of the reach GSDs) does not report errors in the calibration process source reaches GSDs varying within the limits of their specified ranges. The ranges of uncertainty of the reaches' D50 do not seems to increase proceeding downstream, but remains similar to the range of values of the sources D50 that supply the most sediment

to the river branch the reaches belongs to.

An assessment framework for multi-objective analysis was developed to analyze the trade-off between hydropower production and sediment alteration for different dams portfolios (Chapter 3). The identification of Pareto-optimal portfolios was carried using an exhaustive search, evaluating the performances In the assessment framework, we implement a spatially-distributed indicator for sediment alteration instead of a basin outlet indicator like *Schmitt et al.* (2018). The Pareto front was identified and the Pareto-optimal portfolios were divided into three Sets, according to their sediment alteration, power production and type of dams in their portfolios [1].

Among the portfolios on the Pareto frontier identified using this indicator, the Pareto-optimal solutions listed in Set A are to be the most suited for low-impact dam planning. The performance of the indicators for these set of portfolios shows that it is possible to produce up to 50% of the maximum hydropower production in the basin without implementing dams on the lower Vjosa while limiting the sediment alteration to 30% compared to the scenario with all dams implemented.

Portfolios with higher power production heavily rely on the three large dams on the lower Vjosa, the Karbonari, Pocem and Kalivaç. Since in the lower part of the river, where the dams are sited, the load of sediment transported in undisturbed conditions is high, also thanks to the supply from the largest tributary, the Drinos, the sediment alteration reported by the relative indicator for each one of these dams taken individually is the highest among all the dams. However, if all three of these dams are build, in the CASCADE framework they act like a single dam, since their reservoirs are positioned one directly after the other. Therefore the model reports erosion only downstream the last dam, the Karbonari. This fact, together with their large energy output, makes the construction of these dams a competitive option for a high-level hydropower production portfolio, like the ones listed in Set B. The high capacity of construction of the dams in the lower Vjosa, in fact, removes the need to build other infrastructure in the middle Vjosa or on the tributaries, reducing the risk of sediment erosion in these areas.

The sensitivity analysis on the identification and performances of Pareto-optimal solutions, performed by searching for the non-dominated portfolios in scenarios with values of source reach GSDs coarser or finer than the average value, have found that the non-dominated portfolios in for the average scenario are generally robust and perfoms well also in the other scenarios (Section 7.2) Finally, the assessment framework strongly penalizes small reservoirs both

[1] See Section 7.1 and figures 7.4 and 7.5 for further references.

on the main river and the tributaries, since their small energy output does not justify the alteration of sediment transport in the river network.

Over all, the results of the assessment framework, while obtained with a simple analysis, allow for the quantification of the sediment alteration of the dam portfolios and therefore the evaluation of the objectives trade-off.

CASCADE future developments

The CASCADE framework is a versatile tool that allows for the implementation and the description of multiple processes involving the sediment cascades and the sediment entraining and depositing in the reaches. Here, we analyze the limitations of the revised CASCADE framework and explore possible future developments.

CASCADE revised framework aims to increase the level of detail of the modelisation of the sediment transport processes. However, it requires as input the reach GSDs of all the reaches in the network. The latter is difficult to acquire for such a large scale through data collecting on the field. Model B seems to offer a viable, basin scale method to acquire this data, but its results are sensible to the GSDs of the source nodes, as seen in the sensitivity analysis for the bed D50, and the geomorphological features calculated for the reach.

In particular, the bed slope was found by performing operations of river network extraction on two DEMs of the area. However, elevations of the low-flow river bed derived from both of these DEMs are affected by errors. The TanDEM-X DEM presents NaN or outliers in cells situated on the water flow, while the Copernicus DEM has a spatial resolution that does not allow for discernment between the bed elevation and the elevation of the surrounding areas. In confined section, on in gorges, where the river flow through a *U* shaped bed and few of no river bars are present, the elevation reported from the DEM and the actual bed elevation could strongly diverge, and therefore the bed slope could present errors. Employing detailed DEMs together with field measurement of elevation could produce better results in evaluating the reach GSDs.

Furthermore, the definition of the active channel width of a river section depends on a multitude of factor, including the water flow and shape of the section. For braided rivers, identifying the active channel width has often proved very difficult, since multiple channels can be active at the same time in the section, the number of active channel and the water flow passing thought each channel changes with the water low conditions and the channel geomorphology itself can change with time, since these rivers are often highly dynamic. The methodology used in this work to estimate the active channel width as a

function of the water flow, therefore, is bound to present errors in the measurement of the width, since it is employed at a basin scale using a basic power law function.

In this work, the transport capacity of a reach depends only on the reach GSDs of the reach. Therefore, if some sediment classes are present only in small fractions in the reach bed, their frequency in the GSD will be low and the transport capacity for that class will be very small. Because of this, reaches with very coarse GSD have a low or null transport capacity for fine sediment classes and thus presents a high deposition of these classes. Future development of CASCADE could take into account both the reach GSD and the GSD of the incoming sediment cascades to calculate the transport capacity of the reaches for each sediment class.

Another limitation of the current model framework is that all reaches are non-supply limited, and the sediment erosion do not account for availability of sediment to be entrained. Applying thresholds to the availability of sediment in reach could help solving this issue. These threshold could also be dependent ot the length of the reach, therefore avoiding erosion and deposition concentrated in a single reach, as instead happens in the current framework in areas like the one affected by dam construction.

Additionally, a new framework could take into account the sediment abrasion during the transport process, that as reported before is one of the processes causing the downstream fining in grave-bed rivers.

Assessment framework future developments

As stated before, CASCADE allows for the quantification of the alteration caused by the construction of one or more barriers or reservoir in the network. In this work, we have implemented a spatially-distributed indicator for sediment alterations. As seen before, this indicator favors closely packed series of dams, to concentrate the damage form sediment alteration in a portion of the river, while leaving the rest unaltered, at least according to the indicator. *Schmitt et al.* (2018), instead, used an indicator on the delivery of sediment in the output. By using the latter, reservoir situated in the upper part of the Vjosa river system are favored, since they do not alter the sediment delivery to the output as much as the dams sited closely to the river mouth. In a complete multi-objective analysis, both indicators of sediment alteration should be taken into account, since the spatially-distributed one measure the impacts on the whole river system, while the sediment delivery to the outlet is deeply linked with phenomenon of coastal erosion and degradation of the river mouth.

Moreover, the construction of dams also alters the natural water flow regime downstream the reservoir. As seen in the results for model B in Section 6.2, high water flow scenarios are responsible for more than 98% of the annual sediment transport, and the 8 days a year with higher flow are alone responsible to up to 50% of the annual transport . Dams management of water release usually causes a reduction on the peak flow, and therefore we should expect a reduction on sediment transport downstream the dam. Future versions of CASCADE should include an assessment of the dam management operations and therefore alter the natural water flow regime of the reaches downstream the reservoir accordingly, if the reservoir is implemented. Since we expect to see a reduction in water flow in the extreme scenarios, this framework could allow to estimate the reduction of sediment load transported downstream the dam.

The assessment framework here implemented does not account for the ecological damage on fish populations due to river fragmentation. Typically, large dams sited close to the river mouth greatly disrupt the paths of migratory fishes and the connectivity between fluvial ans sea ecosystems. In turn, disappearance of migratory fish species in the upper part of the river can alter the ecological balance of the ecosystem these sited, aggravating the impacts of the dam. Infrastructures like fish passages and fish elevators on the dams can be implemented to contain the damages and restore connectivity to the river, however for large dams their actual benefit is limited. The dams on the lower part of the Vjosa are bound to produce severe damage to the ecosystems on the braided sections and to the ecological connectivity of the river, and to cause problems of coastal erosion due to the decrease of sediment supply to the river mouth.

While indicators of sediment alteration can be used as proxy for a qualitative analysis on the impact on the ecosystem services, no methodology has yet been implemented to quantify and monetize the damages on a specific ecosystems good and service caused by the sediment alteration reported in CASCADE, for example the damage due to coastal erosion, or the loss of habitat due to sediment erosion. For future developments, the assessment framework could benefit from the creation of model frameworks that uses as input the results from CASCADE simulations to quantify the damages due to sediment alteration on a specific ecosystem good or service with a specifically designed indicator.

Bibliography

Ashmore, P., W. Bertoldi, and J. Tobias Gardner (2011), Active width of gravel-bed braided rivers, *Earth Surface Processes and Landforms*, *36*(11), 1510–1521.

Betrie, G. D., Y. A. Mohamed, A. van Griensven, and R. Srinivasan (2011), Sediment management modelling in the blue nile basin using swat model, *Hydrology and Earth System Sciences*, *15*(3), 807.

Brismar, A. (2002), River systems as providers of goods and services: a basis for comparing desired and undesired effects of large dam projects, *Environmental Management*, *29*(5), 598–609.

Castelletti, A., and M. Giuliani (2011), Multi-agent water resources management, in *AGU Fall Meeting Abstracts*.

Chatzinikolaou, Y., V. Dakos, and M. Lazaridou (2008), Assessing the ecological integrity of a major transboundary mediterranean river based on environmental habitat variables and benthic macroinvertebrates (aoos-vjose river, greece-albania), *International Review of Hydrobiology*, *93*(1), 73–87.

Czuba, J. A., and E. Foufoula-Georgiou (2014), A network-based framework for identifying potential synchronizations and amplifications of sediment delivery in river basins, *Water Resources Research*, *50*(5), 3826–3851.

Czuba, J. A., and E. Foufoula-Georgiou (2015), Dynamic connectivity in a fluvial network for identifying hotspots of geomorphic change, *Water Resources Research*, *51*(3), 1401–1421.

De Roo, A. P., et al. (2003), Development of a european flood forecasting system, *International Journal of River Basin Management*, *1*(1), 49–59.

Engelund, F., and E. Hansen (1967), A monograph on sediment transport in alluvial streams, *Technical University of Denmark 0stervoldgade 10, Copenhagen K.*

European Environment Agency (2017), *Copernicus Land Monitoring Service - Reference Data: EU-DEM*, European Environment Agency.

Ferguson, R. (2003), The missing dimension: effects of lateral variation on 1-d calculations of fluvial bedload transport, *Geomorphology*, *56*(1-2), 1–14.

Ferguson, R., M. Church, C. Rennie, and J. Venditti (2015), Reconstructing a sediment pulse: Modeling the effect of placer mining on fraser river, canada, *Journal of Geophysical Research: Earth Surface*, *120*(7), 1436–1454.

Giuliani, M., D. Anghileri, A. Castelletti, P. N. Vu, and R. Soncini-Sessa (2016), Large storage operations under climate change: expanding uncertainties and evolving tradeoffs, *Environmental Research Letters*, *11*(3), 035,009.

Gomez, B., B. J. Rosser, D. H. Peacock, D. M. Hicks, and J. A. Palmer (2001), Downstream fining in a rapidly aggrading gravel bed river, *Water Resources Research*, *37*(6), 1813–1823.

Graf, W., et al. (2017), The fauna of the vjosa river and the adjacent floodplain at poçem.

Hadka, D. (2015), Moea framework-a free and open source java framework for multiobjective optimization. version 2.11, *URL http://www. moeaframework. org*.

Hoey, T. B., and B. J. Bluck (1999), Identifying the controls over downstream fining of river gravels, *Journal of Sedimentary Research*, *69*(1).

Horner, G. J., P. J. Baker, R. Mac Nally, S. C. Cunningham, J. R. Thomson, and F. Hamilton (2010), Forest structure, habitat and carbon benefits from thinning floodplain forests: managing early stand density makes a difference, *Forest ecology and management*, *259*(3), 286–293.

International Energy Agency (2015), World energy outlook special report on southeast asia, *France International Energy Agency (IEA)*.

Jager, H. I., R. A. Efroymson, J. J. Opperman, and M. R. Kelly (2015), Spatial design principles for sustainable hydropower development in river basins, *Renewable and Sustainable Energy Reviews*, *45*, 808–816.

James, L. D. (2015), *Man and Water: The Social Sciences in Management of Water Resources*, University Press of Kentucky.

Jansen, R. B. (2012), *Advanced dam engineering for design, construction, and rehabilitation*, Springer Science & Business Media.

Kondolf, G. M. (1994), Geomorphic and environmental effects of instream gravel mining, *Landscape and Urban Planning*, *28*(2-3), 225–243.

Kondolf, G. M. (1997), Hungry water: effects of dams and gravel mining on river channels, *Environmental management*, *21*(4), 533–551.

Krumbein, W. C., and E. Aberdeen (1937), The sediments of barataria bay, *Journal of Sedimentary Research*, *7*(1).

Kuby, M. J., W. F. Fagan, C. S. ReVelle, and W. L. Graf (2005), A multiobjective optimization model for dam removal: an example trading off salmon passage with hydropower and water storage in the willamette basin, *Advances in Water Resources*, *28*(8), 845–855.

Liébault, F. (2003), Les rivières torrentielles des montagnes drômoises: évolution contemporaine et fonctionnement géomorphologique actuel (massifs du diois et des baronnies), Ph.D. thesis, Lyon 2.

Liu, J., P. Mason, N. Clerici, S. Chen, A. Davis, F. Miao, H. Deng, and L. Liang (2004), Landslide hazard assessment in the three gorges area of the yangtze river using aster imagery: Zigui–badong, *Geomorphology*, *61*(1-2), 171–187.

Merritt, W. S., R. A. Letcher, and A. J. Jakeman (2003), A review of erosion and sediment transport models, *Environmental Modelling & Software*, *18*(8-9), 761–799.

Millennium Ecosystem Assessment (2005), Ecosystem and human well-being: biodiversity synthesis.

Milliman, J. D., and R. H. Meade (1983), World-wide delivery of river sediment to the oceans, *The Journal of Geology*, *91*(1), 1–21.

Moussavi-Harami, R., A. Mahboubi, and M. Khanehbad (2004), Analysis of controls on downstream fining along three gravel-bed rivers in the band-e-golestan drainage basin ne iran, *Geomorphology*, *61*(1-2), 143–153.

Mueller, E. R., J. Pitlick, and J. M. Nelson (2005), Variation in the reference shields stress for bed load transport in gravel-bed streams and rivers, *Water Resources Research*, *41*(4).

Null, S. E., J. Medellín-Azuara, A. Escriva-Bou, M. Lent, and J. R. Lund (2014), Optimizing the dammed: Water supply losses and fish habitat gains from dam removal in california, *Journal of environmental management*, *136*, 121–131.

Piegay, H., A. Alber, L. Slater, and L. Bourdin (2009), Census and typology of braided rivers in the french alps, *Aquatic Sciences*, *71*(3), 371.

Ranzi, R., T. H. Le, and M. C. Rulli (2012), A rusle approach to model suspended sediment load in the lo river (vietnam): Effects of reservoirs and land use changes, *Journal of Hydrology*, *422*, 17–29.

Rice, S. (1999), The nature and controls on downstream fining within sedimentary links, *Journal of Sedimentary Research*, *69*(1).

Richter, B. D., S. Postel, C. Revenga, T. Scudder, B. Lehner, A. Churchill, and M. Chow (2010), Lost in development's shadow: The downstream human consequences of dams, *Water Alternatives*, *3*(2), 14.

Rosenberg, D. M., F. Berkes, R. Bodaly, R. Hecky, C. Kelly, and J. W. Rudd (1997), Large-scale impacts of hydroelectric development, *Environmental Reviews*, *5*(1), 27–54.

Schmitt, R., S. Bizzi, A. Castelletti, and G. Kondolf (2018), Improved trade-offs of hydropower and sand connectivity by strategic dam planning in the mekong, *Nature Sustainability*, *1*(2), 96.

Schmitt, R. J., S. Bizzi, and A. Castelletti (2016), Tracking multiple sediment cascades at the river network scale identifies controls and emerging patterns of sediment connectivity, *Water Resources Research*, *52*(5), 3941–3965.

Schmitt, R. J. P. (2016), Cascade - a framework for modeling fluvial sediment connectivity and its application for designing low impact hydropower portfolios, Phd thesis, Politecnico di Milano, Dipartimento di Elettronica, Informazione e Bioingegneria (DEIB).

Schwanghart, W., and N. J. Kuhn (2010), Topotoolbox: A set of matlab functions for topographic analysis, *Environmental Modelling & Software*, *25*(6), 770–781.

Schwarz, U., and F. Vienna (2017), Hydropower projects on balkan rivers - data update 2017.

Shih, S.-M., and P. D. Komar (1990), Differential bedload transport rates in a gravel-bed stream: A grain-size distribution approach, *Earth Surface Processes and Landforms*, *15*(6), 539–552.

Sivapragasam, C., G. Vasudevan, J. Maran, C. Bose, S. Kaza, and N. Ganesh (2009), Modeling evaporation-seepage losses for reservoir water balance in semi-arid regions, *Water resources management*, *23*(5), 853.

Sklar, L. S., C. S. Riebe, J. A. Marshall, J. Genetti, S. Leclere, C. L. Lukens, and V. Merces (2017), The problem of predicting the size distribution of sediment supplied by hillslopes to rivers, *Geomorphology*, *277*, 31–49.

Sogreah Consultant (2009), Consultants services for assessment of power generation potential of selected albanian rivers.

Soncini-Sessa, R., E. Weber, and A. Castelletti (2007), *Integrated and participatory water resources management-theory*, Elsevier.

Vejnovic, I. (2017), Broken rivers - the impacts of european-financed small hydropower plants on pristine balkan landscapes, *Bankwatch Network*.

Walling, D. E. (1983), The sediment delivery problem, *Journal of hydrology*, *65*(1-3), 209–237.

Ward, J. V., and J. Stanford (1995), Ecological connectivity in alluvial river ecosystems and its disruption by flow regulation, *River Research and Applications*, *11*(1), 105–119.

Wessel, B., T. Fritz, T. Busche, and P. Rizzoli (2016), Tandem-x ground segment - dem products specification document.

Wilcock, P. R., and J. C. Crowe (2003), Surface-based transport model for mixed-size sediment, *Journal of Hydraulic Engineering*, *129*(2), 120–128.

Wild, T. B., and D. P. Loucks (2014), Managing flow, sediment, and hydropower regimes in the sre pok, se san, and se kong rivers of the mekong basin, *Water Resources Research*, *50*(6), 5141–5157.

Wolman, M. G. (1954), A method of sampling coarse river-bed material, *EOS, Transactions American Geophysical Union*, *35*(6), 951–956.

World Commission on Dams (2000), *Dams and Development: A New Framework for Decision-making: the Report of the World Commission on Dams*, Earthscan.

Zarfl, C., A. E. Lumsdon, J. Berlekamp, L. Tydecks, and K. Tockner (2015), A global boom in hydropower dam construction, *Aquatic Sciences*, *77*(1), 161–170.

A

Additional material

A.1 MATLAB coding

Matlab function/script	Description
`CASCADE_script`	The main CASCADE script, composed by the sections: • `graph preprocessing`: contains operations of river network extraction and derivation of topological informations stored in struct *Network*, described in Section 2.3.2, and the operations of slope smoothing; • `Annual cascade routing - Model A`: runs Model A for all the considered water flow scenarios, and collect and join the outputs from the simulations to obtain outputs of annual sediment transport processes, with the formulas described in Section 2.3.5; • `Annual cascade routing - Model B`: runs Model B for all the considered water flow scenarios, and collect and join the outputs from the simulations to obtain outputs of annual sediment transport processes, with the formulas described in Section 5.3.
`Script_River_Network_Vjosa`	Acquires and prepares the DEM and other inputs for function `Extract_River_Network`, generates matrix *AggData* from the function's outputs.
`CASCADE_model_A`	Run the revised CASCADE framework with the methodology of Model A to derive the reach GSDs
`CASCADE_model_B`	Run the revised CASCADE framework with the methodology of Model B to derive the reach GSDs

Matlab function/script	Description
`CASCADE_model_B_optimized`	Run the revised CASCADE framework by receiving as input the reach GSDs obtained by simulations in undisturbed state.
`Extract_River_Network`	Extracts the river network and the geomorphological features of the reaches.
`slope_smoothing`	Smooths the slope reported in *AggData* for each reach by performing a weighted average between the original channel slope and the slope or the neighboring reaches, as described in Section 2.3.
`Script_Assessment_framework`	Calculates the values of the indicators for all the possible dams portfolios and identify Pareto-optimal portfolios.
`getNonDominated`	Receives as input the performances of the indicators for all the possible dam portfolios and returns the list of non-dominated portfolios.
`dam_slope_correction`	Modifies the value of the slope in *AggData* for the reaches inundated by the construction of a dam, with the methodology described in Section 5.3.
`Script_sensitivity_GSD`	Contains the operation to perform the sensitivity analysis on the reach GSDs.
`Script_sensitivity_Pareto`	Contains the operation to perform the sensitivity analysis on the non-dominated portfolios.

Table A.1: *MATLAB functions and scripts from the CASCADE model, assessment and sensitivity frameworks reported in the document.*